ACIBADEM MEHMET ALI AYDINLAR UNIVERSITY
INSTITUTE OF HEALTH SCIENCES

CONSTRUCTION OF BIFUNCTIONAL SUBSTITUTE FOR OSTEOCHONDRAL TISSUE ENGINEERING

DENİZ BAŞÖZ

M.Sc. THESIS

DEPARTMENT OF MEDICAL BIOTECHNOLOGY

SUPERVISOR
Asst. Prof. Dr. Deniz Yücel

SECONDARY SUPERVISOR
Prof. Dr. Vasıf Hasırcı

ISTANBUL-2022

ACIBADEM MEHMET ALI AYDINLAR UNIVERSITY
INSTITUTE OF HEALTH SCIENCES

CONSTRUCTION OF BIFUNCTIONAL SUBSTITUTE FOR OSTEOCHONDRAL TISSUE ENGINEERING

DENİZ BAŞÖZ

M.Sc. THESIS

DEPARTMENT OF MEDICAL BIOTECHNOLOGY

SUPERVISOR
Asst. Prof. Dr. Deniz Yücel

SECONDARY SUPERVISOR
Prof. Dr. Vasıf Hasırcı

ISTANBUL-2022

DECLARATION

I declare that this thesis work is my own work, I had no unethical behavior at any stages from the planning to the writing of the thesis, I obtained all the information in this thesis in accordance with academic and ethical rules, I cited all the information and comments that were not obtained with this thesis work, and I provided resources in the list of references. I also declare that there was no violation of any patents and copyrights during the study and writing of this thesis.

29.06.2022

Deniz BAŞÖZ

PREFACE AND ACKNOWLEDGEMENT

It is a great pleasure to express my sincere appreciation to my advisor and mentor Asst. Prof. Deniz YÜCEL for her continuous support, guidance and encouragement during all the stages of my thesis. I am grateful for her patience, valuable suggestions and endless guidance that have enhanced the quality of this thesis. I cannot thank her enough for her kind attitude, physical and mental support from the first day.

I would like to express my sincere gratitude and deepest respects to my secondary advisor Prof. Dr. Vasıf HASIRCI for his utmost guidance and valuable suggestions. I am grateful for his patience and effort to improve my scientific experience.

I especially grateful to Prof. Dr. Halime KENAR for her valuable suggestions and guidance. Her continuous support, kindness and motivation has been invaluable.

I wish to express my appreciation to Prof. Dr. Gamze TORUN KÖSE for her support.

I am also deeply grateful to Gözde Ervin KÖLE for being invaluable friend and a research partner. I am especially thankful to her for transferring her knowledge and experience to me, and her endless support on academic and personal level.

I would like to thank to Neval ÖZDEMİR and Kübra COŞKUN KIRATLI for their support on both academic and personal level and their invaluable friendship.

I would like to thank to my lab mates Hilal SELAMET, Şeyma IŞIK and Onat KÖYLÜOĞLU for their support on my studies and their friendship.

I would like to thank Selçuk BİRDOĞAN and Senem ÇİTOĞLU for their helps for the scanning electron microscopy studies.

This study was supported by Acıbadem Mehmet Ali Aydınlar University and ACU Biomaterials Center and their facilities are gratefully acknowledged. I would like to thank METU-BIOMATEN for the contributions during my thesis. During this study, I was supported by TUBITAK SBAG 118S587 and 218S717 and these grants scholarships are gratefully acknowledged.

I especially would like to thank to my friends Ece SELEK and Harun İNAN for their patience, support, love and understanding through my studies and more. I feel very lucky to have them in my life.

Finally, I would like to express my deepest gratitude to my parents İsmail BAŞÖZ and Gülten ÇELİK and my brother Ömer Güney BAŞÖZ for their encouragement, love, caring and endless support through my education and my life. I also want to thanks to my aunts Fatma ÇELİK, Münevver ÇELİK, Gülsün ÇELİK, Sebahat Çelik and Ayfer BAŞÖZ and my uncle Mehmet ÇELİK for always being there for me and their endless support. Also, I would like to thanks my cousin Nuray ÇELİK who was very helpful and interested in my education from my childhood.

TABLE OF CONTENTS

LIST OF ABBREVIATIONS \ SYMBOLS

2D	2 Dimensional
3D	3 Dimensional
α-MEM	Alpha-Minimum Essential Medium
AC	Articular Cartilage
ACI	Autologous Chondrocyte Implantation
ALP	Alkaline Phosphatase
β-TCP	Beta Tricalcium Phosphate
BSA	Bovine Serum Albumin
BMP	Bone Morphogenetic Protein
BMSC	Bone Marrow Mesenchymal Stem Cell
CC	Calcified Cartilage
CLSM	Confocal Laser Scanning Microscopy
CS	Chondroitin Sulfate
DAPI	4',6-Diamidino-2-Phenylindole, Dihydrochloride
DMEM	Dulbecco's Modified Eagle Medium
DMF	Dimethyl Formamide
DMSO	Dimethyl Sulfoxide
DP-MSC	Dental Pulp derived Mesenchymal Stem Cell
ECM	Extracellular Matrix
FBS	Fetal Bovine Serum
FDM	Fused Deposition Modelling
FITC	Fluorescein Isothiocyanate
GAGs	Glycosaminoglycans
HA	Hyaluronic Acid
HAp	Hydroxyapatite
MSCs	Mesenchymal Stem Cells
OC	Osteochondral
OC-TE	Osteochondral Tissue Engineering
OCD	Osteochondral Defect

PBS	Phosphate Buffered Saline
PCL	Poly(ε-caprolactone)
PFA	Paraformaldehyde
PVA	Polyvinyl Alcohol
SEM	Scanning Electron Microscope
TGFβ	Transforming Growth Factor β
Try-EDTA	Trypsin-Ethylenediamine Tetraacetic Acid
TCPS	Tissue Culture Polystrene

LIST OF FIGURES

LIST OF TABLES

ÖZET

Osteokondral Doku Mühendisliği için Bifonksiyonel Doku Eşleniği Tasarımı

Travma veya dejeneratif hastalıkların neden olduğu osteokondral defektler, ağrı, şişme, zayıf hareket kabiliyeti ve hatta eklemin hareket kabiliyetini tamamen kaybetmesi gibi semptomlara neden olabilirler. Osteokondral doku mühendisliği, osteokondral defektlerin tedavisi için alternatif bir yaklaşım sunmaktadır. Bu çalışmanın amacı, doğal dokunun histolojik özelliklerini taklit ederek *in vitro* ortamda, süperfisyal fibröz kısım, hücre yüklü kıkırdak, kalsifiye kıkırdak ve hücre yüklü kemik kısımlarından oluşan işlevsel, çok katmanlı bir osteokondral doku eşleniği oluşturmaktır. PCL bazlı çok katmanlı yapı iskelesi ve rastgele lifli yapılar sırasıyla, 3B baskı ve elektroeğirme ile üretildi ve ardından lifli yapılar, 3B basım ile elde edilen yapının kıkırdak tarafına sabitlendi. Kemik tarafına β-TCP kaplandıktan sonra elde edilen doku iskeleleri morfolojik ve mekanik özellikler açısından karakterize edildi. İnsan diş pulpası dokusundan elde edilen mezenkimal kök hücreler (MKH), kemik tarafında osteojenik hücrelere farklılaştırıldı ve hidrojel içinde kıkırdak tarafına yüklenen DP MKH'lardan türetilen kondrositler ile beraber kültür edildi. SEM sonuçları, kıkırdak kısmının gözenek boyutunun, amaçlandığı gibi kemik kısmındakinden daha büyük olduğunu gösterdi. Ayrıca kalsifiye kıkırdak kısmının fonksiyonel bariyer görevi gördüğü gösterildi. β-TCP kaplı nihai yapının Young Modülü 75.7± 5.2 MPa olarak belirlendi. MTS analizi ve immün boyama sonuçları, DP MKH'ların iskele üzerinde başarılı bir şekilde çoğaldığını ve ortak kültürden sonra bile bölgeye özgü hücre farklılaşmasının gerçekleştirildiğini gösterdi. Sonuçlar, iki işlevli, çok katmanlı osteokondral doku ikamesinin *in vivo* çalışmalarda test edilme potansiyeline sahip olduğunu ve klinikte osteokondral defektlerin tedavisi için umut verici bir yaklaşım olabileceğini göstermektedir.

Anahtar Sözcükler: Çok Katmanlı Doku İskelesi, Bifonksiyonel, Osteokondral Doku Mühendsiliği, 3 Boyutlu Basım, Mezenkimal Kök Hücre

ABSTRACT

Construction of Bifunctional Substitute for Osteochondral Tissue Engineering

Osteochondral defects, caused by trauma or degenerative diseases, results in symptoms like pain, swelling, poor mobility and even immobilization of joint. Osteochondral tissue engineering offers alternative approach for treatment of osteochondral defects. The aim of this study was to construct a bifunctional, multilayered osteochondral tissue substitute consisting of superficial fibrous layer, cell-loaded cartilage, calcified cartilage, and cell-loaded bone parts under *in vitro* by mimicking histological properties of native tissue. PCL-based multilayered scaffold and random fibrous mats were fabricated by 3D printing and electrospinning, respectively, and then the fibrous mat was fixed onto the cartilage side of 3D printed construct. After β-TCP coating to the bone side, the obtained scaffolds were characterized in terms of morphology and mechanical properties. Human dental pulp MSCs differentiated into osteogenic cells on the bone side, and DP MSC-derived chondrocytes loaded within the hydrogel to the cartilage side were co-cultured. SEM results showed that pore size of the cartilage part was larger than that of the bone part as intended. In addition, it was shown that the calcified cartilage part acts as functional barrier. The Young's Modulus of β-TCP coated final construct was determined as 75.7± 5.2 MPa. MTS assay and immunostaining results indicated that DP MSCs was successfully proliferated on the scaffold and site-specific cell differentiation was accomplished, even after co-culture. The results indicates that the bifunctional, multilayered osteochondral tissue substitute has a potential to be tested in *in vivo* studies, and could be a promising approach for the treatment of osteochondral defects in clinic.

Keywords: Multilayer Scaffold, Bifunctional, Osteochondral Tissue Engineering, 3D Printing, Mesenchymal Stem Cells

1 INTRODUCTION AND AIM

Osteoarthritis is a disease characterized by degenerative lesions and pain in the bone and cartilage at joints. It is currently thought to affect 25% of adults over the age of 18 (1). It has been observed that osteoarthritis is accounted for 2.9% in total disease burden and ranks seventh in disease burden studies in Turkey (2). Since this disease is common and restricts vital activities, its treatment has a significant impact on public health (1). Recurrent overload of the joints causes articular cartilage damage that can progress to the subchondral bone under the cartilage, resulting in loss of function in the joint (3). Since the articular cartilage has a nonvascular structure, this region has a limited repair capacity (4). The damages affecting both the articular cartilage and subchondral bone are referred to as osteochondral injuries. If osteochondral damage is not treated, it can lead to the development of osteoarthritis and make the healing of this region with low repair capacity very difficult (3).

The most commonly used surgical techniques for the treatment of osteochondral defects include microfracture, fixation, autologous and allogeneic osteochondral transplantation, and mosaicplasty autologous chondrocyte implantation (5). These surgical methods used in the treatment of osteochondral damage may cause unwanted complications in the patient and the complaints may recur after treatment. In addition, there are some limitations in these applications, such as donor site morbidity, disease transmission, immunogenicity, tissue unavailability, and inability to regenerate biologically active articular surface. Besides, classical treatment methods used for osteochondral tissue damage offer palliative treatment rather than restorative, and often cause insufficient healing at the damaged site. Tissue restoration in this region is difficult due to the complex structure and heterogeneity of that region (6). Osteochondral tissue engineering is a promising approach that can overcome these challenges in the treatment of osteochondral defects.

Osteochondral tissue is a heterogeneous tissue composed of layers with different biochemical and mechanical properties. The tissue conjugates to be designed should provide site-specific clues to meet the biochemical and mechanical properties

of the multilayered structure of osteochondral tissue (7). One of the challenges in osteochondral tissue engineering studies is the requirement of different biochemical and mechanical properties of different layers for site-specific tissue-regeneration in one substitute.

In this study, it was aimed to develop a bifunctional, multilayered osteochondral tissue substitute to mimic most of the layers of the native tissue, and to evaluate the multilayered scaffold in *in vitro* conditions (Figure 1). The architeure and cellular compositions of this construct was inspired by the histological properties of the native osteochondral tissue. In this concept, the multilayered scaffold was planned to be fabricated by 3D printing to imitate subchondral bone, calcified cartilage, and hyaline cartilage layers, and electrospun fibrous mat was planned to be fixed onto the cartilage part to act as a superficial layer.

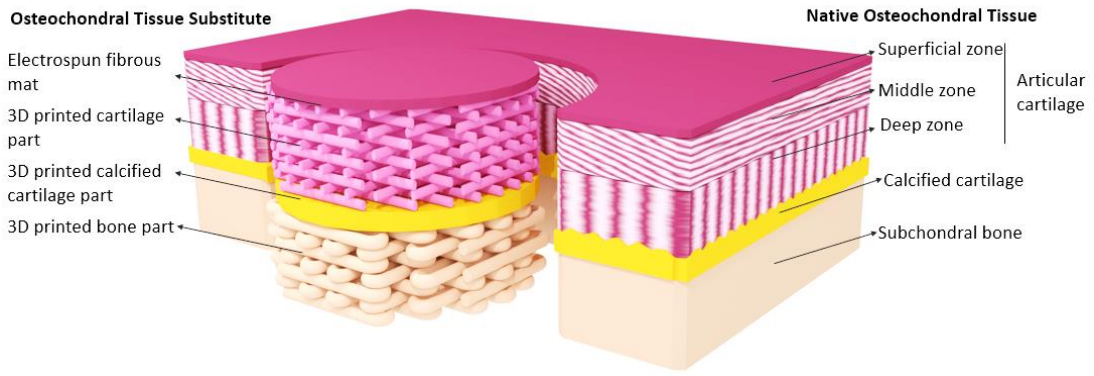

Figure 1. Schematic presentation of the native osteochondral tissue and design of the multilayered osteochondral tissue substitute

In this thesis, considering the structure of the natural tissue, 3D printing technology, hydrogel, and electrospinning methods were used together. It was planned to use human dental pulp mesenchymal stem cells for osteogenic and chondrogenic cell differentiation. Chondrogenic cell differentiation aimed to be done by spheroid culture. It was planned to differentiate DP MSCs into osteogenic cells on the bone side, and to load DP MSC-derived chondrocytes within the hydrogel to the cartilage side, and then to do co-culture of these cells to obtain tissue substitute.

2 BACKGROUND

2.1 Histology of Osteochondral Tissue

The human body can perform a wide variety of movements by articular joints such as knees, hips, shoulders, and elbows. Some of these joints carry 2-3 times the body weight while walking, jumping, or climbing stairs (8). Distal ends of the articulating joints are covered with specialized articular cartilage (AC) tissue and an underlying subchondral bone and these cartilage and bone tissues form osteochondral (OC) unit together (Figure 2). The unique structure of osteochondral tissue has an essential role in the smooth joint movement, and dispersion of the force loaded from the skeleton. Osteochondral tissue provides an efficient load-bearing property with the organization of different tissue layers. It also has a lubricating low friction surface which allows the movement of the joints normally pain-free, usually for a lifetime (9). Osteochondral tissue, starting from the superficial layer consists of a specialized type of hyaline cartilage called as articular cartilage, calcified cartilage and subchondral bone part merging into the underlying trabecular bone (Figure 2). Articular cartilage is composed of superficial, middle and deep layers. This well-organized osteochondral complex is crucial for human movement, and the patients' quality of life may be severely affected upon its damage (10). Osteochondral tissue has unique structure with its heterogeneous, viscoelastic, nonlinear, and anisotropic properties (9). To understand the structural and biomechanical properties, it is crucial to examine the histology of this complex tissue (Figure 2).

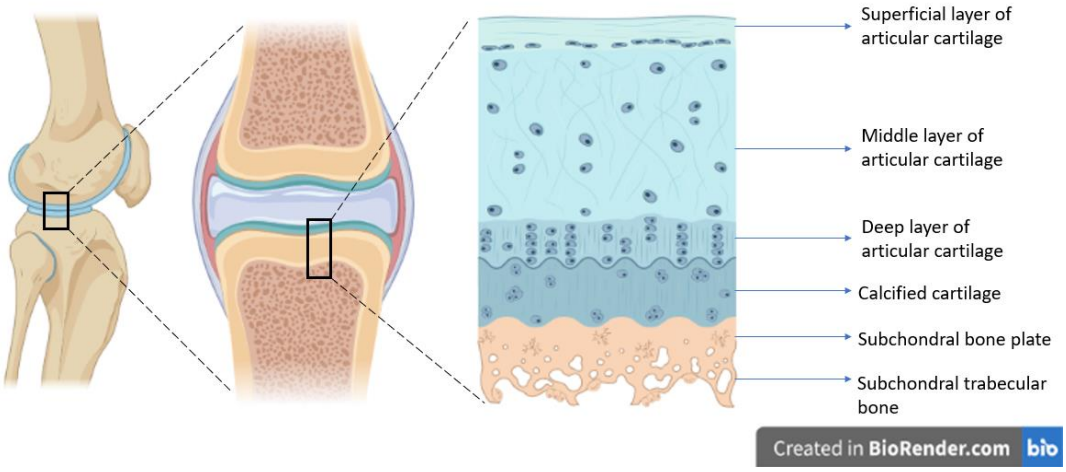

Figure 2. Schematic presentation of the location of the osteochondral tissue and the organization of different histological layers of the osteochondral tissue. Created with BioRender.com

2.1.1 Articular cartilage

Cartilage is a specialized connective tissue, and there are three types of cartilage having different structures and compositions. These are fibrocartilage, elastic cartilage, and hyaline cartilage. Articular cartilage (AC), a specialized type of hyaline cartilage, covers the distal ends of bones and is vital for the smooth movement of the joints (11). AC is an aneural and avascular tissue obtaining the needed nutrients from synovial fluid. Due to being avascular tissue, articular cartilage has a low regeneration capacity (12). AC is composed of chondrocytes, a mature cell type, and a distinctive extracellular matrix (ECM) surrounding the chondrocytes, which contains collagen, proteoglycans, glycosaminoglycans, and absorbs water that comprises 65-80% of tissues volume (13).

Chondrocytes are the only consisting cell type found in articular cartilage tissue. Even though they consist of only 2-5% volume of the total tissue, they are the metabolic units maintaining the articular cartilage tissue (12). Chondrocytes are differentiated from mesenchymal stem cells (MSC), and they have a unique and specialized role in maintaining and repairing the ECM. Chondrocytes synthesize and turnover the large portion of ECM around it, including collagens, proteoglycans, and glycoproteins (14). The microenvironment synthesized by chondrocytes entraps the

chondrocytes within, separating them from each other. The chondrocytes are located within the spaces, called lacunae, which maintain chondrocytes survival and functionality. Chondrocytes have a distinguished spherical shape that depends on the zonal location within the articular cartilage. Chondrocytes having very low mitotic activity leads to the low regenerative capacity of articular cartilage (15).

Collagen is the most abundant ECM macromolecule and makes up to 50% of the dry weight of AC. There are different types of collagen present in the AC, the most abundant one is collagen type-II (90-95%), and it is a cartilage-specific marker (16). The highly organized fibril network of the ECM is made of collagen type II fibrils, synthesized by chondrocytes located in the superficial and middle zone. Collagen type X is synthesized by deep zone chondrocytes and has the role of mineralization in the calcified cartilage (9, 14). Polypeptides, assembled from procollagen, form collagen, and then they are assembled into microfibrils. The polypeptide chains consist of amino acids, mostly glycine and proline. While hydroxyproline produces the stability with hydrogen bonds along the molecule chain, hydroxylysine creates covalent crosslinks that stabilize the formed collagen fibrils (13). Type IX and XI collagens are also present in the AC and are involved in cross-linking of collagen type II fibers (15). The organization of collagen fibrils and chondrocytes differs depending on where they are located, and this provides an extraordinary biomechanical property of the AC (10, 12). Collagen fibrils are intertwined with proteoglycan molecules (16).

Proteoglycans are secreted into cartilage ECM by the chondrocytes and constitute 10-15% of the dry weight of ECM (13). Aggrecan is the main proteoglycan of articular cartilage and is considered a key marker for chondrogenesis. Aggrecans are made of core proteins covalently binding to glycosaminoglycans (GAGs), such as chondroitin sulfate and keratan sulfate, which have highly negative charges. The sum of these negative charges causes osmotic pressure in the tissue and attracts water molecules. Thus, water trapped in the ECM causes swelling and leading to the high compression modulus of the cartilage. Swelling also ensures the ability of articular cartilage to distribute loads effectively and the frictionless movement at the joints (9, 17).

2.1.1.1 Zonal organization of articular cartilage

Articular cartilage is a 2-4 mm thick tissue that has a characteristic tissue organization and biomechanical structure compared to other hyaline cartilage types, which enables it to have a high load-bearing capacity with low friction for the joint motion (15, 18). There are four layers of the articular cartilage as the superficial zone, the middle zone, the deep zone, and the calcified cartilage zone with different structural and biochemical organizations (Figure 3). This complex organization and distribution of chondrocytes, collagen fibrils, and proteoglycans bring in distinctive biological, biochemical and biomechanical properties in each zone.

The superficial (tangential) zone is the thinnest layer of the articular cartilage and consists of 10-20% of the tissue. In the superficial zone, which has the highest concentration of chondrocytes among the articular cartilage layers, chondrocytes are flat and organized parallel to the articular surface (Figure 3). The superficial zone chondrocytes synthesize dense collagen type II fibrils that are aligned parallel to the synovial joint surface (19). Collagen fibrils in this zone are the thinnest fibers and at the highest concentration among the articular cartilage zones. This dense and parallel fibril organization provides a high tensile strength and acts as a pressure-resistant region. In addition, as being the closest layer to the articular surface it protects the underlying tissue. Chondrocytes within this layer secrete a protein called lubricin that ensures a decrease in the friction force for joint movement (20). Moreover, this layer takes role in diffusion of nutrients and oxygen to the underlying tissue from synovial fluid; on the other hand, it acts as a barrier preventing the large macromolecules from passing through the synovial joint (21).

The middle (transitional) zone is right below the superficial zone, and it houses sparsely, randomly distributed, round-shaped chondrocytes, which are larger than the ones in the superficial zone (Figure 3). In this zone collagen type II fibers are thicker than the ones in the superficial zone and display random organization (21). Proteoglycan concentration is the highest in the middle zone, thus providing compression strength to the articular cartilage tissue (12).

The deep (radial) zone is between the middle zone and the calcified cartilage and it consists of less number of round-shaped chondrocytes. Chondrocytes are arranged in columns perpendicular to the articular surface and the subchondral bone (Figure 3) (22). The deep zone collagen type II fibers are the thickest collagen fibers in the articular cartilage tissue. These fibers are found between cellular columns along the long axis of the long bone and organized perpendicular to the articular surface. This organization provides a high compression strength to the articular cartilage. In the middle zone and the deep zone, chondrocytes and its 4-6 μm thick pericellular matrix (PRM) surrounding that is rich in collagen type IV form chondron (21).

The calcified cartilage (CC) zone is a thin mineralized tissue layer, tightly integrated between bone and articular cartilage enhancing the mechanical integrity of the OC tissue and having an important role in the transmission of the force loaded (21, 23) . Perpendicularly organized collagen fibrils of the deep zone that are anchored to the calcified cartilage zone prevent the partitioning of articular cartilage from bone (Figure 3) (24). The calcified cartilage prevents the vascularization of the articular cartilage from bone and helps maintaining the needed hypoxic environment of the articular cartilage (21, 23). The calcified cartilage is a transitional layer between the articular cartilage and subchondral bone and consists of hydroxyapatite, collagen type II and X, and GAGs. The calcified cartilage is characterized by very sparsely distributed hypertrophic chondrocytes that synthesize the collagen X molecules (22). Collagen type X provides stiffness to the tissue and also initiates the mineralization of calcified cartilage (25)

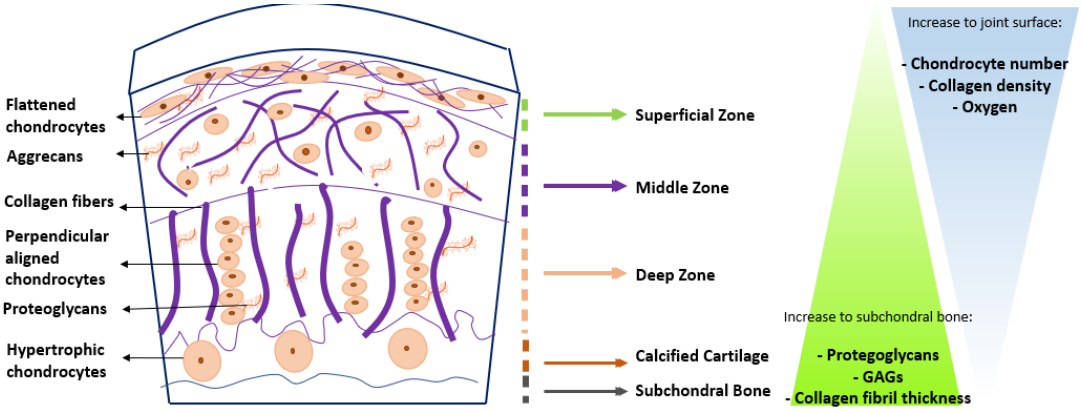

Figure 3. Schematic presentation of the organization of zones of the articular cartilage and their composition.

2.1.2 Subchondral bone

The subchondral bone is an approximately 1 mm thin layer right under the articular cartilage and consists of two layers as subchondral bone plate and subchondral trabecular bone (Figure 4) (26). Subchondral bone plate is a dense, highly mineralized tissue with 85% hydroxyapatite concentration, providing a firm support against loading at joint (23), while the subchondral trabecular bone has a more elastic structure and it provides shock absorption (27). The subchondral bone absorbs most of the mechanical loads, and due to its characteristic structure it effectively distributes the loads and contributes to maintain the health of the articular cartilage tissue (28).

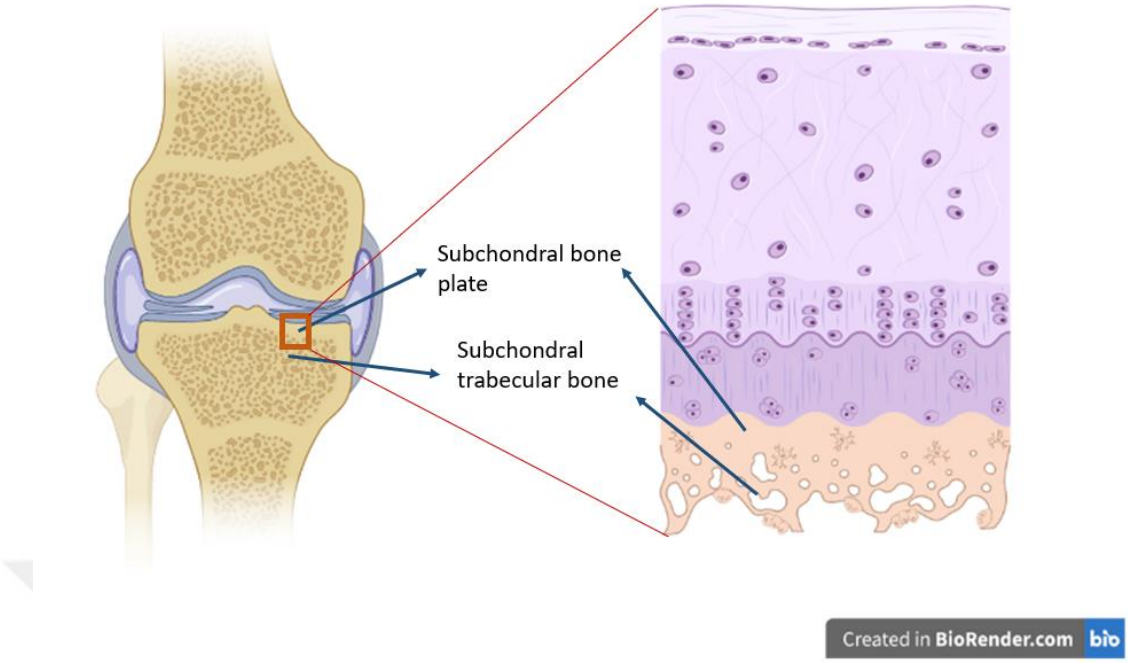

Figure 4. Schematic presentation of the subchondral bone. Created with BioRender.com

Bone tissue is composed of various types of cells, organic and inorganic ECM, and water. Bone is a mineralized tissue that provides maximum load-bearing strength with minimum weight due to its structure (29). There are four kinds of cells in bone tissue as bone lining cells, osteoblasts, osteocytes, and osteoclasts (19). Bone lining cells, osteoblasts, and osteocytes are originated from mesenchyme, while osteoclasts are originated from macrophage-monocyte cell lineage. Bone lining cells are flat and elongated inactive cells, since these are immediate precursors of osteoblasts they are also called as inactive osteoblasts. Osteoblasts are partially differentiated cells from osteoprogenitor cells that synthesize and regulate the ECM molecules (30). These precursor cells also synthesize the alkaline phosphates enzyme. In their active form, osteoblasts have cuboidal shape and found at the periphery of the bone. Osteoblasts are differentiated into osteocytes, while they are entrapped within the surrounding mineralized matrix. Osteocytes, mature bone cells, are found within a small space in the ECM, called lacunae, and these cells have connections with each other and the blood vessels via tiny channels, called canaliculi. Osteoclasts are very large multinucleated phagocytic cells that are involved in bone resorption, which occurs under normal conditions before bone tissue synthesis during bone remodeling.

The organic component of the bone ECM consists of collagenous and non-collagenous proteins. Collagenous proteins are collagen type I, collagen type III, and collagen type V. Collagen type I is the most abundant protein found in the bone ECM (90%), synthesized by osteoblasts, and provides mechanical strength, and serves as a scaffold for the bone cells (31) Collagen type I is in the form of collagen fibrils containing triple helix polypeptides. With the help of other collagens and non-collagenous proteins, collagen fibrils become collagen fibers and bundles. Non-collagenous proteins consist of proteoglycans such as chondroitin sulfate, heparan sulfate, keratan sulfate, hyaluronic acid, and dermatan sulfate. In addition, glycoproteins such as osteocalcin, osteonectin, and osteopontin are also non-collagenous proteins. Mostly they are endogenic proteins produced by the bone cells and they have roles in mineralization, bone formation, and collagen fibrillogenesis. For example, osteocalcin is involved in binding of calcium molecules during mineralization, and osteonectin has a bridging function between the mineral components and collagen fibrils (30). The inorganic component of the ECM is mainly composed of calcium phosphate crystals in the form of hydroxyapatite ($Ca_{10}(PO_4)_6(OH)_2$), (HAp), which makes up 60-70% of the bone weight (32). The deposition of HAp occurs by the biomineralization process and provides stiffness and mechanical strengths to the bone tissue (31).

2.2 Osteochondral Defects (OCD) and Classification

The osteochondral tissue has required biomechanical properties to absorb the shock and to exert the loaded force efficiently to the underling cancellous bone tissue. When the capacity of the tissue is exceeded due to mechanical (e.g., major trauma, overuse of the joint leading to repetitive minor trauma) or biological reasons (e.g., osteochondral dissecans, osteonecrosis), or when there is a traumatic injury at joints due to accident or sports, a defect occurs in the articular cartilage (5). Defect formation begins with a decrease in proteoglycan synthesis and an increase in synthesis of degradation enzymes (e.g., metalloproteases) in the articular cartilage. This leads to apoptosis of the chondrocytes and loss of a part of the articular cartilage. Thus, the

defect disrupts the frictionless surface and leads to deterioration of the load-bearing capacity (5, 10).

Outerbridge classification is a broadly used system to evaluate the cartilage defects. Outerbridge classifies the cartilage defects as “grade 1: there are softening and swelling of the cartilage; grade 2: there are fragmentation and fissuring in an area half an inch or less in diameter; grade 3: is the same as grade 2 but an area more than half-inch in diameter is involved; in grade 4 there is an erosion of the cartilage down to the bone”, the schematic presentation of this classification system is shown in Figure 5 (33).

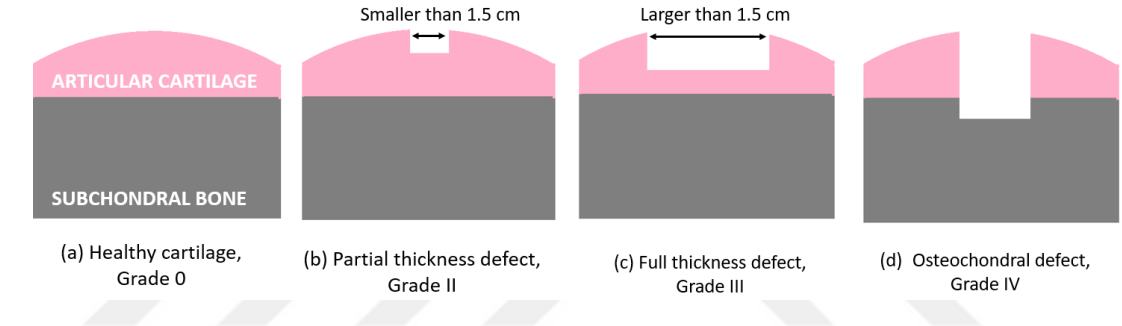

Figure 5. Schematic presentation of Outerbridge Classification System. (a) Grade 0: healthy cartilage; (b) Grade II: defect with a partial thickness lesser than 1.5 cm in diameter; (c) Grade III: defect with a full thickness more than 1.5 cm in diameter; (d) Grade IV: osteochondral defect reaching to subchondral bone.

Osteochondral defects (OCDs) are characterized by the symptoms like pain, swelling, inflammation, stiffness and impairment in function (34). When a large focal defect is left untreated, it may progress to an end-stage osteoarthritis. Osteoarthritis (OA) is the most commonly seen joint disease characterized by degeneration of the tissue and leads to pain and swelling at the articulating joints. OA is accounted for 2.9% in total disease burden and ranks seventh in disease burden studies in Turkey (2).

2.3 Classical Treatment Approaches for Osteochondral Defects

Due to the low self-regeneration capacity of AC, treatment of the OCD remains a challenge on which orthopedic surgeons and researchers have been working for a long time. Treatment of OCD is to relieve the patient from symptoms like pain and swelling and to regain the joint function (6). Small defects in articular cartilage may transform into large focal lesions and full joint degradation if it is left untreated. Conventional methods like using anti-inflammatory drugs and physiotherapy can be solutions in the early stages of defect. For severe cases like larger defects or prolonged defects there are several surgical options available that are summarized in Table 1. Due to the complex structure of the OC tissue, none of these treatment options has demonstrated a complete functional repair of the joint. In addition, classical treatment methods used for osteochondral tissue damage offer palliative treatment rather than restorative, and often cause insufficient healing at the damaged site. Tissue regeneration or restoration in this region is difficult due to the complex structure and heterogeneity of this region (6). Therefore, alternatives treatment strategies like tissue engineering may have the potential to offer a permanent solution, and may ensure complete recovery of the OCD.

Table 1. Classical treatment methods for OCD with their advantages and disadvantages.

Method	Application	Advantages	Disadvantages
Microfracture	It is a bone marrow stimulation method. With drilling in the subchondral bone, MSCs migrate to the AC surface and fill the defect with fibrocartilage (38)	-It is an easy and cheap application - It maintains short-term improvements(34)	- It has weak mechanical properties due to formation of fibrocartilage (34)
OC Allografts	OC plugs harvested from cadaver are used to fill the defect area. OC plugs can be composed of both hyaline cartilage and subchondral bone (34)	- It can be used in very large defects - It shows hyaline cartilage characteristics (34) - It is suitable for osteochondral lesions reaching to subchondral bone	- It may have a risk of immunologic reaction or disease transmission. - It may have a limited supply (35)
Autologous osteochondral transplant (OAT), Mosaicplasty	Autologous OC plugs from non-load-bearing parts of the joint are removed. The lesion filled with one big autologous OC plug is called OAT. The lesion filled with multiple autologous OC plugs is called mosaicplasty (37)	- There is a high survival of chondrocytes. - It shows hyaline cartilage characteristics. - There is no risk of immune rejection. - It is suitable for osteochondral defects reaching to bone (37)	- There may be a donor site morbidity. - There may be a fibrocartilage formation between plugs. - Poor surface matching (contour mismatch) may be occurred. - There is a need of a specialized operator (34, 36)
Autologous Chondrocyte Implantation (ACI)	The autologous chondrocytes are isolated from healthy cartilage of the patient. After reproducing the autologous chondrocytes at monoculture, implantation is done at the lesion site after 3-5 weeks (39)	-Hyaline cartilage can repair. - There is no risk of immune rejection. (36)	- It may not be suitable for OC defects reaching to bone - Multiple procedures are needed. - High cost is required. - There is a need of a specialized operator. - Patients activity may be restricted for one year to allow integration (35, 36)
Matrix assisted autologous chondrocyte implantation (MACI)	It is a third generation of ACI method. Isolated autologous chondrocytes are seeded on a scaffold *in vitro* before implantation on lesion site (36)	- There are better outcomes than ACI and mosaicplasty in some ongoing studies. - Hyaline cartilage can repair. - There is no risk of immune rejection (36)	- Multiple procedures are needed and a high cost is required. - There is a need of a specialized operator. - Patients activity may be restricted for one year to allow integration - There have been no long-term results (34, 36)
Full knee replacement	The total or partial joint is replaced with metal-plastic prostheses.	- There are successful results for patients with sedentary lifestyle.	- It is a highly invasive method. - There may be a risk of losing joint function postoperatively. -It may not be a suitable solution for physically active patients.

2.4 Tissue Engineering

The demand for organ transplantation or tissue replacement has rapidly increased due to vital organ or tissue failures or loss caused by the increased living age of the population. However, available donor numbers are not matching with the number of patients on the transplant waiting lists and this causes an organ shortage crisis (40). According to Health Resources and Services Administration (HRSA), there are more than 100 000 patients on the national transplant waiting list and another patient is added to the waiting list every 9 minutes.

The failure or loss of an organ, a tissue, or a part of a tissue, is one of the most frequent and major problems in human health care (41). Beside the organ transplantation, reconstructive surgical treatments using decellularized tissues or autograft transplantation methods are other methods utilized by physicians for the treatment of organ and tissue loss (42). All these procedures aim to restore or re-functionalize the lost organ or tissue. Although these treatment methods have saved and improved the lives of many patients, they remain temporary and imperfect solutions with lots of drawbacks like donor shortage, need for immunosuppressive therapy, donor site morbidity, transmission of virus, and need for repetitive surgeries.

By the improved understanding of cell biology and the development of biomaterial technologies, a new alternative approach called tissue engineering has emerged with the convergence of these disciplines (43). Vacanti and Langer, the pioneers of this field, define tissue engineering as “an interdisciplinary field that applies the principles of engineering and the life sciences towards the development of biological substitutes that restore, maintain or improve tissue functions” (41). The first idea was formed when Joseph Vacanti who was working at the children’s hospital at the time, made contact with Robert Langer to construct cell-loaded scaffolds, customed for children in need of transplants to overcome the donor shortage (44).

The primary goal of tissue engineering is to restore or support the function of the defective tissue with a constructed tissue substitute that includes living elements to

provide and support the regeneration of the defected area. Apart from the regeneration of the defective tissue, tissue engineering prospects and methods can be applied to design *in vitro* models of healthy and diseased tissues. *In vitro* models can be utilized for the further understanding of biological pathways and disease mechanisms, as well as to evaluate new therapies and pharmaceuticals (45).

There are three main components of the tissue engineering; (i) physically and biochemically adequate scaffold, (ii) appropriate cell source to adhere and fill the scaffold, and (iii) bioactive agents to support the survival, proliferation and/or differentiation of the cells to enhance healing process (46, 47) (Figure 6).

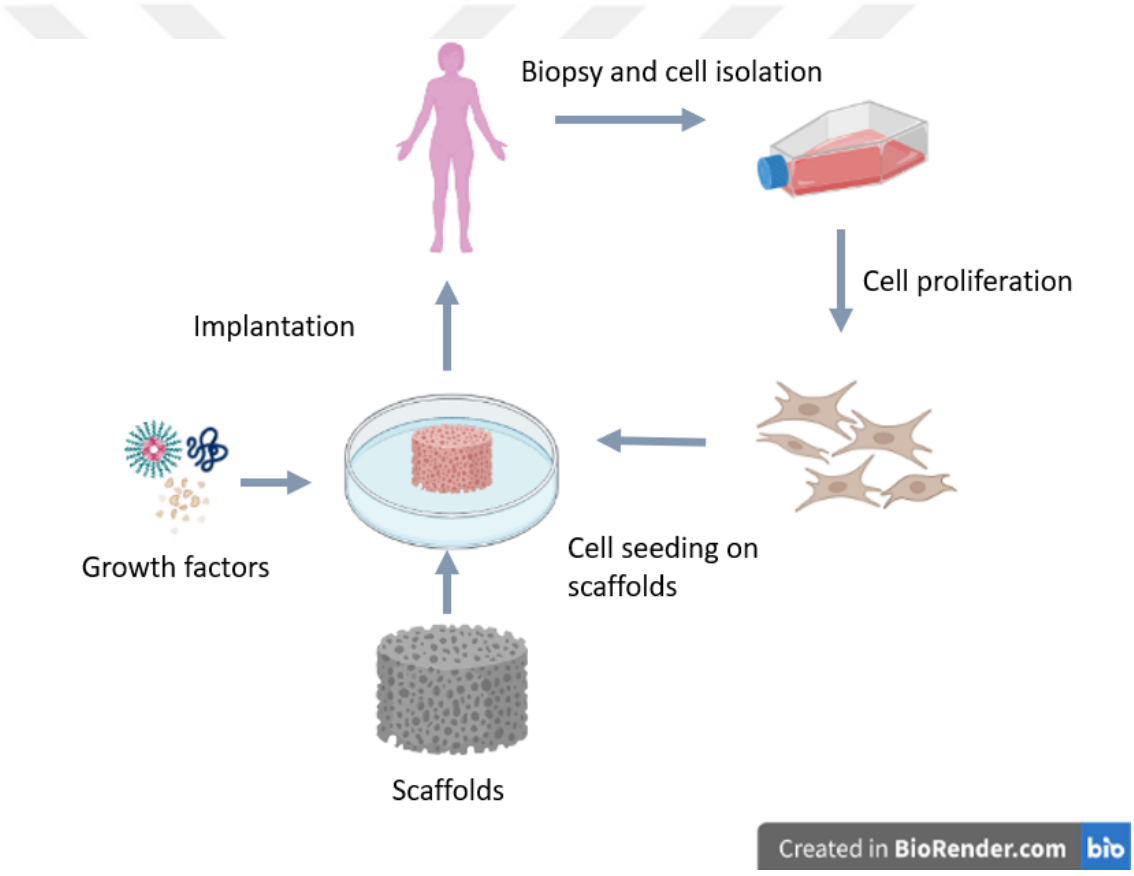

Figure 6. Schematic presentation of tissue engineering process. Created with BioRender.com

In tissue engineering the scaffolds should mimic the properties of native ECM as closely as possible to meet the requirements for neogenesis. Scaffolds should provide a porous, 3D environment and should imitate the 3D geometry and biochemistry of the native ECM for cells to adhere, proliferate, and/or differentiate

into the target tissue (48). Scaffolds should provide appropriate mechanical and chemical properties, and they serve as temporary templates guiding the cells during the regeneration of the target tissue. Therefore, they should be composed of biodegradable biomaterials and the rate of degradation should be compatible with the rate of new tissue formation. In addition, pore size and interconnectivity within the pores are important factors for cells to connect with each other and proliferate. The different pore sizes of scaffolds can induce different pathways. For example, in bone tissue engineering the scaffolds with a pore size of 100-400 μm induce osteoconduction, while larger pore sizes (>300 μm) induce bone formation by vascularization; therefore, scaffold properties should be adjusted according to the purpose of the study. Another critical factor is that the mechanical properties of the scaffolds should meet that of the the native tissue. It is intended to obtain scaffolds with high compression modulus for bone tissue engineering, while for vascular tissue engineering scaffolds with high elastic properties are aimed (49, 50).

The top-down tissue engineering approaches rely on seeding and extending the cells on 2D or 3D scaffolds to form tissue substitutes (42). The selection of the cell source and its ability to proliferate and differentiate into the targeted tissue is an important issue. The cells isolated from the patient's healthy tissue (i.e., autologous cells) can be considered the first choice, but the donor site morbidity and the shortage of cell numbers can be limitations. Isolated autologous cells can be expanded under tissue culture conditions but this may take a little long time such as weeks. Another option is to isolate cells from donors of the same species (i.e., allogeneic cells) or different species (i.e., xenogenic cells). However, viral transmission and immune response are the serious drawbacks that should be considered (47, 51). As a result of the mentioned issues, stem cells have found a significant role in the tissue engineering field due to their ability to differentiate into various cell types and their high proliferation capacity (52).

2.5 Osteochondral Tissue Engineering

Osteochondral tissue is mainly composed of three layers such as articular cartilage, bone-cartilage interface and subchondral bone. The main purpose of the OC tissue engineering is to develop an implant that will integrate with the native tissue while having adequate mechanical and biochemical properties to support tissue regeneration at each layer of the OC unit. Apart from the bone and cartilage layers it is very crucial to understand the structure and function of the bone-cartilage interface and introduce it to the design of OC tissue substitute (53). The main purpose of tissue engineering studies is to mimic biological and mechanical properties of the native tissue, and thus to ensure its function. Since there is a comprehensive relation between tissue structure and its function, it is a challenge to develop an biomimetic tissue substitutes in tissue enginnering, especially for load bearing tissues.

2.5.1 Scaffolds for osteochondral tissue engineering

Osteochondral tissue engineering remains a challenge due to the spatial complexity of the OC tissue, low self-healing and regeneration ability of the articular cartilage, and the chondrocyte's tendency to dedifferentiate in 2D environments. Therefore, osteochondral scaffold to be constructed should provide the certain following features to overcome these issues (54) ;

1) From compositional point; scaffold should be biocompatible and biodegradable. Degradation rate of the scaffold should match to the rate of new tissue formation.

2) From structural point; while having a stratified orientation it should provide an appropriate pore size and porosity to enable cell attachment and growth at each layer, and to ensure cell-to-cell interactions. In addition, scaffold should be able to remain the phenotype and morphology of the bone and cartilage cells.

3) From functional point; scaffold should ensure the mechanical properties of the native tissue such as compression strength to withstand the cyclic loading from the joint movement and a frictionless surface to maintain smooth joint movement.

There are four main types of scaffold design for OCTE; monolayered, gradient, bilayered, and multilayered scaffolds as seen in Figure 6 (6) .

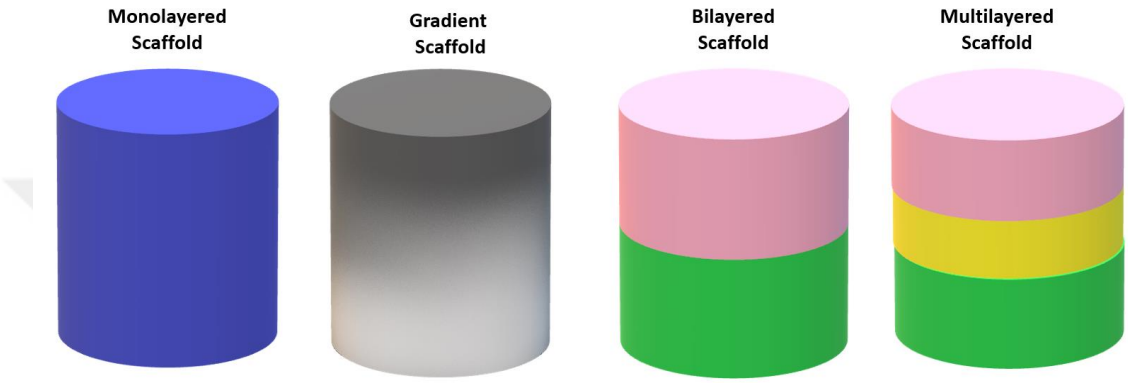

Figure 7. Different types of scaffolds for osteochondral tissue engineering

Monolayered scaffolds were the first scaffolds used for OCTE. These biomaterials can be composed of one single component or a composite, creating a homogenous structure (54). There are no biological or physical spatial variations within the scaffold. Scaffold should have a uniform architecture and porosity all along. There are *in vivo* studies using monolayered scaffolds, indicating cell recruitment when implanted on OC models. For instance, in one of the study it was reported that bone morphogenetic protein-2 (BMP-2) loaded PCL scaffold was used for the OCD model (55). Even though chondrocyte seeded scaffolds produced cartilaginous tissue, *in vivo* testing of the scaffolds showed higher expression of hypertrophic chondrocytes. It was revealed that this indicated the endochondral ossification of the seeded chondrocytes. Monolayer scaffolds with a homogenous structure do not address zonal differences of the native AC tissue. Therefore, there are limitations in promoting site-specific tissue regeneration and matrix deposition. It has been reported in the monolayered scaffold studies that the regenerated tissues were deficient and homogenous, unlike the native tissue (6).

Gradient scaffolds can be categorized as monolayer scaffolds due to the use of a single material or single composite in the design, but they provide the gradient change within the scaffold (56). Similar to gradual changes in the properties of the native tissue, these scaffolds may provide site-specific regeneration. Gradient features of the scaffold can be prepared by many properties like mechanical stimuli, chemical stimuli, structural properties (i.e., pore size, porosity), loaded cells (i.e., chondrocytes, osteoblasts), and/or loaded molecules (i.e., HAp, BMP).

Bilayered and multilayered scaffolds can be categorized as hierarchical scaffolds due to providing a tissue-specific microenvironment with varied mechanical, biological, and chemical properties within the scaffold. Hierarchical scaffolds can be constituted of different components and dissimilar architectures (57). Bilayered and multilayered scaffold studies were listed in Table 2.

Bilayered scaffolds aim for simultaneous regeneration of cartilage and bone tissue layers which have significant differences in their mechanical and biological features (58). Each layer can be optimized for tissue-specific regeneration respective to the native tissue. The bilayered scaffold can be based on chemical and/or physical factors such as using two different materials for different layers and/or using a single material for both layers which have a significantly different porosity or architecture. Also, the bilayered function can be based on the biological factors by using different cell types at different layers or providing different biological microenvironments for cells at each layer. One of the limitations of bilayered scaffolds is the lack of optimized combining methods of two layers (57). Even though fibrin sealant and press-fitting are commonly used methods, there is a risk of delamination and phase separation due to the lack of a transitional zone between layers. In one of the studies, a bilayered osteochondral tissue substitute was developed and implanted at the OCD in a rabbit model (59). The cartilage part of this scaffold was composed of fibrillar collagen or hyaluronic acid-chitosan composite, while the bone part was composed of polylactic acid (PLA) and hyaluronic acid. Even though hyaline cartilage formation was observed at the cartilage layer, an abnormal dissociation of collagen type-II and GAG expression was seen indicating the improper hyaline-cartilage regeneration. The results showed

the inadequacy of the bilayered scaffold to produce a functional bone-cartilage interface that exists in native tissue (6).

As a consequence, OC TE studies have shifted towards the design of three-layer or multilayered scaffolds in order to better mimic the osteochondral tissue (60). The structural and biomechanical integrity of the multilayered OC TE scaffolds could be ensured with the linkage between cartilage and bone layers (57). A functional interface is vital for the integration of the layers within the scaffold and with the native tissue. Multilayered scaffolds aim to mimic and regenerate cartilage, calcified cartilage (interface), and bone parts simultaneously. This transitional interface zone maintains the load distribution through cartilage and bone parts, and also improves structural integrity. Multilayered features can be based on physical and biological factors like in the bilayered scaffolds. The transitional zone between layers can facilitate site-specific tissue regeneration by allowing the seeding of distinct cell types to the appropriate part of the multilayered scaffold (61, 62). In one of the study, a tri-layered scaffold was constructed using collagen type I, collagen type II, and hyaluronic acid for the cartilage part; collagen type I, collagen type II, and HAp for the calcified cartilage part; and collagen type I and HAp for the bone part (63). *In vivo* studies were held with a caprine model, and histological and macroscopic results of 6-12 post-implantation studies showed the success of tissue-specific regeneration due to the presence of the scaffold.

Table 2. Bilayered and multilayered osteochondral tissue engineering studies.

	Cartilage Part	Interface	Subchondral Part	Cells	Study/ Outcome	Ref
Bilayered Scaffolds	Collagen	-	Collagen and HAp	hBMSC	*In vitro* study, chondrogenic and osteogenic differentiation at appropriate layers	(64)
	Gelatin, CS, SH	-	Gelatin and ceramic bovine bone	Chondrocytes and hBMSCs	*In vivo* study (rabbit), bone formation and hyaline like cartilage at 36 weeks post implantation	(65)
	PGA	-	PLGA, PEG	Chondrocytes and osteoblasts	*In vitro* study, GAG synthesis on cartilage side and mineralization at bone side was observed after 2 weeks of culture.	(66)
Multilayered Scaffolds	PCL, decellularized ECM	PCL	PCL, TCP	hASC	*In vitro* study, Site specific osteochondral tissue properties were seen at week 4.	(67)
	Col-I, Col-II, HA	Col-I, Col-II, HAp	Col-I, HAp	-	*In vivo* study (rabbit), cartilage and subchondral bone repair in 12 weeks	(68)
	PCL	Col-I, HAp	TCP	BMSC	*In vivo* study (rabbit), cartilage formation was seen	(69)

*CS: chondroitin sulfate, SH: sodium hyaluronant. PGA: polygolic acid, PCL: poly-ε-caprolactone, ECM: extracellular matrix, Col-I: collagen type-I, co-glycolic acid, PEG: polyethylene glycol Col-2: Collagen type-II, HA: hyaluronic acid, HAp: hydroxyapatite, PLGA: poly-lactic, TCP: tricalcium phosphate, BMSC: bone mesenchymak stem cells, hASC: human adipose derived stem cells

2.5.1.1 Scaffold materials

There are different kinds of biomaterials used for OC TE such as natural and synthetic polymers, ceramics and composites. Advantages and disadvantages of these biomaterials were shown in Table 3 (54, 70, 71). Due to the heterogeneous structure of the OC tissue composites of polymers and bi-ceramics have been widely used for OC TE applications.

Table 3. Examples of biomaterials used for OC TE with their advantages and disadvantages

	Materials	Advantages	Disadvantages
Natural Polymers	• Collagen • HA • CS • Silk fibroin	- high biocompatibility - high biodegradability - increased cell attachment due to natural molecular domains	- risk of transmission of disease and hazardous agent - purification problems - variation between batches - weak mechanical properties
Synthetic Polymers	• PLA • PLGA • PCL	- ease of processing - wide range of mechanical properties - biodegradability - no risk of disease transmission - no limitation in supply	- cytotoxic degradation product - eliciting inflammatory response
Ceramics	• TCP • HAp	- biocompatibility - osteoinductive and osteoconductive properties - promoting bone-like apatite when implanted	- poor mechanical stability
Composites	• Polymer-Polymer • Polymer-Bioceramics	- adjustable properties according to need - novel properties	- disadvantage of the used material

*HA: hyaluronic acid; CS: chondroitin sulfate; PLA: poly (l-lactic acid); PLGA: poly(lactide-co-glycolide); PCL: poly(ε-caprolactone); TCP: tricalcium phosphate; HAp: hydroxyapatite.

Natural polymers such as collagen, hyaluronic acid (HA), gelatin and chondroitin sulfate (CS) are mostly used in OC TE applications as they exist in the natural ECM of the cartilage (72). They have high biocompatibility and biodegradability, and they provide a chemical composition resemblance with native ECM. Due to their high biodegradability and weak mechanical properties, they are mostly used as a combination with synthetic polymers and ceramics (68, 73, 74).

A wide range of synthetic polymers are used for the OC TE approaches such as poly(caprolactone) (PCL), poly (L-lactide acid) (PLA), poly(glycolic acid) (PGA).

Synthetic polymers can be tailored according to the specific applications; for instance, adjusting their chemistry or molecular weight to control the mechanical properties and degradation rate. However, they have low biocompatibility and are mostly hydrophobic, and thus the cell attachment on these polymers is less due to lack of specific binding motifs. To overcome these issues hydrophobic and hydrophilic polymer composites can be used as a scaffold material. For example, in a study, a hydrophilic polymer polyvinyl alcohol (PVA) was blended with hydrophobic polymer PCL to produce nanofibrous scaffold (75). It was revealed that PVA-PCL blend increased hydrophilicity of the scaffolds and enhanced cell proliferation on them, and improve chondrogenic differentiation of MSCs on these scaffolds compared to only PCL scaffolds.

Calcium phosphate-based ceramics such as hydroxyapatite and β-TCP are widely used at the subchondral part of the osteochondral construct due to their osteoconductive and osteoinductive properties. It was shown that these ceramics integration into the subchondral part of the construct promoted mineralization and bone regeneration when osteochondral construct was implanted (76).

2.5.1.2 Scaffold fabrication techniques

The scaffold used in tissue engineering aims to provide appropriate surfaces in 2D or 3D for cells to adhere and proliferate, and also to implement adequate mechanical properties and transport of nutrients as well as allowing coordination of multicellular process (77). Scaffold fabrication is one of the important issues to obtain a successful tissue substitute in tissue engineering. Scaffold material, the architecture of the scaffold design, and also its application strategy should be taken into consideration while selecting the scaffold fabrication technique. There are wide variety of fabrication techniques such as particulate leaching, freeze-drying, electrospinning and 3D printing.

2.5.1.2.1 Conventional scaffold fabrication techniques

Particulate leaching is a basic and cost-efficient technique to fabricate porous polymeric scaffolds. Polymer solution is mixed with an easy- dissoluble particulate such as salt or sugar particles. After the solvent of the polymer solution evaporates, the particulates within the solid construct are leached out with solvent of the particulate. Pore size and porosity of the scaffold can be adjusted by particulate size and amount (78). Freeze-drying also known as lyophilization is a technique based on the phase separation between the solvent and the polymer. Polymer solvent is sublimated using low temperature under vacuum conditions, and a porous scaffold is obtained. A scaffold having up to 90% porosity with interconnected pores can be produced via this method. Pore size and porosity can be controlled with polymer concentration, solvent type and freezing temperature (79).

2.5.1.2.2 Electrospinning

Electrospinning is another widely used method in tissue engineering studies. Electrospinning method basically consists of a syringe containing polymer solution which is pushed with syringe pump at a certain flow rate, power supply and metal collector on which ejected fibers are deposited. The increased voltage between the needle of syringe and the metal collector creates repulsive and attractive forces between two poles. When the repulsive force overcomes the surface tension of the polymer injected, polymer droplet at the tip of the needle in the form of Taylor cone is ejected. During ejection of polymer solution towards the collector, the solvent evaporates and thin, dry polymeric fibers are collected on the metal collector, and thus fibrous mat is deposited on the collector (80) .

2.5.1.2.3 3D printing via additive manufacturing

Control of the scaffold's internal structure is difficult even almost impossible with conventional scaffold fabrication methods. There are limitations such as

uncontrolled/random porosity, irreproducibility and insufficient mechanical properties in the scaffolds produced by conventional techniques such as freeze drying and solvent casting. 3D printing via additive manufacturing is rapidly emerging technique also in the field of tissue engineering, since it enables the production of complex and multilayered scaffolds with high precision and reproducibility (81, 82). The combined use of computer-aided design (CAD) programs and 3D printing technologies makes it possible to print high-precision, efficient and customizable scaffolds with a complex microarchitecture. Most common 3D printing methods are fused deposition modelling (FDM), stereolithography (SLA), selective laser sintering (SLS) and inkjet printing (83). Main advantage of the 3D printing technique is to have precise control over the scaffold's micro and macro architecture. 3D printing can fabricate scaffolds with adjustable pore size and controllable porosity including interconnected pores as intended. In addition, 3D printing methods are widely used for the fabrication of patient specific implants. For patient specific treatments, firstly the defect size information obtained from magnetic resonance imaging (MRI) or computed tomography (CT) is converted to 3D scaffold design (84). Then, the predetermined size of scaffold is 3D printed so that the implant is personalized to the patient's use.

FDM is a widely used method due to its simplicity and high mechanical strength of the thermoplastics that can be used with this method (85). FDM method consists of a vertically moving extrusion nozzle and a horizontally moving build plate. A melted thermoplastic polymer gets extruded out of extrusion tip with the help of screws or pressure. With the FDM method 3-D printer prints out the 3D model obtained by CAD. Before printing, a software is used to slice the 3D model. Once printing parameters such as printing temperature, pressure, speed and layer height are entered, software converts the 3D model into a digital file, which is a set of instructions. This conversion is called "slicing". Extruder head moves according to this instruction moving with the speed in the instructions and creates the model in a layer-by-layer fashion. After each layer is created building plate descends along z-coordinate according to programmed layer height and starts the next layer and a 3D model is fabricated with the fusion of these layers.

2.5.2 Cell sources used in osteochondral tissue engineering

Using cells with scaffolds influences the interaction of the tissue engineered substitute with the surrounding tissue, and it is universally accepted that cells improve the synthesis of tissue-specific ECM, and enhance tissue regeneration and healing process at the implantation site (54). There are several cell types used in tissue engineering field such as mature somatic cells, embryonic stem cells and mesenchymal stem cells. Mostly used cell types for the osteochondral tissue engineering are autologous mature chondrocytes and mesenchymal stem cells (86).

Autologous mature chondrocytes can be considered most direct cells for the treatment of OCDs. The use of autologous chondrocytes for OCDs is a very common approach because chondrocytes are the only cells that have the perfect capacity to regenerate native articular cartilage (76). However, there are serious drawbacks such as (i) additional injury to the articular cartilage while harvesting mature chondrocytes, (ii) limited supply of cells due to less amount of donor tissue and inefficient isolation, (iii) need for multiple surgeries (46). Moreover isolated autologous cells are proliferated in *in vitro* culture before implantation, and the common risk of chondrocytes to dedifferentiate in monolayer cultures precludes the success of tissue engineered substitute (86).

The use of stem cells would overcome these issues. One of the stem cell types used in tissue engineering is embryonic stem cell (ESC). ESCs has unlimited self-renewal capacity and ability to differentiate any desired cell or tissue. But there are drawbacks such as controlling the specific lineage differentiation *in vivo*, risk of teratoma formation in undifferentiated state and ethical issues to use ESC lineages (46). Induced pluripotent stem cells (IPSCs) were used to remove ethical problems since they are formed from somatic cells. IPSCs behave like ESCs in terms of high self-renewal capacity and high differentiation potential. However, they have also risk of teratoma formation in undifferentiated state, therefore their implantation potential is limited like ESCs. But, IPSCs are promising cell source to develop *in vitro* disease

models to be used in patient specific drug screening or analyzing disease mechanism (54).

Considering all tissue layers of the OC complex are originated from mesenchyme, mesenchymal stem cells are the preferred cell source for that tissue substitute. Indeed, with their tendency to differentiate into both cartilage and bone cells MSCs become very prevalent in the osteochondral tissue engineering by overcoming the challenges that can be faced with mature chondrocytes and other stem cells. Using a single autologous cell source like MSC that can differentiate into both osteogenic and chondrogenic cells may provide all cellular components of OC tissue as well as eliminates the risk of immune response (87, 88).

2.5.2.1 Mesenchymal stem cells

Mesenchymal Stem Cells (MSCs) are non-hematopoietic stromal cells with a potential of multi-lineage differentiation. They are the reservoir of reparative cells in the body, they can migrate to injury site and differentiate into adult stage functional cells and/or release some bioactive agents such as growth factors to repair injured tissue (89). They were first isolated from bone marrow by the Friedenstein (90) and bone marrow was then considered the main source for MSCs. However, they have been isolated from various tissues such as adipose tissue (91), dental pulp (92), amnion fluid (93) and umbilical cord (94). MSCs are naturally able to differentiate into connective tissue lineages like bone, cartilage and adipose tissue (Figure 8) (95). Afterwards, it has been shown that they can differentiate into other cell types such as vascular cells (96) and neural cells (97) in the presence of appropriate signals. MSCs isolated from different sources may have different characteristics and differentiation potentials towards different cell types. This should be considered during the selection of an appropriate MSCs for the targeted tissue (95). Dental tissues including dental pulp are rich in stem cells and can be obtained during standard dental operations. Since they are discarded as surgical waste, tissue harvesting from these tissues is non-invasive and do not raise ethical concerns (98). Dental pulp stem cells can be isolated from dental pulp tissue and they have mesenchymal characteristics as they can

differentiate into various cell types including osteoblasts, adipocytes, chondrocyte-like cells and neural cells (99).

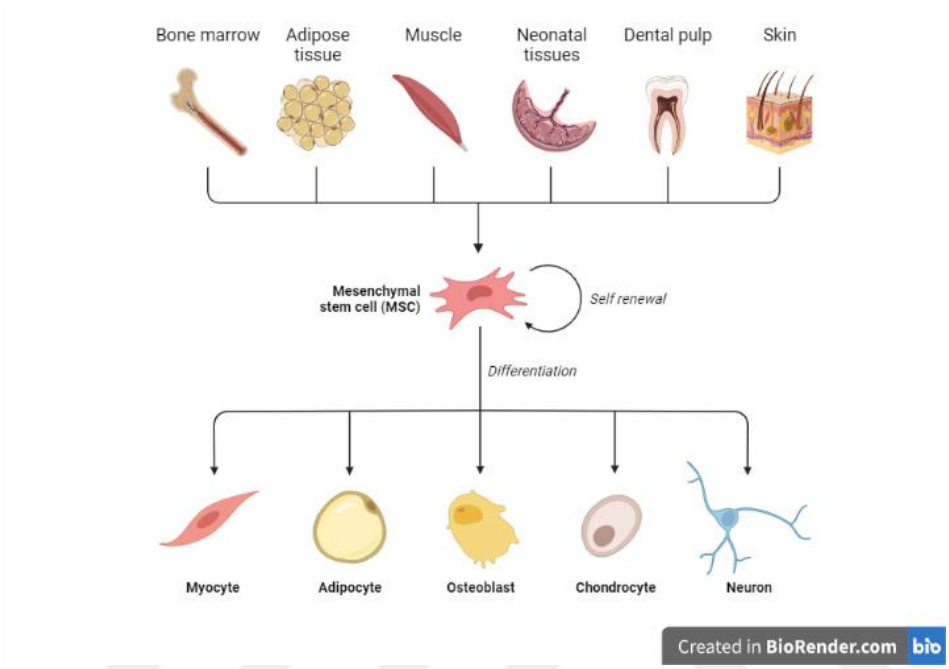

Figure 8. Source and differentiation potential of MSCs. Created with BioRender.com

3 MATERIALS AND METHODS

3.1 Materials

Polycaprolactone (PCL) (MW 50000 g/mol) was purchased from Polysciences, Inc. Chloroform, beta-tricalcium phosphate (β-TCP), FITC-phalloidin, DAPI, WST-1 kit, dexamethasone, silver nitrate, sodium thiosulfate, alcian blue, insulin transferrin selenite, sodium pyruvate, proline and alizarin red were purchased from Sigma. DMF was purchased from Merck. Alpha-MEM, DMEM Low Glucose medium, DMEM High Glucose medium, Fetal Bovine Serum (FBS), Penicillin/Streptomycin (pen/strep) and Try-EDTA were purchased from Gibco. All antibodies and isotypes for flow cytometry were obtained from BD Biosciences. β -glycerophosphate was purchased from AppliChem. ALP kit was obtained from Randox. Live/Dead assay was purchased from Thermo Scientific. Aggrecan and Collagen type-II antibodies were purchased from Abcam and Invitrogen, respectively, while secondary antibodies conjugated with Alexa Fluor 488 and Alexa Fluor 555 were purchased from Thermo Fisher.

3.2 Methods

3.2.1 Construction of the multilayered osteochondral scaffold

3.2.1.1 Designing the 3D printed part of the multilayered scaffold

Osteochondral tissue is a unique composite tissue that can transfer the load during joint movement. The composition and organization of cells and extracellular matrix molecules in each region are different and it affects the mechanical properties and functions of these regions (100). Collagen fibril structures in each layer of AC are arranged to distribute the load equally (101). The osteochondral tissue substitute implanted in the joint would be introduced to a dynamic biomechanical environment with a constant change in forces such as stress, strain and fluid pressure. To achieve a cartilage-bone defect repair using a multilayer scaffold, it is important that each layer

of the scaffold has mechanical properties that match the surrounding tissue and have mechanical properties to withstand the cyclic physiological load of the joint (3)

Osteochondral tissue is composed of three main tissues, starting from synovial surface, articular cartilage, calcified cartilage and bone (53). Hereinafter, articular cartilage part of the construct would be referred as cartilage part. 3D scaffold model was designed to have three parts which mimic bone, calcified cartilage and cartilage layers of the native tissue, and each layer has a different architecture. Computer programs, SketchUp (Trimple Inc, USA) and Blender (Blender Foundation, Netherlands), were used to design the 3D model of the scaffold.

The architecture of the multilayers in scaffold was designed considering the pore size and filament radius for the bone and cartilage layers to enable the cells to adhere and proliferate in those regions. In this study, the bone part of the scaffold was designed to have a pore size of 400-500 µm and appropriate mechanical properties to withstand the load applied to the area. In the scaffold design, each layer was composed of parallel filaments with a certain distance between them, and layers were added on top of each other with a 90° angle between subsequent layers (Figure 9). The bone part of the scaffold was composed of two repeats of four layers. In order to increase cell adhesion, a 150 µm shift of struts was applied to the layers facing the same direction within repetitive four layers.

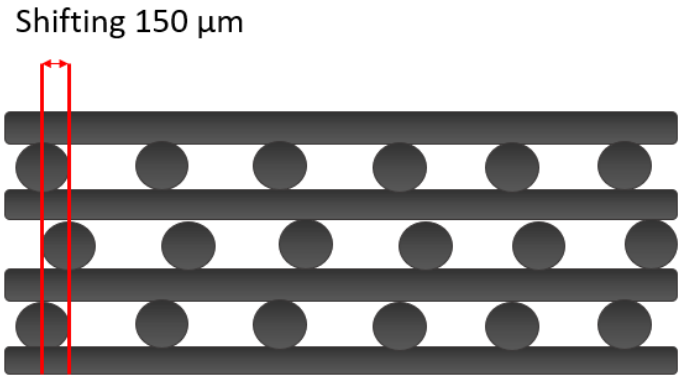

Figure 9. Schematic presentation of the bone part of the 3D printed multilayer scaffold design showing the organization of the filaments in a cross-sectional view of the scaffold.

In the natural OC tissue calcified cartilage layer prevents vascularization and migration of bone cells to cartilage side and enhances mechanical integrity (102). The non-porous design of this layer was made to fulfil the role of natural calcified cartilage tissue. Calcified cartilage part was designed as a single layer of parallel filaments with 200 μm diameter with no space between them (Figure 11). It was aimed to obtain the non-porous layer with the fusion of filaments.

Figure 10. Schematic presentation of the calcified cartilage part design of the 3D printed multilayer scaffold showing the organization of the filaments in a cross-sectional view of the scaffold.

Cartilage part of the scaffold was designed in a similar fashion to the bone part. It was composed of eight layers including two repeats of four layers. Each layer was made-up of parallel filaments with a certain distance between them, adding layers on top of each other along the Z-axis by turning the following layer 90° (Figure 11). In the cartilage part design, the filament diameter was thinner and the distance between filaments were longer than the ones in the bone part, which would increase the pore size to allow hydrogel solution to enter between the pores. In addition, to mimic the perpendicular orientation of collagen fibers at the deep zone of the articular cartilage half of the layers in cartilage part were designed without shifting of filaments. However, in order to mimic the random orientation fibers at the middle zone in the other half of the layers it was designed to have 150 μm shifting of filaments within the layers facing the same direction.

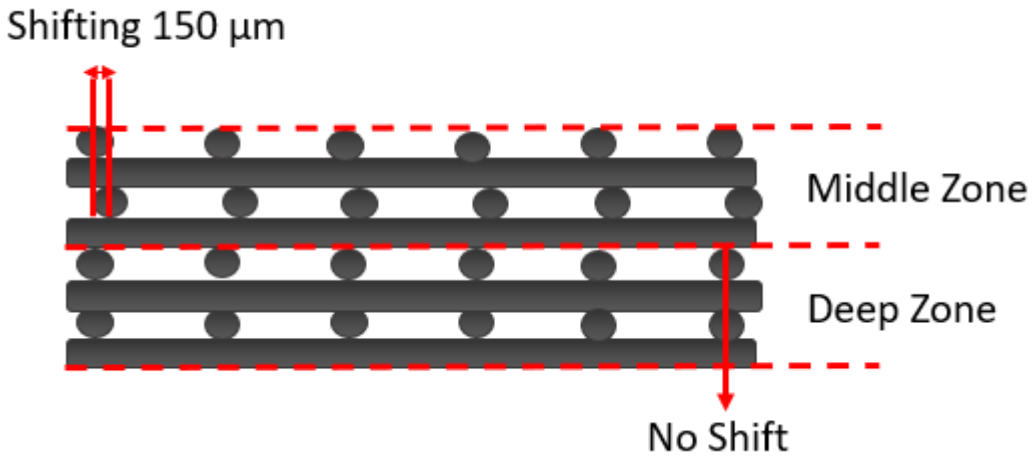

Figure 11. Schematic presentation of the cartilage part of the 3D printed multilayer scaffold design showing the organization of the filaments in a cross-sectional view of the scaffold.

3.2.1.2 3D printing of the multilayered scaffolds: optimization of parameters

3D scaffold was printed using fused deposition method (FDM) with an Allevi 2 3D Printer (3D Systems, USA). This pneumatic 3D printer, uses pressure to extrude the molten polymer through printing tip. In this study, 3D printing of PCL polymer was performed at 100°C and 100 psi as recommended by the firm Allevi (103).

Scaffolds were printed according to the architecture of the model using poly(ε-caprolactone) (PCL) by melting and extrusion of PCL. To obtain accurately the desired filament diameters and pore size, different designs with different filament dimensions were printed. In addition, the printing parameters such as layer height and printing speed were adjusted, and optimized for 3D printing process. Moreover, the effect of needle tip type on the geometry of 3D printed scaffolds was investigated. The optimization of 3D printing parameters was held separately for the bone and the cartilage parts (Table 4 and Table 5). After optimization of the design parameters for bone and cartilage part separately, the common printing parameters obtained for each were chosen. During optimization studies, 3D printed scaffolds were examined under stereomicroscope (Stemi 508, Zeiss, Germany).

Table 4. The optimization parameters of 3D printing for the bone part of the multilayer scaffold.

Scaffold / Parameter	A	B	C	D	E	F	G	H	I	J	K
Needle tip (Ga)	27						25				
Designed filament diameter (μm)	400										500
Designed distance between filaments (μm)	600			400			600				800
Layer Height (μm)	100	200		100	200						
Speed (mm/s)	2	2	1	2	2	1	2	3	4	6	4

Table 5. The optimization parameters of 3D printing for the cartilage part of the multilayer scaffold.

Scaffold / Parameter	A	B	C	D	E	F
Needle tip (Ga)	27			25		
Designed filament diameter (μm)	200		300		400	
Designed distance between filaments (μm)	800		900		1200	
Layer Height (μm)	200	100	200	100	200	
Speed (mm/s)	1	2	1	2	3	4

3.2.1.3 Fabrication of electrospun fibrous mats

Electrospun fibrous mat that was planned to be the outer layer of the cartilage part of the 3D printed scaffold mimicking the superficial layer of the articular cartilage was fabricated by electrospinning.

Electrospinning system was composed of syringe pump (New Era Pump Systems Inc., USA), 10 mL syringe with a 21 Ga needle with cut blunt tip, high voltage power supply (Gamma High Voltage, USA) and the metal collector (Figure 12). Polymer solution was prepared as 20% (w/v) PCL solution in chloroform: DFM (9:1) and was placed into a syringe placed on syringe pump. Electrospun fibrous mat was collected with a 14 cm needle-to-collector distance, 0.4 mL/h flow rate of the polymer from syringe tip and a 20 kV potential from the power supply. Random electrospun mats were obtained after 5 minutes of electrospinning process

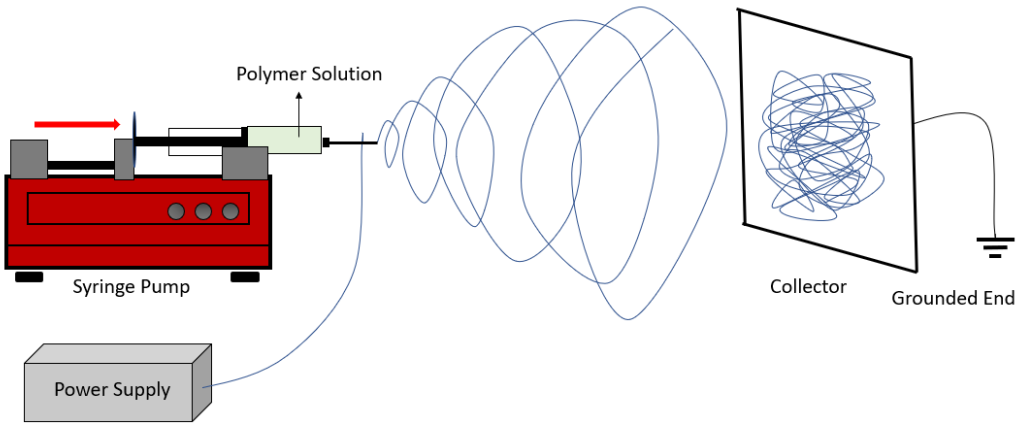

Figure 12. Schematic presentation of electrospinning set-up

3.2.1.4 Construction of the multilayered osteochondral scaffold

3D scaffolds composed of cartilage, calcified cartilage and bone parts were printed with Allevi 3D printer (Allevi 2, 3D Systems, USA) by fused deposition method using the optimized parameters in Section 3.2.1.2. PCL powder was loaded into the metal syringe head of the 3D printer and heated to 100°C. After PCL was

melted, a pressure of 100 psi was applied for printing. Multilayered scaffold was printed with a 4 mm/s printing speed, 0.2 mm layer height and using 25 Ga extruder tip. Consequently, the scaffolds containing cartilage, calcified cartilage and bone parts were produced as a whole by 3D printing without weak interphase.

The final multilayered scaffolds were obtained by integration of the electrospun fibrous mat with 3D printed scaffolds. For that purpose, firstly the electrospun fibrous mats were cut circular according to the diameter of the 3D printed scaffolds. Then, chloroform was sprayed on the cartilage part of the 3D printed scaffolds and the fibrous mats were fixed on the top surface of the cartilage part immediately after spraying. Fixation of these two parts was checked by trying to seperate the combined structure to see whether there was any detachment.

3.2.1.5 Coating of β-TCP onto the bone part of the multilayered scaffolds

The multilayered scaffolds were treated with oxygen plasma (power 50-watt, 5 min). After this treatment, the bone parts of the scaffolds were coated with β-tricalcium phosphate (β -TCP) solution in water (1%, w/v). Coating process was applied twice with 1 h wait after each coat. After the second coat and 1 h wait period, the scaffolds were immersed into 70% EtOH to speed up the drying of the scaffolds.

3.2.2 Characterization of the multilayered scaffold

3.2.2.1 Scanning electron microscopy

Morphology of the multilayered scaffolds was examined with Scanning Electron Microscopy (SEM) (EVO 10, Zeiss, Germany). For that purpose, the scaffolds at different stages of preparation were mounted on aluminum stubs, and coated with 50 nm thick gold under vacuum (Q150RS, Quorum, UK).

3.2.2.2 Mechanical analysis

Mechanical properties of the multilayered scaffolds were determined with Mechanical Testing Machine (Shimadzu AGS-X Series Universal Test Machine, Japan) by a compression test at 1 mm/s of testing speed, and the results were analyzed with Mechanical Testing Software (Trapezium, Shimadzu, Japan). Samples were dimensions of 10 mm diameter and 8 mm height. Data was acquired as load-displacement graph (N/mm), and coverted into stress-strain curve. The Young's Modulus (E) values of samples were calculated using the following equation, where (E) is the Young's Modulus, (σ) is the stress, (ε) is the strain, (F) is the applied force, (A) is the cross-sectional area of the sample on which stress was applied, ($\Delta\ell$) is displacement and (ℓ_0) is the initial length of the sample.

$$E\ (Young's\ Modulus) = \frac{\sigma\ (stress)}{\varepsilon\ (strain)}$$

$$\sigma(N/mm^2) = F\ (N)/\ A\ (mm^2)$$

$$\varepsilon = l/l_o$$

Test samples were labeled as;

- (Group 1) FullOC - the final multilayered scaffolds
- (Group 2) BONE - scaffolds composed of only the β-TCP coated 3D printed bone part.
- (Group 3) CARTILAGE - scaffolds composed of only 3D printed cartilage part and electrospun mat.

3.2.2.3 Investigation of impermeability of the calcified cartilage barrier

Calcified cartilage layer found between the bone part and the cartilage part of 3D printed multilayered scaffold was designed to prevent cell migration from bone side to cartilage side, and fabricated as a non-porous layer as explained in Section 3.2.1.1. Therefore, the impermeability of this layer was tested using a blue dye. A set of scaffolds were fabricated including bone, calcified cartilage and cartilage part, while the other set of scaffolds were fabricated without calcified cartilage. A blue dye was

placed on bone side of the scaffolds, and whether there was any passage of blue dye to the cartilage layer through time was followed. Then, the scaffolds were examined under stereomicroscope (Stemi 508, Zeiss, Germany). In addition, the blockage of cell passage through calcified cartilage was investigated with Phalloidin/DAPI staining after cell seeding only to the bone part. The detailed information about this method was given in Section 3.2.3.5.1.

3.2.3 *In vitro* studies

3.2.3.1 Isolation and characterization of human DP-MSCs

3.2.3.1.1 Isolation of DP-MSC

Human dental pulp-derived mesenchymal stem cells (DP-MSCs) used in this study were previously isolated by explant culture for a study of Dr. Deniz Yücel at Acıbadem Mehmet Ali Aydınlar University. The approval of the ethical committee for the use of these isolated DP-MSCs in this study was given in Appendix 8.1 (Acıbadem Mehmet Ali Aydınlar University, Istanbul, ATADEK-2022/02).

Briefly, dental pulp tissues were obtained from the deciduous teeth of 6-12 years old healthy children. The tissues were cut into small pieces, placed on cell culture plates, and then 1 mL of growth media containing Alpha MEM (αMEM) medium, 10% Fetal Bovine Serum (FBS) and penicillin/streptomycin (100 U/mL, 100 µg/mL) was added. Tissues were cultured in a CO_2 incubator (5% CO_2) at 37^o C. After 12 h incubation, another 1 mL of the growth media was added onto the tissues, and the culture continued by changing the growth media every 3 days. When cells reached 70-80% confluency, they were passaged (subcultured). For passage of cells, the cells were detached from flask surface via trypsinization using 0.05% Try-EDTA, centrifuged at 2200 rpm for 5 min and then transferred to large surfaces to continue culture. Cells were stored in liquid nitrogen after gradual freezing in growth media containing 10% DMSO to be used in the further experiments.

3.2.3.2 Characterization of human DP-MSCs

The Mesenchymal and Tissue Stem Cell Committee of the International Society for Cellular Therapy defines three minimal criteria to qualify a cell as human MSC (104). The first of three criteria is that when maintained in standard culture conditions MSC must be plastic-adherent; the second is that MSC must have expression of specific surface molecules as CD73, CD44, CD90 and CD105 and must be lack of CD34, CD 45 and HLA-DR expression; and the third is MSC must be able to differentiate into osteoblasts, chondroblasts and adipocytes.

In the light of this information, in order to prove that the isolated DP-MSCs in this study were MSCs the morphology of DP-MSCs was evaluated under standard culture conditions, expression of the indicated cell surface markers were analyzed with flow cytometry, and their differentiation capacity into osteoblast and chondroblast were investigated. In addition, the growth kinetics of DP-MSCs was determined.

3.2.3.2.1 Morphology of DP-MSCs

In order to investigate the morphology of human DP-MSCs, the cells were examined under light microscope; in addition, they were examined with confocal laser scanning microscopy (CLSM) after staining with FITC conjugated Phalloidin for the cytoskeletal organization and 4', 6-diamidino-2- phenylindole (DAPI) for the nucleus. DP-MSCs were seeded on 24 well plates and cultured within the growth medium for 5 days. Then, the cells were fixed with 4% PFA (in PBS) for 30 min at room temperature. After washing with PBS (10 mM, pH 7.4), they were incubated for 5 min in 0.1% (v/v) Triton X-100 for cell permeabilization, and then washed with PBS again. The cells were incubated in 1% (w/v) BSA solution for 30 min to prevent non-specific binding, and then they were incubated with FITC conjugated Phalloidin at for 1 h at 37°C to stain actin filaments of cells. After washing with PBS to remove excess dye, the cells were counter-stained with DAPI (1:5000 in PBS) for 10 min to stain the nucleus of the cells. After washing with PBS, the cells were examined with CLSM (LSM 900 Airyscan 2, Zeiss, Germany).

3.2.3.2.2 Flow cytometry analysis

Specific cell surface antigens' expressions of the isolated DP-MSCs at passage 3 (P3) were analyzed by flow cytometry. The cell surface antigens were CD105, CD73, CD44 and CD90 as MSC markers, hematopoietic lineage markers (CD34 and CD45) and immunogenic antigens (HLA-DR (MHC Class 1) and HLA-ABC (MHC Class 2)). After human DP-MSCs reached 70-80% confluency, the cells were detached from surface with trypsinization as explained in Section 3.2.3.1.1 and centrifuged at 2200 rpm for 5 min. After resuspension of the cell pellet in the growth medium, the cells were counted and transferred to tubes as to be $5x10^5$ cells/ tube. Then, cells were resuspended with 1% (w/v) BSA (in PBS) and centrifuged at 2200 rpm for 5 min at $+4^0$C. The cell pellets were resuspended, and the cells were incubated with fluorochrome-conjugated antibodies (FITC-CD105, PerCp-CD73, PE-CD44, PerCp-CD90, PE-CD34, FITC-CD45, PerCp-HLA-DR, PE-HLA-ABC) in a 1% (w/v) BSA solution for 1 h at +4ºC. Following incubation, the cells were washed twice with PBS, and fixed with 1% PFA for 10 min. Then, the cell surface markers were analyzed with flow cytometer (FACS Verse, BD Biosciences). Isotype controls were used to eliminate non-specific binding signal, and thus percentage of positive cells were determined.

3.2.3.2.3 Growth kinetics of human DP-MSCs

To investigate the growth behavior and to determine the doubling time of the isolated DP-MSCs a cell proliferation assay, WST-1, was done. DP-MSCs were seeded on 24 well plates at a density of 10^4 cells/well, and they were cultured in the growth medium at 37°C in CO_2 incubator. Samples were studied as triplicates (n=3). The cell number was determined by Cell Proliferation Reagent WST-1 at the end of 24, 48, 72, 96, 144, 192 and 240 h incubation.

WST-1 assay is based on the conversion of tetrazolium salt to formazan by the cellular activity (mitochondrial dehydrogenases) of the viable cells. Therefore, the formazan production is directly proportional with the number of the viable cells. The

formed formazan can be quantified with its absorbance at 440 nm. For this assay, at the end of the incubation periods the growth medium was removed, and 500µL of prepared WST-1 working solution (20:1, growth medium: WST-1) was added onto the cells. Then, the cells were incubated at 37°C in CO_2 incubator for 2 h. After 2h incubation, 200 µL of the colored product was transferred into a 96 well plate. Absorbance of the formed product was determined at 440 nm with Fluorescence Plate Reader (Victor Nivo, Perkin Elmer). The measured absorbance values were converted into the cell number by the use of a calibration curve (Appendix 8.2).

3.2.3.2.4 Osteogenic differentiation of human DP-MSCs

DP-MSCs at P3 were seeded onto 24 well plates at a density of $5x10^3$ cells/well. The cells were incubated in the growth medium for 24 h, and then the growth medium was changed with an osteogenic induction medium composed of Dulbecco's Modified Eagle Medium (DMEM) Low Glucose supplemented with 10% FBS, penicillin/streptomycin (100 U/mL, 100 µg/mL), 100 nM dexamethasone, 50 µg/mL ascorbic acid, 10 µM β-glycerophosphate to ensure osteogenic differentiation. The osteogenic induction medium was applied for 21 days by changing the medium every 3 days. Undifferentiated DP-MSC cultured in the growth medium in equal terms was used as a control group. After 21 days of osteogenic differentiation of DP-MSCs was assessed with alkaline phosphatase (ALP) assays and von Kossa staining.

Alkaline phosphatase (ALP), dephosphorylates compounds and is known to be produced by osteoblasts. It is involved in mineralization of bone. Therefore, it is widely used indicator for early bone formation (105). ALP assay is based on dephosphorylation of p-nitrophenyl phosphate to p-nitrophenol with the presence of ALP enzyme, shown with the reaction given in the following equation (Equation 1)

(Equation 1)

To evaluate the osteogenic differentiation with ALP activity, the cells on 24 well plates were lysed with 0.1% (v/v) Triton X-100 (in 0.1 M, pH 7.6 Tris Buffer), and then the cell lysates were transferred into 1.5 mL centrifuge tubes. The cell lysates were exposed to freeze/thaw cycle by keeping them at -20°C for 10 min followed by 37°C for 10 min, and this freeze/thaw process repeated three times. After cell lysates were sonicated (Sonoplus, Bendelin, Germany) for total of 10 min with 30 s breaks, they were centrifuged at 5000 rpm for 10 min at 4°C. 50 µL of supernatant and 50 µL of 0.1% (v/v) Triton X-100 were added into 96 well plates, and as a blank 100 µL of 0.1% (v/v) Triton X-100 was used. ALP substrate, p-nitrophenyl phosphate (20 µL) was added onto all samples. Absorbance of the product (p-nitrophenol) was measured at 405 nm for 16 min in every 2 min. ALP activity of the samples was expressed as µM of substrate converted to product per min, considering the calibration curve for the enzymatic product (Appendix 8.3 Figure A3). Specific ALP activity of the samples was determined by dividing the ALP activity to total protein amount. BCA assay was used to determine the total protein amount in the cell lysate (Appendix 8.3 Figure A4).

Von Kossa staining was performed to show accumulation of calcium-phosphate mineralization by osteoblasts. On 21st day of culture, the cells were washed with PBS, and fixed with 4% PFA solution for 30 min. After washing with PBS, the cells were exposed to ultraviolet light (UV) within 1% (w/v) aqueous silver nitrate solution for 1 h, and they were incubated in 5% (w/v) sodium thiosulfate for 5 min. After washing the cells with distilled water, the samples were examined under light microscope (Primovert, Axiocam ERC55, Zeiss, Germany).

3.2.3.2.5 Chondrogenic differentiation of human DP-MSCs

DP-MSCs at P3 were seeded into 24 well plates at a density of 5x10^3 cells/well. The cells were cultured in a chondrogenic induction medium composed of DMEM Low Glucose supplemented with 10% FBS, penicillin/streptomycin (100 U/mL, 100 µg/mL), 1% (w/v) Insulin-Transferrin-Selenium (ITS), 100 nM dexamethasone, 1 µM ascorbate-2-phospate, 1% (w/v) sodium pyruvate and 40 µM proline. Undifferentiated DP-MSCs cultured in the growth medium was used as a control group. After cells were

cultured for 21 days in a CO_2 incubator at 37°C, they were washed with PBS and fixed with 4% PFA for 30 min.

Chondrogenic differentiation of the cells was assessed with Alcian Blue staining at an acidic pH. Alcian blue was used as an indicator of the presence of glucosaminoglycans and proteoglycans like aggrecan which is typically found in ECM of articular cartilage tissue. Cartilage tissue components such as carboxylate and sulfate groups of hyaluronic acid, heparan sulfate, dermatan sulfate, and chondroitin sulfate get ionized at a pH of 2.5 and form a negative charge (106). Therefore, proteoglycans and hyaluronic acid components in cartilage tissue were specifically stained with Alcian Blue at a pH of 2.4-2.5 and appears as blue color after staining. After fixation, the cells were stained with 1% (w/v) Alcian Blue solution (in 3% acetic acid, pH 2.4) for 30 min. After washing with distilled water, the samples were examined under light microscope (Primovert, Axiocam ERC55, Zeiss, Germany).

3.2.3.3 Spheroid culture and chondrogenic differentiation

3.2.3.3.1 Formation of spheroid culture and chondrogenic induction

DP-MSCs at P3 were seeded into 24 well plates at a density of $5x10^3$ cells/well. The cells were cultured in a chondrogenic induction medium composed of DMEM Low Glucose supplemented with 10% FBS, penicillin/streptomycin (100 U/mL, 100 µg/mL), 1% (w/v) Insulin-Transferrin-Selenium (ITS), 100 nM dexamethasone, 1 µM ascorbate-2-phospate, 1% (w/v) sodium pyruvate and 40 µM proline. Undifferentiated DP-MSCs cultured in the growth medium was used as a control group. After cells were cultured for 21 days in a CO_2 incubator at 37°C, they were washed with PBS and fixed with 4% PFA for 30 min.

Chondrogenic differentiation of the cells was assessed with Alcian Blue staining at an acidic pH. Alcian blue was used as an indicator of the presence of glucosaminoglycans and proteoglycans like aggrecan which is typically found in ECM of articular cartilage tissue. Cartilage tissue components such as carboxylate and sulfate groups of hyaluronic acid, heparan sulfate, dermatan sulfate, and chondroitin

sulfate get ionized at a pH of 2.5 and form a negative charge (106). Therefore, proteoglycans and hyaluronic acid components in cartilage tissue were specifically stained with Alcian Blue at a pH of 2.4-2.5 and appears as blue color after staining. After fixation, the cells were stained with 1% (w/v) Alcian Blue solution (in 3% acetic acid, pH 2.4) for 30 min. After washing with distilled water, the samples were examined under light microscope (Primovert, Axiocam ERC55, Zeiss, Germany).

Table 6. Composition of chondrogenic induction media used in spheroid culture for chondrogenic differentiation

	Induction Medium 1 (109)	**Induction Medium 2**	**Induction Medium 3**	**Control Medium**
Basal Media	DMEM High Glucose	DMEM Low Glucose	DMEM High Glucose	Alpha MEM
FBS (%)	-	10	-	10
Pen/Strep (U/mL, µg/mL)	(100, 100)	(100, 100)	(100, 100)	(100, 100)
ITS (%)	1	1	10	-
Dexamethasone (nM)	100	100	100	-
Proline (µg/mL)	-	40	-	-
Ascorbic acid (µM)	200	1	1	
Sodium pyruvate (%)	-	1	1	
TGFβ1* (ng/mL)	10	-	10	-

*TGFβ1: Transforming growth factor beta-1

3.2.3.3.2 Evaluation of chondrogenic differentiation by Alcian Blue staining

Chondrogenic differentiation of cells in spheroid culture was assessed by Alcian Blue staining at an acidic pH to evaluate the synthesis of cartilage ECM with the presence of glucosaminoglycans and proteoglycans. After 21 days of culture, the spheroids were washed with PBS and fixed with 4% PFA for 1 h. The spheroids were embedded in OCT (Optimal Cutting Temperature, TissueTek), and then the samples were sliced into 5-6 µm thick sections by cryomicrotome (CM1520, Leica, Germany). The slices were placed onto positively charged slides, and after air drying the slides were kept at -20°C. The cryosections were brought to room temperature and stained with 1% (w/v) Alcian Blue solution (in 3% acetic acid, pH 2.4) for 1 h. After washing with distilled water, the spheroid sections were examined under light microscope (Primovert, Axiocam ERC55, Zeiss, Germany). The appropriate chondrogenic

induction medium for further studies was selected according to the Alcian Blue staining results.

3.2.3.3.3 Evaluation of chondrogenic differentiation by immunostaining

Collagen type II and aggrecan are typically found in articular cartilage tissue; therefore, expression of these markers at protein level was studied by immunostaining. At day 21 of spheroid culture, the spheroids were treated with 0.25% Try-EDTA for 5 min, and then the cells were dissociated by pipetting to obtain a homogenous cell suspension. In order to dilute and reduce Try-EDTA activity, the medium was added and the cells were centrifuged at 1400 rpm for 5 min. The cell pellet was resuspended in the induction medium, and the cells were seeded on cover glass and cultured with chondrogenic induction medium. After 5 days of culture, the cells were fixed with 4% PFA for 1 h at room temperature. The samples were kept in 100 mM glycine solution (in PBS) for 15 min at room temperature to saturate reactive PFA groups. After washing with PBS, the cells were permeabilized by 0.1% (v/v) Triton X-100 for 5 min and washed with PBS. Then, the cells were incubated in 1% BSA solution (in PBS) for 30 min at 37° C to block non-specific binding of antibodies. The cells were incubated in solutions of primary antibodies, anti-collagen type II (1:100) and anti-aggrecan (1:500). After washing with PBS, the cells were incubated at 37° C for 1 h in Alexa Fluor 555 labeled secondary antibody solution (1:200), against both anti-collagen type II and anti-aggrecan. The samples were washed with PBS, and counterstained with DAPI (1:5000) at room temperature for 10 min. After washing with PBS, the samples were examined with CLSM (LSM 900 Airyscan 2, Zeiss, Germany)

3.2.3.4 Cell integration to the multilayered osteochondral scaffolds

3.2.3.4.1 DP-MSCs seeding into the bone part of the scaffold

Bone part of the 3D printed scaffolds was treated with oxygen plasma, and then coated with β-TCP as indicated in Section 3.2.1.5. After coating, the scaffolds were sterilized in 70% EtOH for 1 h and dried in a laminar flow hood. DP-MSCs were

seeded at a density of $5x10^4$ cells/scaffold onto the bone part of the scaffolds, and then incubated for 2 h at 37^0C and 5% CO_2 to ensure cell attachment. In order to examine viability, organization and proliferation of DP-MSCs on the bone part of the scaffolds, the cells were cultured in the growth medium and at the end of incubation period Live/Dead and MTS assays and Phallodin/DAPI were performed as indicated in Section 3.2.3.5.1. On the other hand, for the evaluation of differentiation of MSCs on the scaffolds and for co-culture studies the cells were cultured in the growth medium for a day, and then the culture of cells on the scaffolds continued for 21 days in the osteogenic induction media.

3.2.3.4.2 Chondrogenic cell loaded hydrogel application into the cartilage part of the scaffold

DP-MSCs were differentiated into chondrogenic cells via spheroid culture within the determined chondrogenic induction medium composed of DMEM High glucose medium, penicillin/streptomycin (100 U/mL, 100 μg/mL), ITS (1%), dexamethasone (100 nM), ascorbic acid (100 μM) and TGFβ-1 (10 ng/mL) for 21 days as explained in Section 3.2.3.3.1. At the 21st day of spheroid culture, the spheroids were disrupted by treatment with 0.25% Try-EDTA for 5 min and resuspending in the induction medium. The activity of Try-EDTA was reduced by dilution with the medium, and then the cells were centrifuged at 1400 rpm for 5 min. The pellet was resuspended in the chondrogenic induction medium and the cell number was determined. The cells were combined with collagen type I solution (3%, w/v) of which composition was given in Table 7. The cell loaded hydrogel (100 μL) was injected into the cartilage part of the scaffold, and the samples were kept at 37° C for 45 min to form gelation. The cells were cultured within the scaffolds for 7 days by changing the chondrogenic induction media every other day.

Table 7. Components of collagen-based hydrogel solution

Ingredient	Percentage (% v/v)
10X DMEM	7
NaOH 2.8 M	2.5
Sodium Bicarbonate (7.5% solution)	1
1X DMEM High Glucose	13
Atelocollagen solution in acetic acid (5 mg/mL)	60
Cell suspension	16.5

3.2.3.4.3 Co-culture of chondrogenic and osteogenic cells on the osteochondral multilayered scaffolds

DP-MSCs were seeded onto the bone part and differentiated into osteogenic cells as explained in Section 3.2.3.4.1. On the other hand, DP-MSCs were cultured in spheroids with chondrogenic induction media for 21 days (Section 3.2.3.3.1). After 21 days of osteogenic induction of DP-MSCs on the scaffolds, the chondrogenic differentiated cells within hydrogel were loaded onto the cartilage part of the multilayered construct as indicated in Section 3.2.3.4.2. Then, chondrogenic and osteogenic cells derived from DP-MSCs were co-culture in the multilayered scaffold for one week using the determined chondrogenic induction medium to prevent de-differentiation of chondrocytes (Figure 13).

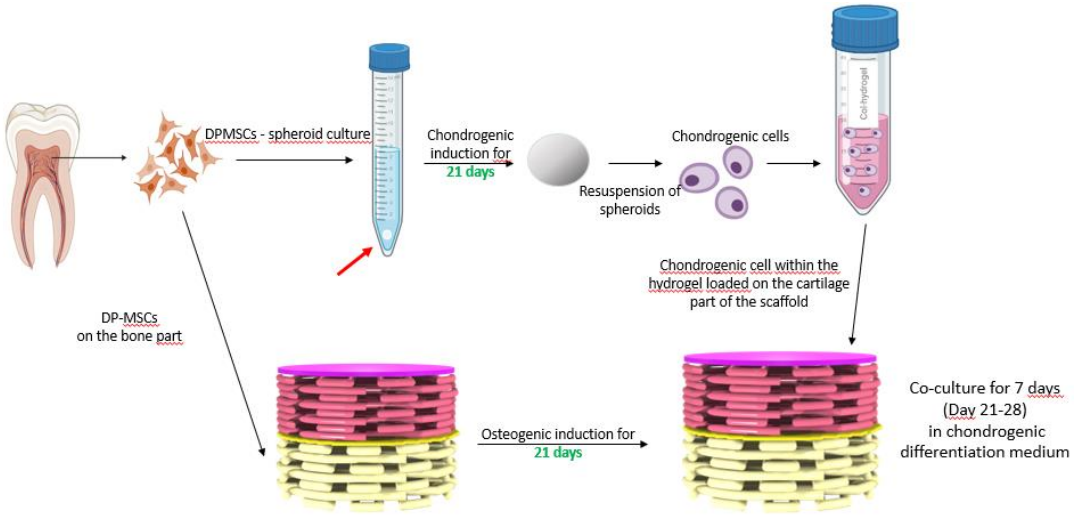

Figure 13. Schematic presentation of cell seeding on bone and cartilage parts of the multilayered scaffold for co-culture studies

3.2.3.5 Cell behavior on the multilayered scaffolds

3.2.3.5.1 Viability, proliferation and organization of DP-MSCs on the bone part of the scaffold

Live/Dead assay, MTS assay and Phalloidin/DAPI staining were performed to investigate the viability, proliferation and organization of DP-MSCs within the multilayered scaffold. For that purpose, DP-MSCs were seeded at a density of $5x10^4$ cells/scaffold on the multilayer scaffold as indicated in Section 3.2.3.4.1. After culturing in the growth media for 5 days, Live-Dead assay was performed to assess the viability of the cells on the scaffolds and Phalloidin/DAPI staining was done to investigate the organization of the cells within the bone part of the scaffolds.

For Live/Dead assay cell containing scaffolds were washed with PBS and the cells were stained with Calcein AM (1:2000) and ethidium homodimer-1 (1:500) in PBS. After staining for 30 min, the cells on the scaffolds were examined with CLSM (Zeiss LSM 900, Germany). In addition, a set of samples were fixed with 4% PFA and were stained with Phalloidin/DAPI as mentioned in Section 3.2.3.2.1. and examined under CLSM. Moreover, the presence of cells on the bone and cartilage parts of the

scaffold were separately examined with CLSM after the scaffold was cut horizontally to evaluate cell migration through the calcified cartilage to show barrier function.

The proliferation of the cells on these scaffolds was analyzed by MTS assay, which was performed on days 1,7,14 and 21 of the culture to determine the cell numbers on the scaffolds. Similar to WST-1, MTS assay is based on the conversion of MTS solution to a colored formazan product with the presence of metabolic activity of the cells. The working solution of 10% MTS working solution was prepared in the growth medium, and 1 mL of MTS working solution was added onto the cell seeded scaffolds on days 1,7,14 and 21 of the culture. After incubation for 2 h at 37° C, 200 µL sample was transferred into 96 well plate and the absorbance was measured at 490 nm with multi-plate reader. A calibration curve was used to convert the absorbance values to the cell numbers (Appendix 8.2 Figure A2).

3.2.3.5.2 Evaluation of cell differentiation on the bone part of the scaffold

Osteogenic differentiation of DP-MSCs on the multilayered scaffold was determined with ALP assay, Alizarin Red staining and mineralization assay.

DP-MSCs were seeded at a density of $5x10^4$ cells/scaffold on the bone part of the scaffolds as explained in Section 3.2.3.4.1. After culturing in the growth medium for 24 h, the cells were cultured with osteogenic induction medium for 21 days by changing the medium every 3 days. A set of DP-MSCs on the scaffolds were cultured in the growth medium as a control. ALP assay was carried out to investigate the osteogenic differentiation of DP-MSCs on the scaffolds according to the protocol given in Section 3.2.3.2.4. In addition, Alizarin Red staining was conducted to the cells on the multilayered scaffolds to detect calcium deposition, which is an indicator of osteogenic differentiation. The cells on the scaffolds were fixed with 4% PFA on day 21 of culture, and then they were treated with Alizarin Red solution (2% w/v) for 15 min at room temperature. After washing 3 times with distilled water to remove excess dye, the samples were examined under stereomicroscope (Stemi 508, Zeiss, Germany). The other method used to prove osteogenic differentiation was tetracycline staining in which newly formed calcium phosphate was labelled to demonstrate mineralization by

osteoblasts (110). Tetracyclines are composed of 4 carboxylic rings which help binding the tetracycline molecules to calcium ions of mineralized tissue. This binding process creates the fluorescence signal on the scaffold from tetracycline after binding to mineralized tissue (111). DP-MSCs were seeded onto the multilayered scaffolds as mentioned above; however, at the third day of culture Pen/Strep (100 U/mL-100 µg/mL) in the osteogenic induction medium was replaced with tetracycline (10 µg/mL). After 21 days of culture, the samples were washed with PBS and 70% EtOH, and then the samples were fixed with 96% EtOH at 4°C for 6 h. After removal of 96% EtOH, the samples were allowed to dry at dark and the formed mineralization was examined via CLSM with an excitation wavelength of 480 nm.

3.2.3.5.3 Cell viability and proliferation analysis after co-culture of chondrogenic and osteogenic cells on the osteochondral scaffolds

After 21 days of osteogenic induction of DP-MSCs on the scaffolds, chondrogenic cells obtained by spheroid culture was loaded on the scaffolds within hydrogel and these cells were co-cultured for a week as explained in Section 3.2.3.4.3. The viability and proliferation of the cells on the bone and the cartilage were separately analyzed by MTS. For the cells on the bone part MTS assay was done on day 1, 21 and 28 according to the method given in Section 3.2.3.5.1. At 28-day of culture scaffolds were cut in half horizontally along the calcium cartilage barrier. MTS Assay was performed on the bone part to determine the cell viability on 7^{th} day of co-culture which corresponds to 28^{th} day of osteogenic differentiation. In addition, the viability and proliferation of chondrogenic cells on the cartilage part was analyzed by MTS on 1^{st} and 7^{th} day of co-culture according to the protocol given in Section 3.2.3.5.1.

3.2.3.5.4 Immunostaining for the expression of osteogenic and chondrogenic markers of the cells after co-culture studies

After 7 days of co-culture of osteogenic and chondrogenic cells on the multilayered scaffolds, the cells were fixed with 4% PFA, and then the scaffold were cut in half horizontally along the calcium cartilage barrier. After washing with PBS,

the cells on the bone and cartilage parts of the scaffold were immunostained for the expression of osteogenic and chondrogenic markers. To evaluate osteogenic differentiation the antibodies against osteopontin and osteonectin were used, while collagen type II and aggrecan were chosen as chondrogenic markers. Cells were incubated in 100 mM glycine for 15 min at room temperature for saturation of PFA groups. After samples were washed with PBS, they were incubated in 1% BSA solution (in PBS) for 30 min at 37° C to block non-specific binding of antibodies, and then the samples were incubated overnight at 4°C in primary antibody solutions of which dilutions were given in Table 6. After washing with PBS, samples were incubated in secondary antibodies at 37° C for 1 h. The samples were washed with PBS, and then counterstained with DAPI (1:5000) at room temperature for 10 min. After washing with PBS, the cells were examined under CLSM (LSM 900, Zeiss, Germany)

Table 8. Antibodies and dilution factors (DF) used in immunostaining

Primary antibody	**DF**	**Secondary antibody**	**DF**
Rabbit anti-Osteonectin	1:500	Alexa Fluor 488 labeled Anti Rabbit Goat Antibody	1:100
Mouse anti-Osteopontin	1:25	Alexa Fluor 555 labeled Anti Mouse Goat Antibody	1:200
Mouse anti-Collagen type II	1:100	Alexa Fluor 555 labeled Anti Mouse Goat Antibody	1:200
Mouse anti-Aggrecan	1:500	Alexa Fluor 555 labeled Anti Mouse Goat Antibody	1:200

3.2.4 Statistical analysis

Statistical analysis was performed using the R program. To compare the averages obtained from the results of MTS assay, ALP assay and mechanical test experiments; ANOVA test was used for two-to-many comparisons and the t-test was used for two independent samples between two groups. The p values less than 0.05 ($p < 0.05$) were considered statistically significant.

4 RESULTS

4.1 Construction of Multilayered Scaffold

4.1.1 Design of 3D plotted part of the multilayered scaffold

3D model of the multilayered scaffold was designed with SketchUp and Blender programs (Figure 14 and 15). This scaffold was made of three parts that mimics the bone, calcified cartilage and cartilage tissues of the OC tissue. For that purpose, bone, cartilage and calcified cartilage parts were designed separately, and then combined to form the multilayered scaffold. Bone and cartilage parts were designed to have a porous structure with different pore sizes and inner structures to ensure cell attachment and proliferation on these layers of the multilayered scaffold. However, there was a non-porous layer between the bone and cartilage parts to mimic the calcified cartilage, which provides mechanical integration between bone and cartilage tissues and prevents vascularization and cell migration through this barrier (102, 112)

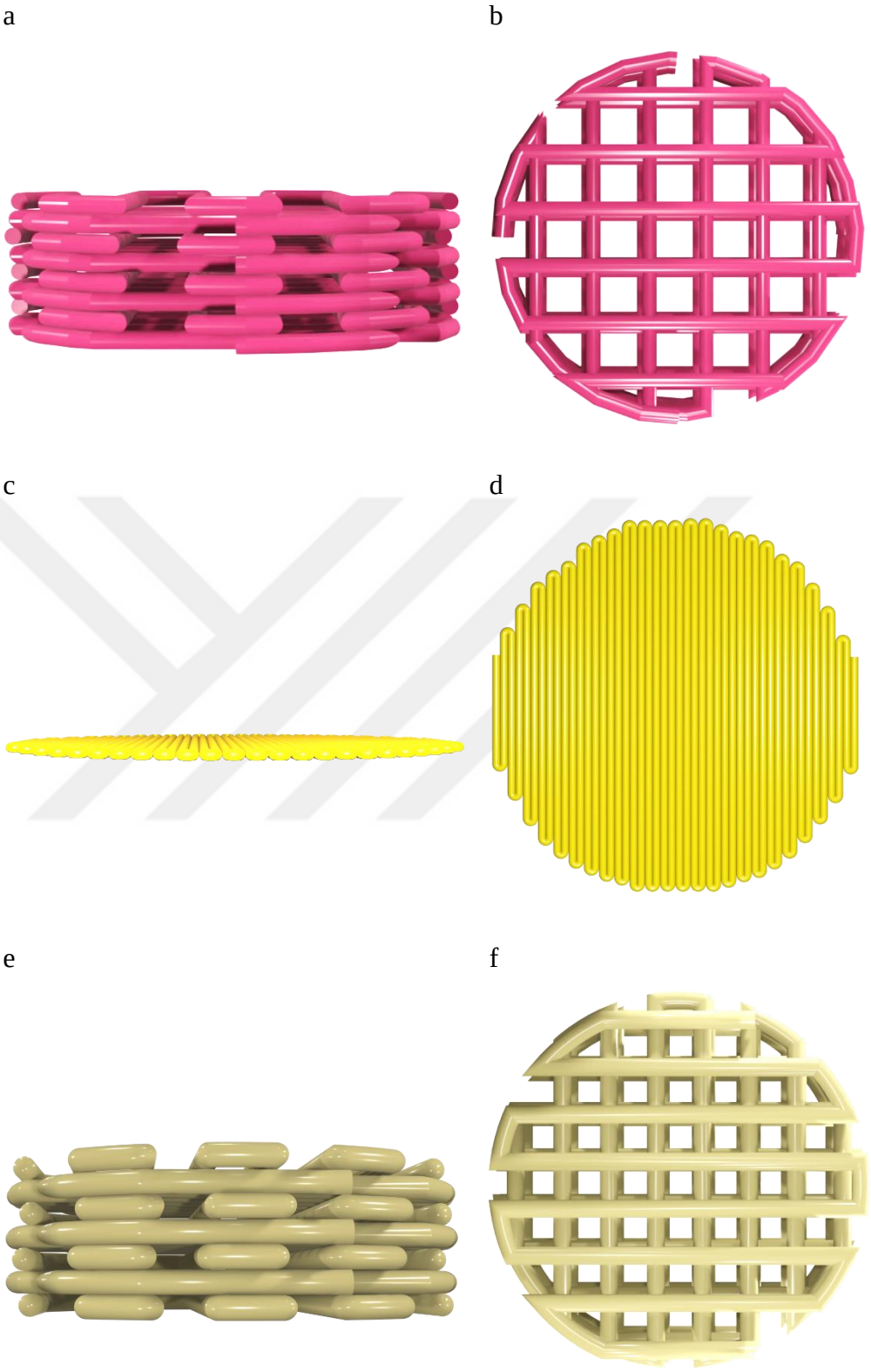

Figure 14. 3D model designs of different parts of the multilayered scaffold. Images show the design of cartilage part from (a) side and (b) top, calcified cartilage part from (c) side and (d) top and bone part from (e) side and (f) top.

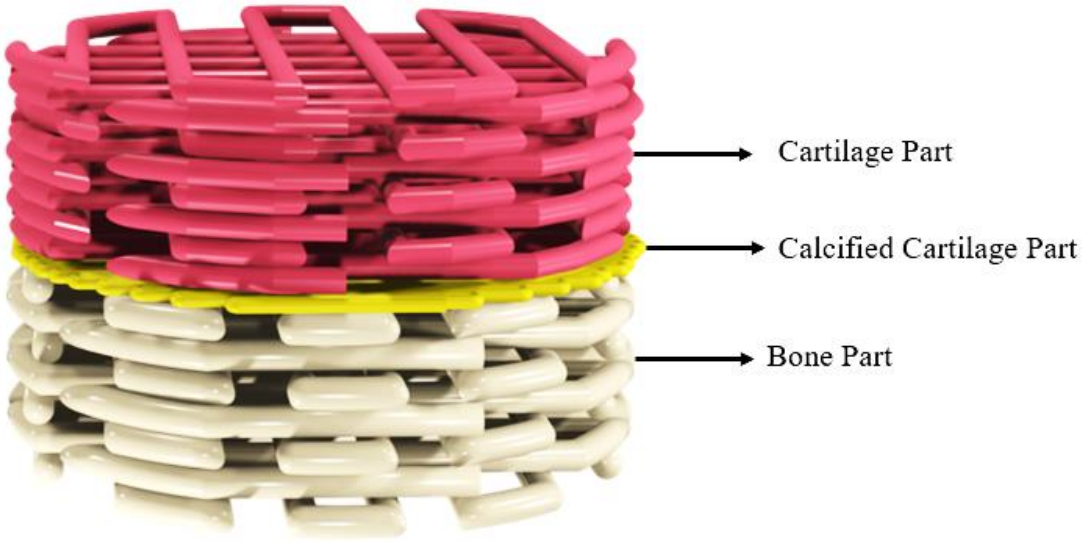

Figure 15. Designed 3D model of the multilayered scaffold including all 3 components; cartilage part, calcified cartilage part and bone part.

4.1.2 Optimization of 3D printing parameters

3D printing of the multilayered scaffold was conducted by FDM that involves melting a thermoplastic material and depositing the molten material in a single layer in the triaxial system. While adding multiple layers on top of each other, the layers fused and create the desired 3D object (113). 3D printing parameters such as printing speed, layer height and needle tip diameter were optimized to obtain well-printed scaffolds having a desired architecture. In addition, 3D models were designed with different fiber diameters and fiber spacing were 3D printed to obtain the intended pore size. The scaffolds were printed by changing the parameters that were given in Section 3.2.1.2. and the stereomicroscope images of the obtained scaffolds' bone and cartilage parts were given in Figure 16 and 17. The filament diameter and pore size measured from the images were given in Table 9 and 10. According to the pore size and structural integrity, the optimum 3D printing parameters to be used in the further studies were determined and presented in Table 11.

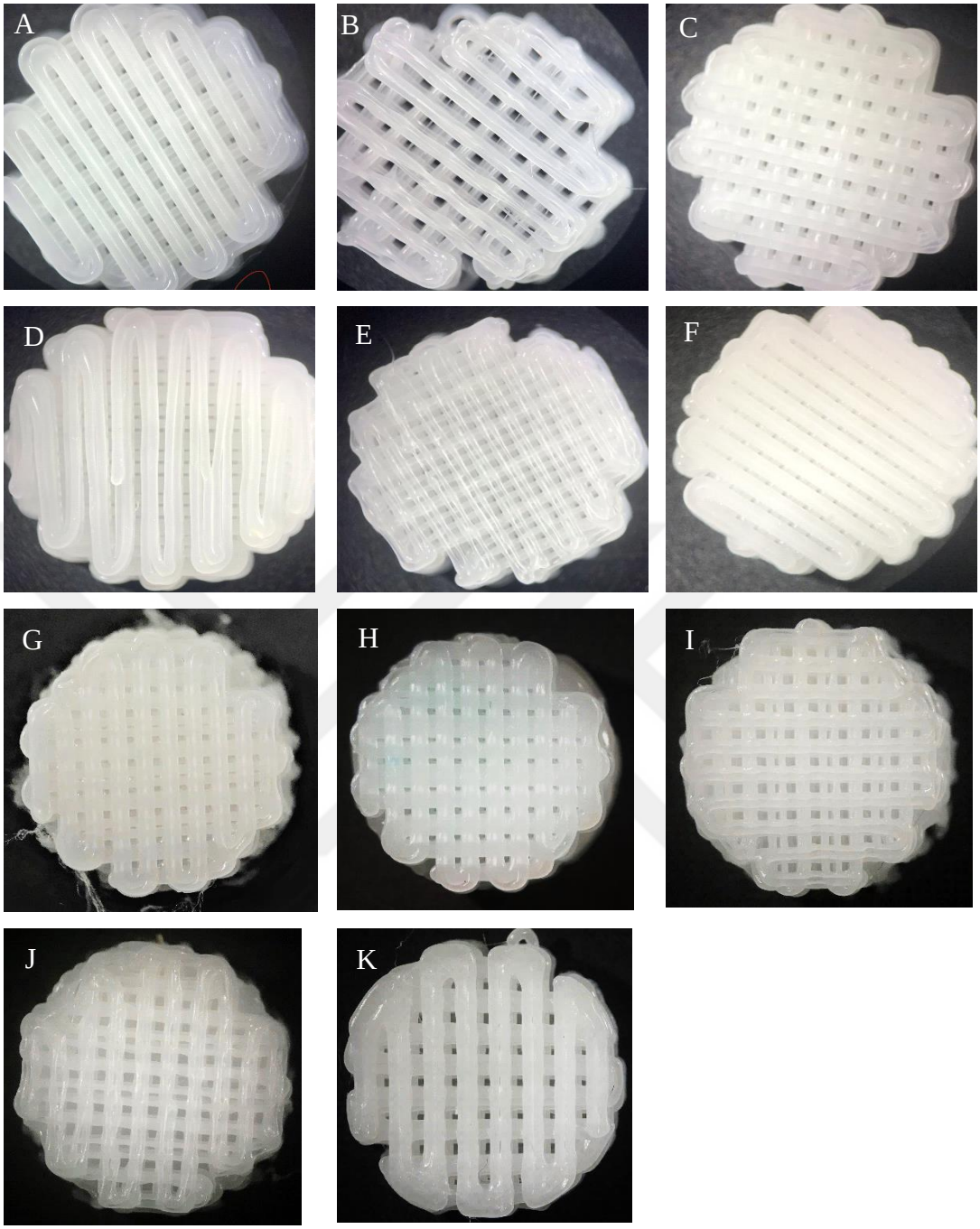

Figure 16. Stereomicroscope images of the bone part of the scaffolds (A-K) that were printed with the parameters shown in Table 4.

Table 9. The fiber diameters and the distance between fibers obtained for bone part of the 3D printed PCL scaffolds using different printing parameters.

<table>
<tr><th></th><th>Needle Tip (G)</th><th>Layer height (mm)</th><th>Speed (mm/s)</th><th>Designed fiber diameter (µm)</th><th>Measured fiber diameter (µm)</th><th>Designed distance between fibers (µm)</th><th>Measured distance between fibers (µm)</th></tr>
<tr><td>A</td><td rowspan="6">27</td><td>0.1</td><td>2</td><td rowspan="11">400</td><td>595±26</td><td rowspan="3">600</td><td>348 ±28</td></tr>
<tr><td>B</td><td>0.2</td><td>2</td><td>562 ±72</td><td>535 ±70</td></tr>
<tr><td>C</td><td>0.2</td><td>1</td><td>564 ±18</td><td>345 ±14</td></tr>
<tr><td>D</td><td>0.1</td><td>2</td><td>599 ±27</td><td rowspan="3">400</td><td>362 ±42</td></tr>
<tr><td>E</td><td rowspan="6">0.2</td><td>2</td><td>448 ±59</td><td>329 ±25</td></tr>
<tr><td>F</td><td>1</td><td>601 ±29</td><td>191 ±21</td></tr>
<tr><td>G</td><td rowspan="5">25</td><td>2</td><td>691±24</td><td rowspan="4">600</td><td>332±25</td></tr>
<tr><td>H</td><td>3</td><td>744±34</td><td>336±25</td></tr>
<tr><td>I</td><td>4</td><td>529±45</td><td>451±21</td></tr>
<tr><td>J</td><td>6</td><td>566±28</td><td>473±24</td></tr>
<tr><td>K</td><td>4</td><td>500</td><td>751±15</td><td>800</td><td>438±27</td></tr>
</table>

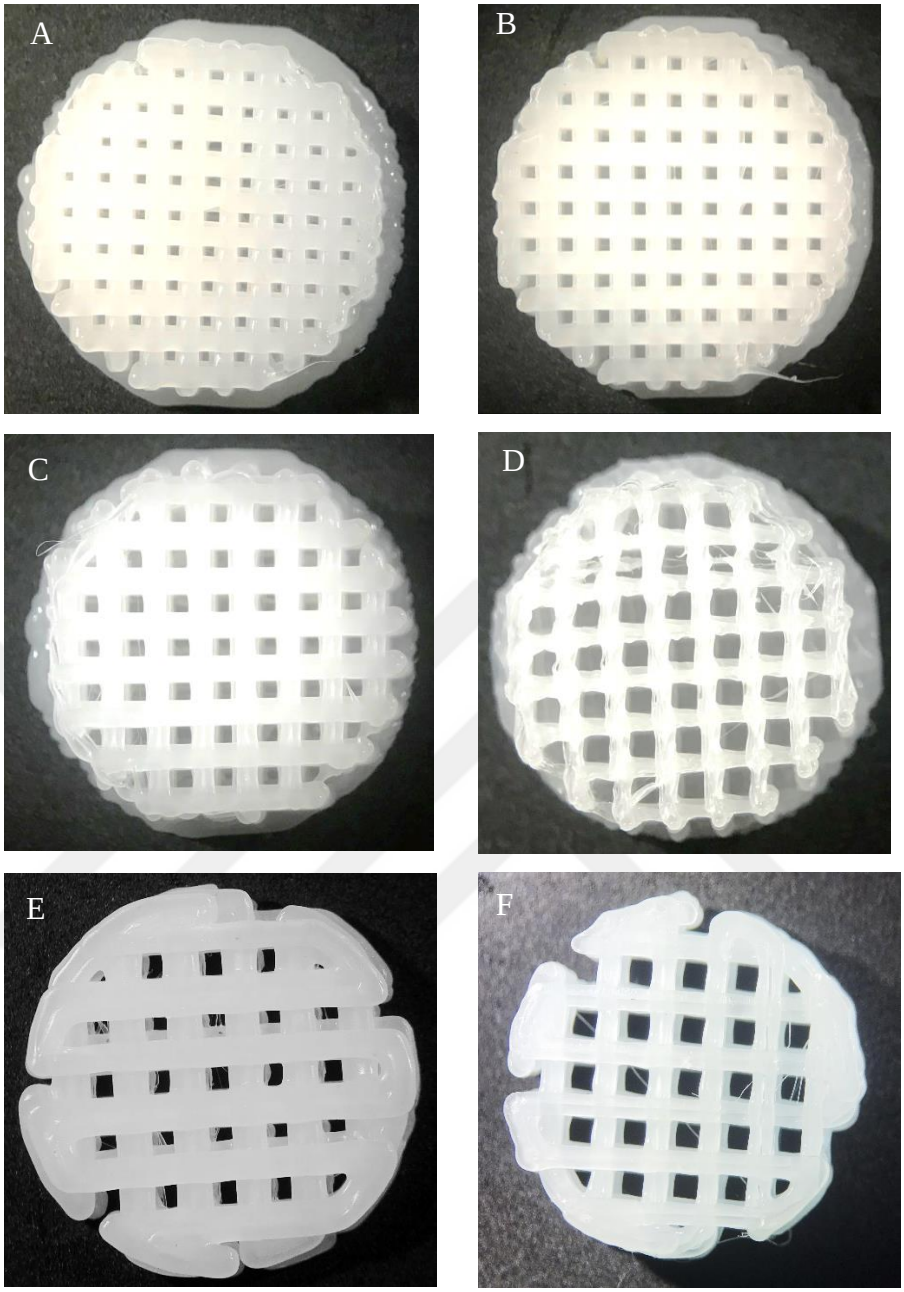

Figure 17. Stereomicroscope images of the cartilage part of the scaffolds (A- F) that were printed with the parameters shown in Table 5.

Table 10. The fiber diameters and the distance between fibers obtained for bone part of the 3D printed PCL scaffolds using different printing parameters.

	Needle Tip (G)	Layer Height (mm)	Speed (mm/s)	Designed Fiber Diameter (μm)	Measured Fiber Diameter (μm)	Designed Distance Between Fibers (μm)	Measured Distance Between Fibers (μm)
A	27	0.2	1	200	540±47	800	555±26
B		0.1	2		520±32		509±33
C		0.2	1	300	570±24	900	656±42
D		0.1	2		469±30		763±21
E	25	0.2	3	400	909±51	1200	645±49
F		0.2	4		656 ± 50		833±48

Table 11. The optimized parameters for 3D printing of the multilayered scaffold

Printing Speed		4 mm/s
Layer Height		0.2 mm
Nozzle Diameter		25 G
Designed Fiber Diameter	Bone Part	500 μm
	Calcified Cartilage Part	200 μm
	Cartilage Part	400 μm
Real Fiber Diameter	Bone Part	751±15 μm
	Calcified Cartilage Part	Fibers were fused
	Cartilage Part	656 ± 50 μm
Designed Distance Between Fibers	Bone Part	800 μm
	Calcified Cartilage Part	No space
	Cartilage Part	1200 μm
Real Distance Between Fibers	Bone Part	438±27 μm
	Calcified Cartilage Part	No space
	Cartilage Part	833±48 μm

4.2 Characterization of the Multilayered Osteochondral Scaffold

4.2.1 Scanning electron microscopy analysis

4.2.1.1 Morphology of 3D printed multilayered scaffold

SEM images of the 3D printed multilayered scaffolds were given in Figure 17. Three layers, bone, calcified cartilage and cartilage parts were printed successfully by FDM method without any interphase (Figure 18 c, d). The fiber diameter and distance between the fibers (pore size) at the cartilage part of the multilayered scaffold were measured as 562±55 μm and 940±51 μm, respectively, while at the bone part they were measured as 730±60 μm and 453 ±44 μm, respectively. (Figure 18 a,b) It was observed that the pore size of the cartilage part was larger than that of the bone part, as it was intended. The calcified cartilage part was printed as a non-porous layer without any space with fusion of filament without any pores. This barrier structure was critical for preventing cell migration between bone and cartilage parts, and would also be important for potential *in vivo* studies to avoid vascularization in cartilage part.

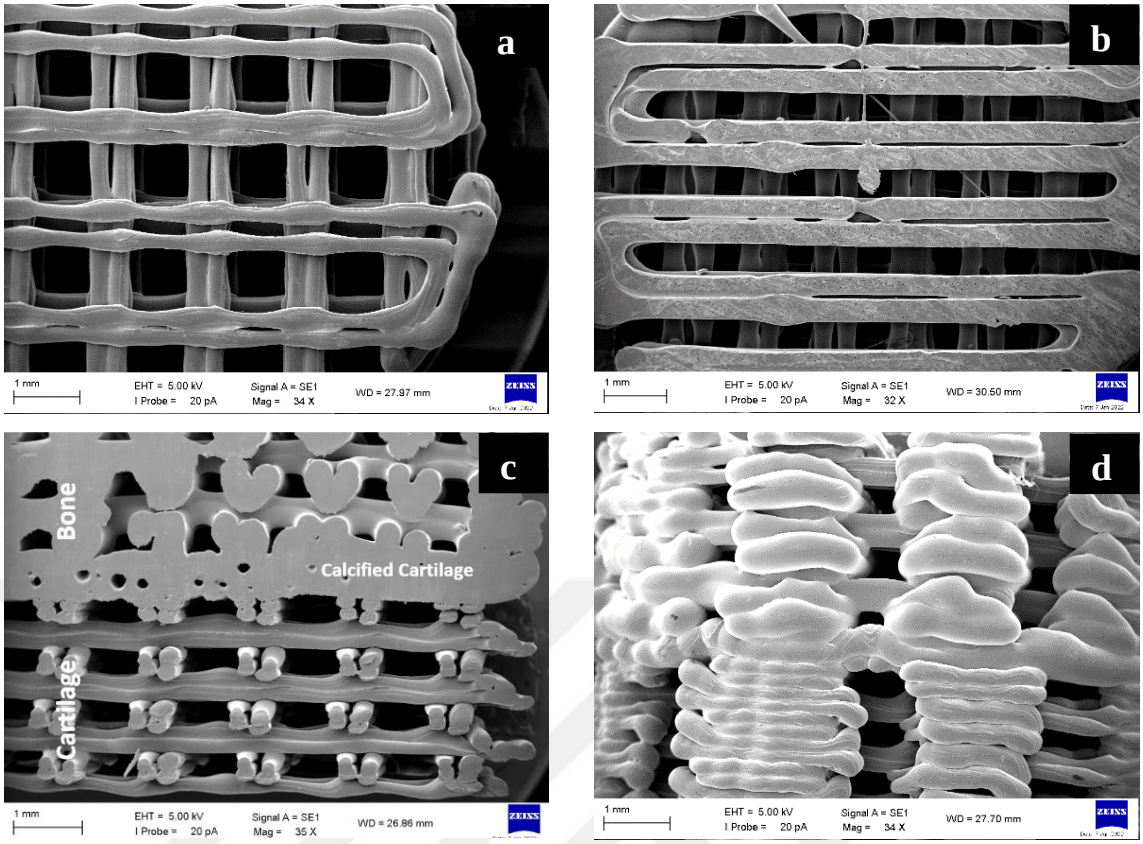

Figure 18. SEM images of the 3D printed multilayered scaffold. Top view of (a) the cartilage part, (b) the bone part, (c) vertical cross-section of the multilayered scaffold, (d) vertical outside view of the multilayered scaffold. Magnifications: (a, d) X34, (b) X32, (c) X35; scale bar: 1mm.

4.2.1.2 Morphology of the electrospun fibrous mat

Electrospun fibrous mat was successfully fabricated using the determined parameters given in Section 3.2.1.3. SEM results showed that the fibers were randomly organized and homogenous all around the mat, as intended (Figure 19).

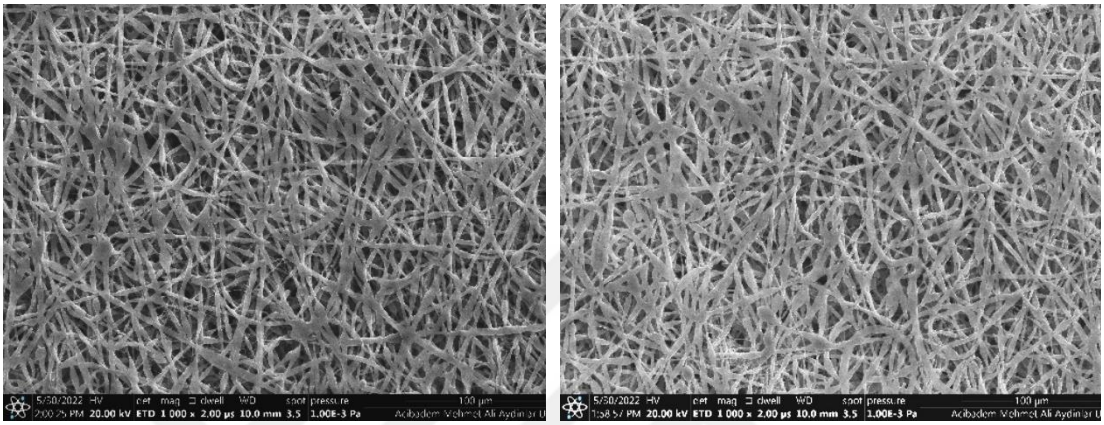

Figure 19. SEM micrographs of the random fibrous mat fabricated by electrospinning. Magnifications: X100, scale bar 100 μm.

4.2.1.3 Coating of β-TCP on the bone part of the multilayered scaffold

The multilayered scaffold was 3D printed using PCL, which is a hydrophobic polymer therefore it might exhibit a lack of bioactivity and low cell attachment at the surfaces (114). In bone tissue engineering integration of β-TCP to the scaffolds is a commonly used approach to encourage osteogenic microenvironment and to induce osteogenic differentiation. For this reason, after fabrication of the multilayered scaffold the bone part was coated with β-TCP to increase hydrophilicity of the scaffold and to enhance cell attachment and osteoconductivity. SEM results showed that β-TCP was successfully coated onto the filaments of the bone part of the scaffolds (Figure 20). β-TCP particles were seen on the filaments in both top view and vertical cross-section view of the scaffolds. In addition, SEM results showed that β-TCP particles were also coated in the depth of the bone part. However, β-TCP particles did not pass

the calcified cartilage barrier (Figure 20 c and 21 d). Thus, it was concluded that β-TCP was homogenously coated on the bone part of the multilayered scaffold.

The scaffolds would be sterilized with EtOH before cell seeding, therefore it was examined with SEM whether the β-TCP coating remained on the surfaces after sterilization (Figure 21). The results showed that after sterilization the β-TCP particles were slightly decreased which could be negligible, especially at the outer surface of scaffold. As a conclusion, it was observed that sufficient and homogenous β-TCP coating was present on the bone part of the multilayered scaffolds even after sterilization process.

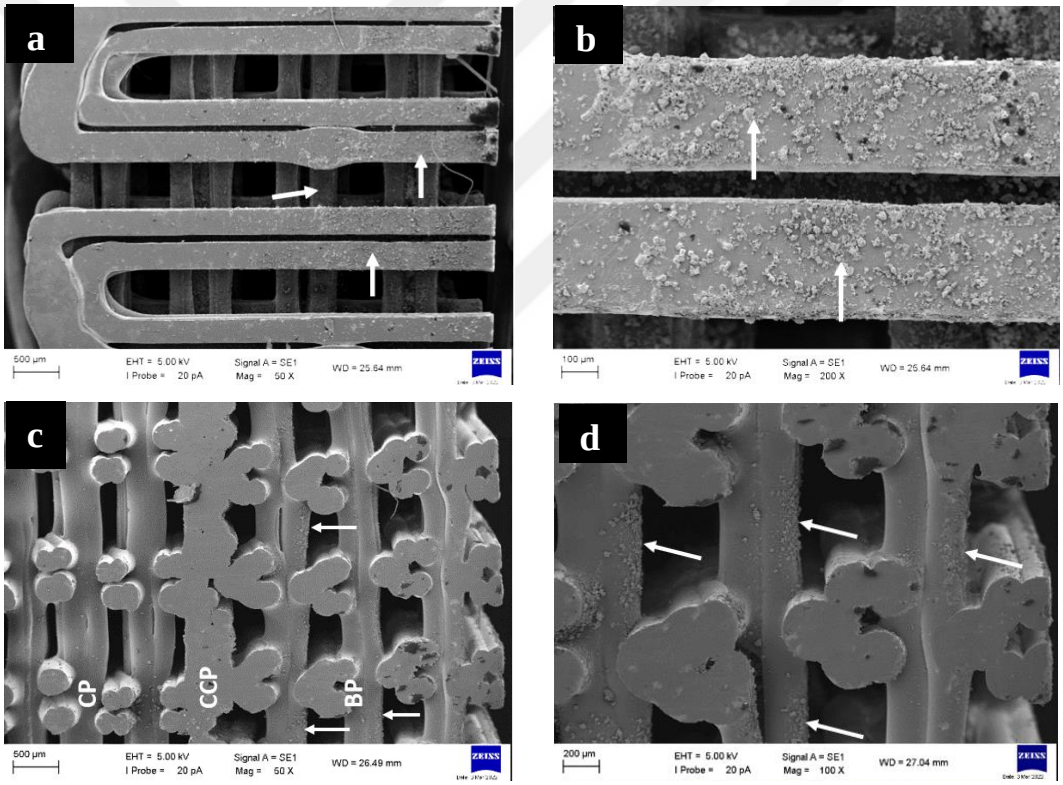

Figure 20. SEM micrographs of the β-TCP coated multilayered scaffold. (a, b) Top views and (c, d) side views of the scaffold. Magnifications: (a, c) X50, (b) X200, (d) X100; scale bars: (a, c) 500 µm, (b) 100 µm, (d) 200 µm. The arrows show the β-TCP particles. Cartilage part (CP), Calcified cartilage part (CCP), Bone part (BP)

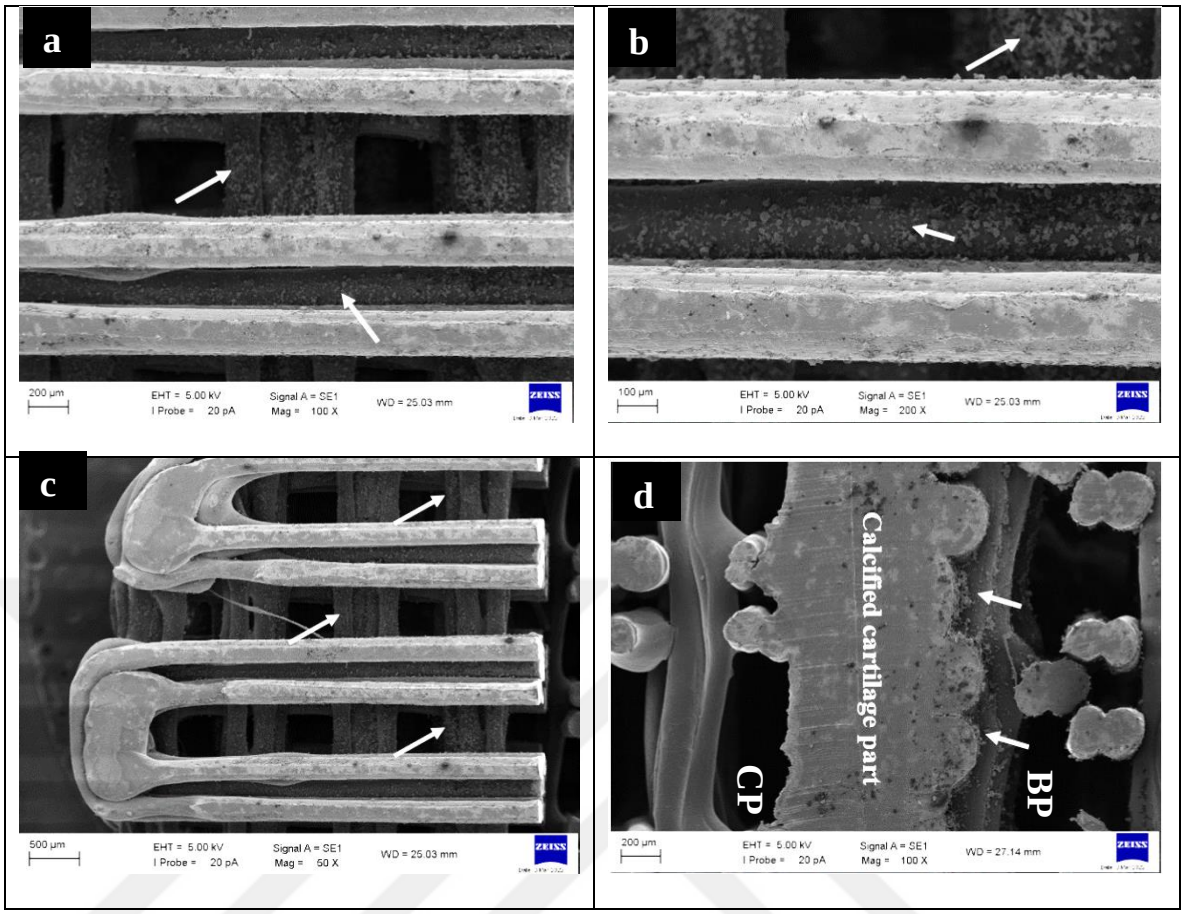

Figure 21. SEM micrographs of the β-TCP coated multilayered scaffold after sterilization with EtOH. (a,b,c) Top views and (d) side view of the scaffold. Magnifications: (a,d) X100, (b) X200, (c) X50; scale bars: (a,d) 200 µm, (b) 100 µm, (c) 500 µm. The arrows show β-TCP particles. Cartilage part (CP), Bone part (BP)

4.2.1.4 Morphology of the ultimate multilayered osteochondral scaffold

The ultimate multilayered osteochondral scaffold was obtained by combining the multilayered 3D printed scaffold and the elecrospun fibrous mat. The successful integration of electrospun mat on to the cartilage part of the 3D printed multilayered scaffold was seen in Figure 22 a, and d. The thickness of the electrospun fiber mat was determined around 420 µm (Figure 22 b). In Figure 22c and d, the non-porous calcified cartilage layer was clearly seen between the bone and the cartilage parts. β-TCP particles were only seen in the bone part due to that β-TCP could not reach to the cartilage part with the presence of calcified cartilage part as seen at Figure 22 c. This also indicated the barrier function of the calcified cartilage part. In addition, it was

shown that the pore size was larger in the cartilage part compared to the bone part, as it was intended (Figure 22 c).

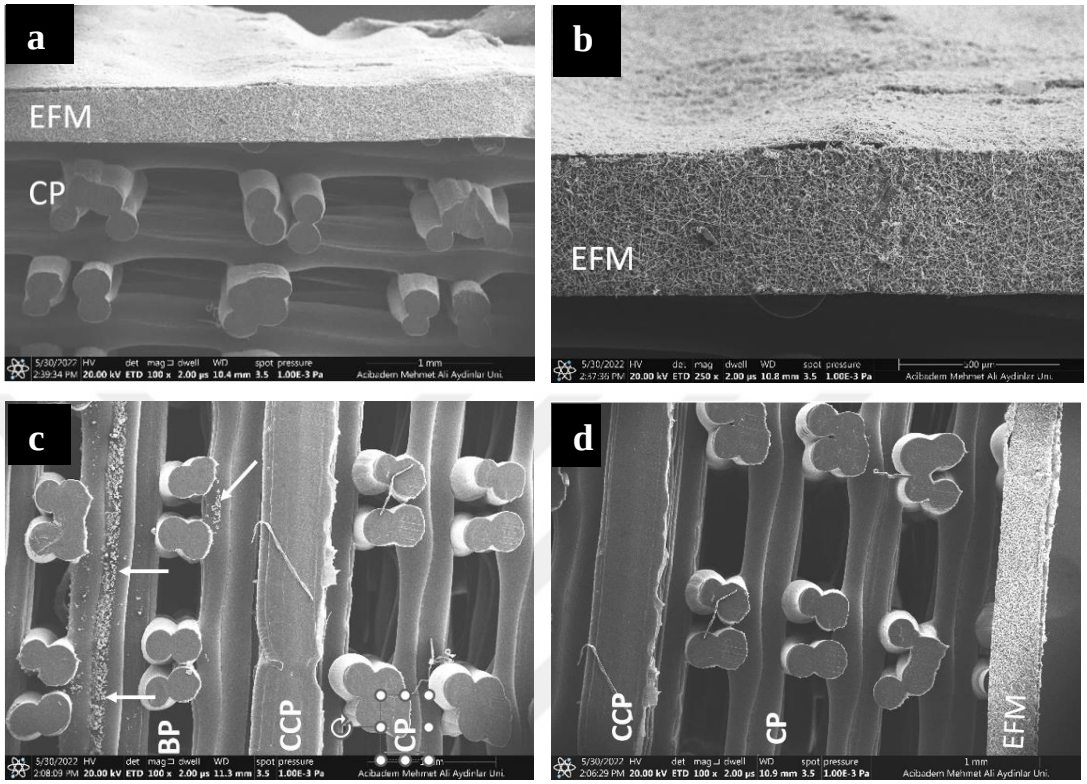

Figure 22. SEM micrographs of the multilayered osteochondral scaffold. The osteochondral scaffold is composed of, starting from the top; electrospun fibrous mat (EFM), the cartilage part (CP), the calcified cartilage part (CCP), the β-TCP coated bone part (BP). Side view of the scaffolds' (a, b) at the cartilage part with intact EFM, (c) at the cartilage, calcified cartilage and β-TCP coated bone parts, (d) at the calcified cartilage and cartilage parts with intact EFM. Magnifications: (a, c, d) X100, (b) X250; scale bars: (a, c, d) 1mm, (d) 200 μm. The arrows show the β-TCP particles

4.2.2 Mechanical Analysis

Articular cartilage and subchondral bone of human osteochondral tissue have a compression modulus of 2-10 MPa and 90-400 MPa, respectively (3). In addition, the calcified cartilage layer increases the mechanical integrity of the osteochondral unit (112). It was reported that designed osteochondral implant should have matching mechanical properties with the surrounding natural tissue; therefore, it should contain

a bone part with a high compression modulus, while a softer cartilage part to promote chondrocyte proliferation (115)

In this study compression test was performed to determine the mechanical properties of the bone phase, cartilage phase and the multilayered osteochondral scaffolds as mentioned in Section 3.2.2.2. The bone and cartilage parts were designed to have different mechanical properties than each other by adjusting the microarchitecture and pore size of the scaffolds. Compression moduli of the scaffolds was calculated using the stress-strain curves obtained by the compression tests (Figure 23). Compression modulus of the bone part, the cartilage part and the whole multilayered osteochondral scaffold including electrospun fibrous mat and β-TCP coating were determined as 61.1± 6.2, 38.9± 5.3 and 75.7± 5.2 MPa, respectively (Figure 24). The results showed that the bone part had a higher compression modulus than the cartilage part, as intended. In addition, it was observed that by combination of bone and cartilage parts and formation of the final multilayered osteochondral scaffold the compression strength of the construct was increased

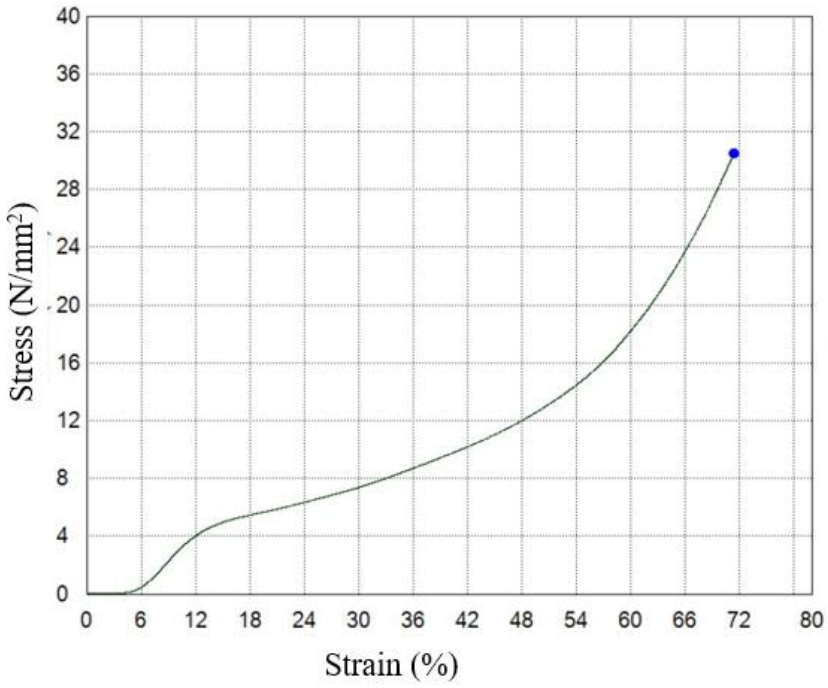

Figure 23. A representative stress-strain curve of scaffold.

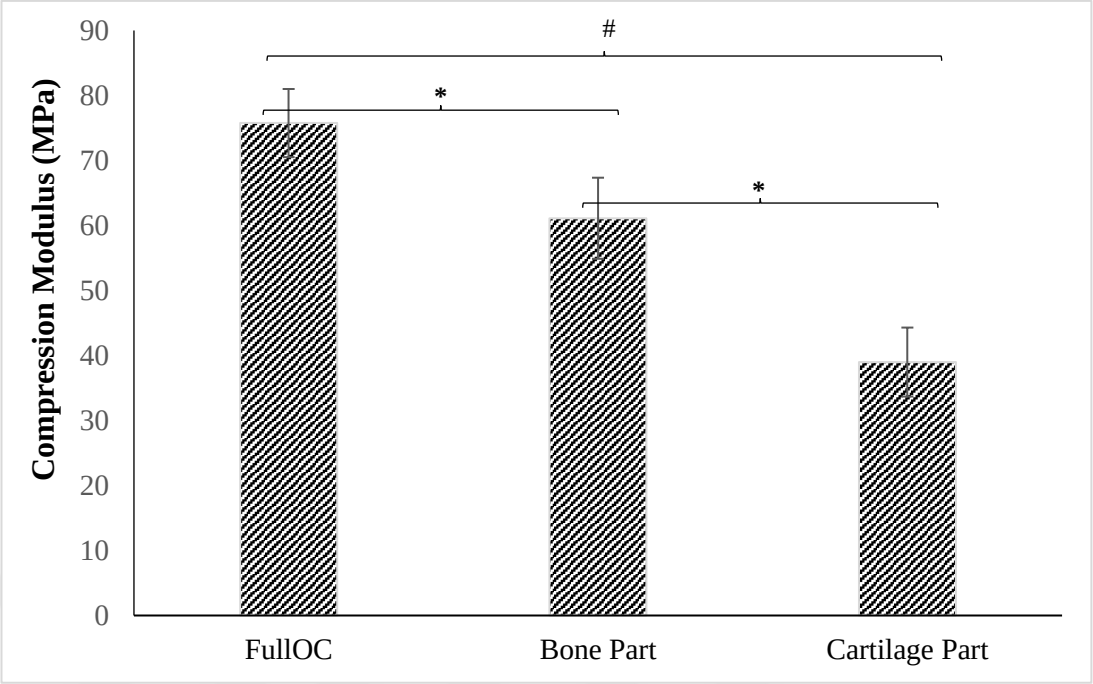

Figure 24. Compression modulus of the bone part, the cartilage part and the multilayered osteochondral scaffold (FullOC) (*p value < 0.05, #p value < 0.0001)

4.2.3 Evaluation of impermeability of the calcified cartilage part

3D printed scaffolds with and without calcified cartilage part were fabricated for the evaluation of impermeability of the calcified cartilage part as mentioned in Section 3.2.2.4. The permeability test was performed by dripping a blue dye from the cartilage side and it was examined whether the dye penetrated the bone part (Figure 25). The images taken after application of the dye showed that in the 3D printed scaffolds with calcified cartilage part the blue dye penetrated deep into the cartilage part, but the presence of the calcified cartilage part didn't allow the passage of the blue dye to the bone part. However, it was observed that the blue dye could pass freely from cartilage part to the bone part. It was concluded that the calcified cartilage part of the multilayered scaffold provided a barrier function in our design.

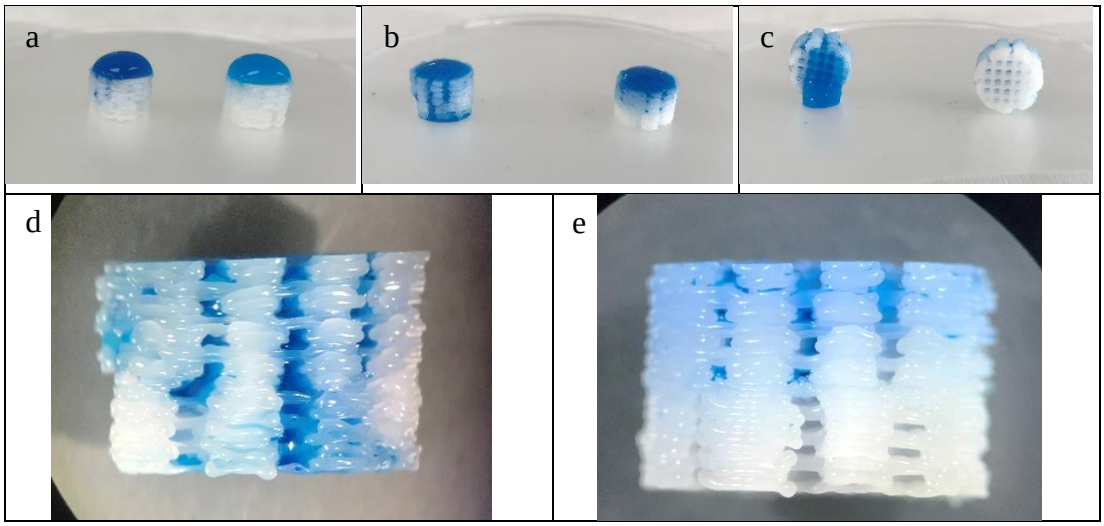

Figure 25. 3D printed scaffolds after application of the dye. (a, b, c) Photographs of the scaffolds with the calcified cartilage part (the ones on the right) and the scaffolds without the calcified cartilage part (the ones on the left). Images of the scaffolds (a) just after adding a blue dye from the cartilage part, (b, c) waited for a while after dye application. Stereomicroscope images of the scaffold fabricated (d) without a calcified cartilage part scaffolds and (e) the scaffold with the calcified cartilage part.

4.3 *In Vitro* Studies

4.3.1 Characterization of human DP-MSCs

4.3.1.1 Cell morphology

One of the criteria to define a cell as a MSC is that the cell adherence to the plastic surfaces when standard culture conditions were applied (104). In this study, DP-MSCs were cultured on plastic flasks as mentioned in Section 3.2.3.2.1. The morphology of DP-MSCs were examined under light microscope and the results showed that they showed plastic-adherent behavior. In addition, it was observed that the cells had spindle shape and fibroblastic morphology (Figure 26). The organization of cytoskeleton and nucleus of DP-MSCs was examined after Phalloidin/DAPI staining. It was observed that DP-MSCs displayed well-organized actin filaments (Figure 27).

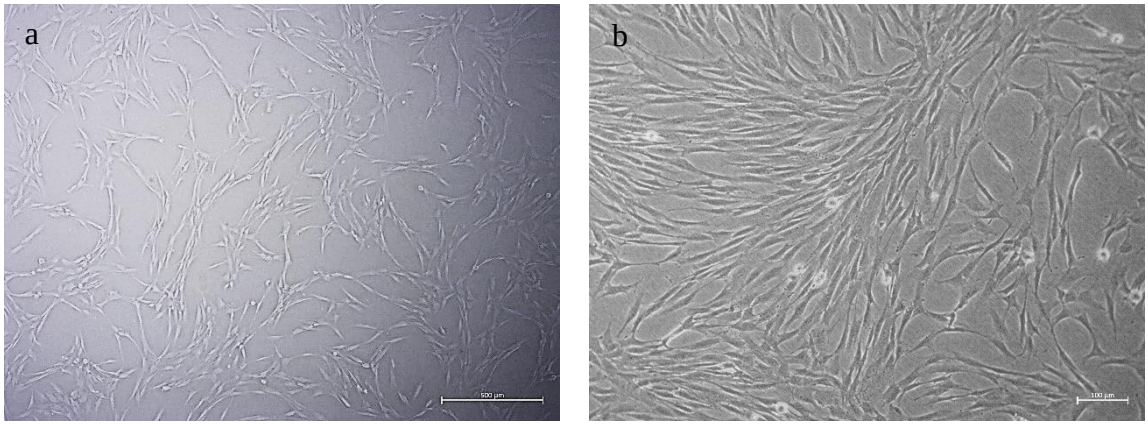

Figure 26. Light microscope images of DP-MSCs isolated from human dental pulp tissue. Magnification: (a) X4, (b) X10: scale bar: (a,b) 100 μm

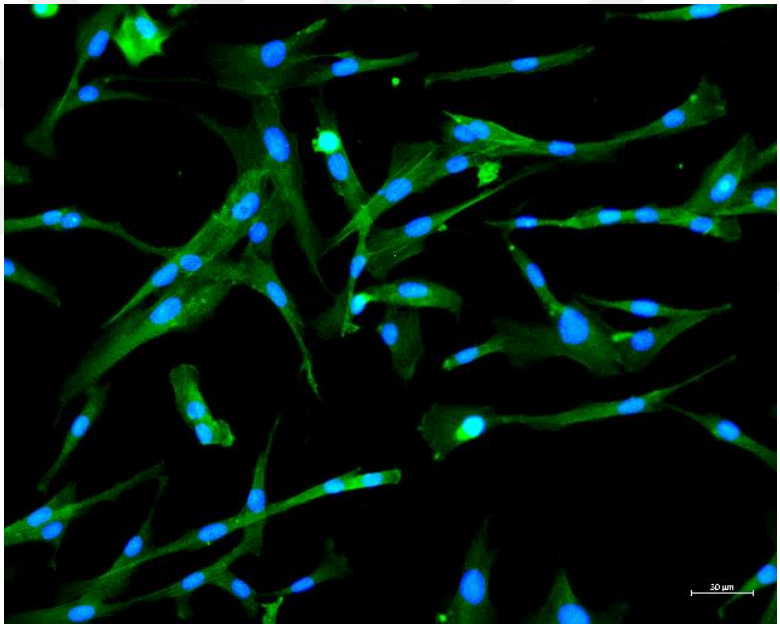

Figure 27. Fluorescence micrographs of DP-MSCs after staining with Phalloidin-FITC and DAPI for actin filaments (green) and nuclei (blue), respectively. Magnification: X20; scale bar: 50 μm.

4.3.1.2 Flow cytometry analysis

Flow cytometry analysis was conducted to determine specific surface antigens expressed by the isolated DP-MSCs (P3). The absolute positive cells were counted considering the immunoglobulin isotypes. The representative histograms for positive and negative expression of antigens obtained by flow cytometry were shown in Figure

28. The percentage of cells that expressed the cell surface antigens were given in Table 12. The results showed that DP-MSCs were positive for MSC markers CD44, CD78, CD90 and CD105, and also for immunogenic antigen HLA-ABC, while they had negative expression for hematopoietic lineage markers CD34 and CD45 and also for immunogenic antigen HLA-DR. These results revealed that the isolated DP-MSCs used in this study showed characteristic surface antigen expression of MSCs according to standards of Mesenchymal and Tissue Stem Cell Committee of the International Society for Cellular Therapy (104).

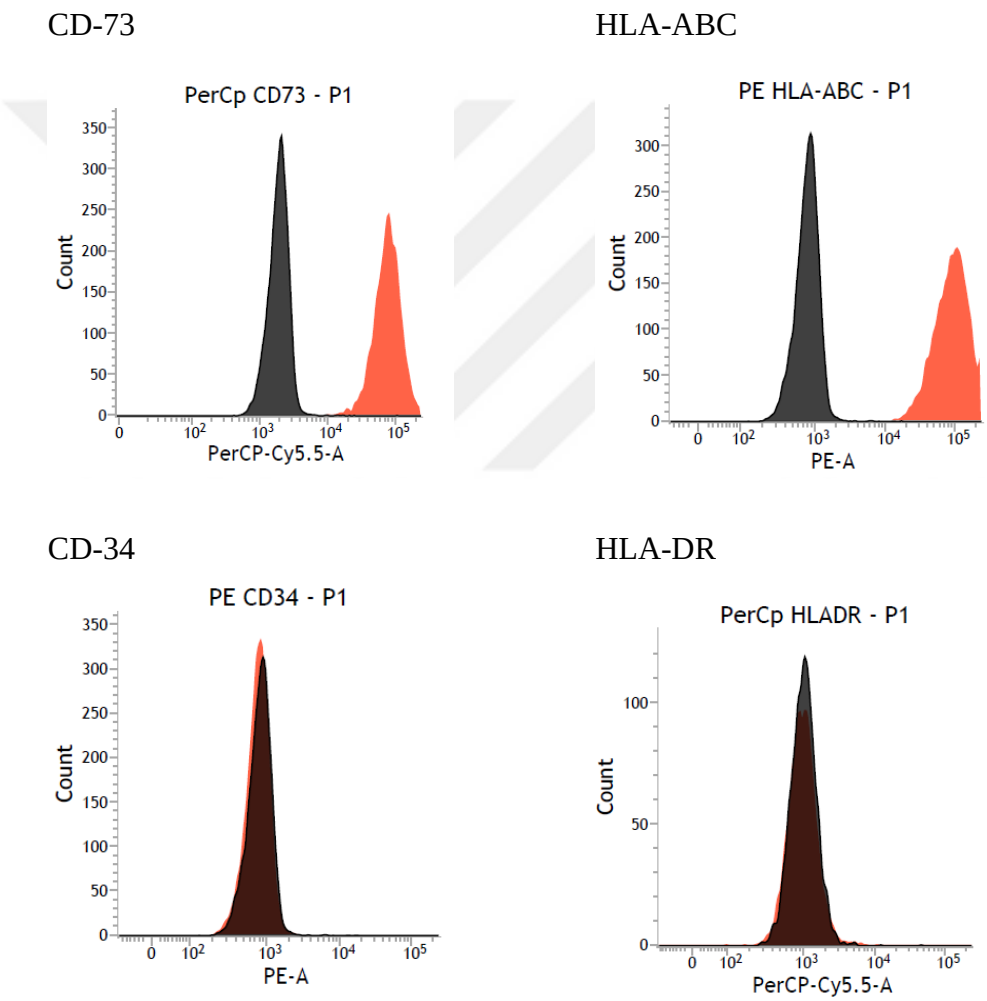

Figure 28. The representative histograms of flow cytometry results for different antigen expression: positive expression of CD73 and HLA-ABC, negative expression of CD34 and HLA-DR.

Table 12. The expression of cell surface antigens of dental pulp derived DP-MSCs

Surface Antigen	Surface Antigen	DP MSC (%)
MSC Markers	CD105	96.73 ± 4.12
	CD73	99.67 ± 0.46
	CD90	99.87 ± 0.14
	CD44	99.87 ± 0.17
Immunogenic Antigens	HLA-DR	0.06 ± 0.08
	HLA-ABC	97.65 ± 3.27
Hematopoietic Lineage Marker	CD34	0.17 ± 0.19
	CD45	1.41 ± 0.67

*Percentage of the positive cells /Intersection of isotype control and positive sample considered for calculation of absolute positives)

4.3.1.3 Growth kinetics of human DP-MSC

The growth curve of DP-MSCs was obtained by plotting the logarithmic number of cells against time (Figure 29). The number of cells was determined by WST-1 assay using calibration curve (Appendix 8.2 A1). The curve showed that DP-MSCs reached growth saturation after 150 h of incubation. The doubling time of the cells which shows the time needed to double the number of cells was determined as 27.2 h using the log phase of the curve.

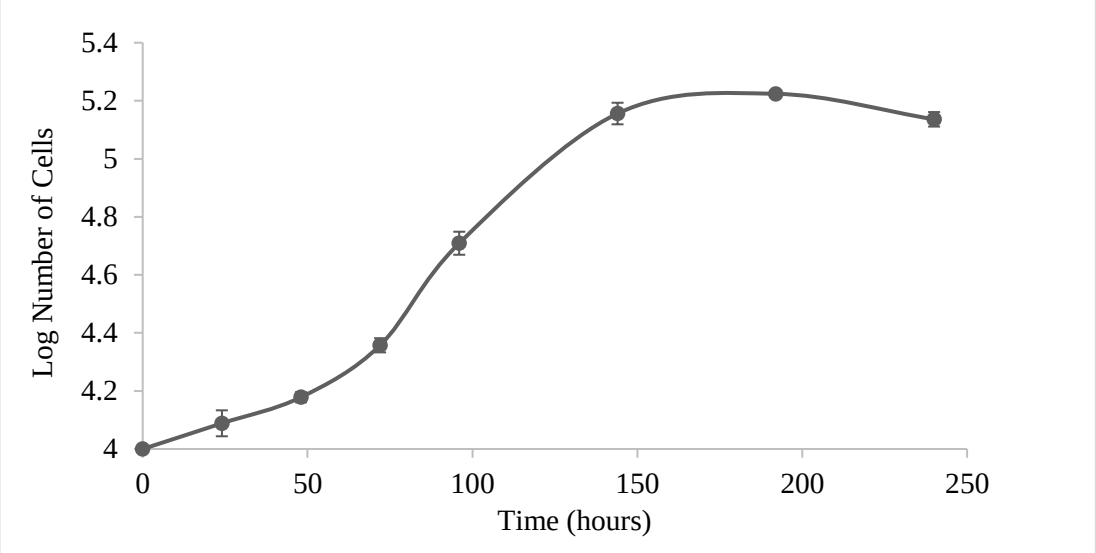

Figure 29. Growth curve of the DP-MSCs

4.3.1.4 Osteogenic differentiation of human DP-MSC

Mesenchymal stem cells have a tendency to differentiate into osteogenic, chondrogenic and adipogenic cells (116) Therefore, in order to confirm that the isolated DP-MSCs display MSC behavior osteogenic differentiation was conducted. ALP assay and von Kossa staining methods were used to determine osteogenic differentiation of the isolated DP-MSCs.

Alkaline phosphatase (ALP) is an enzyme produced by osteoblasts and takes role in bone mineralization. Therefore, in this study ALP activities of differentiated DP-MSCs after osteogenic induction and undifferentiated DP-MSCs as control were determined. After 21 days of osteogenic induction differentiated cells showed 9.15 times higher specific ALP activity compared to undifferentiated MSC control group (Figure 30).

Moreover, von Kossa staining method was used to detect calcium deposition formed by osteogenic differentiation. Compared to the undifferentiated control cells, in the osteogenic differentiated cells the calcium depositions stained with silver nitrate were seen as dark colored regions (Figure 31)

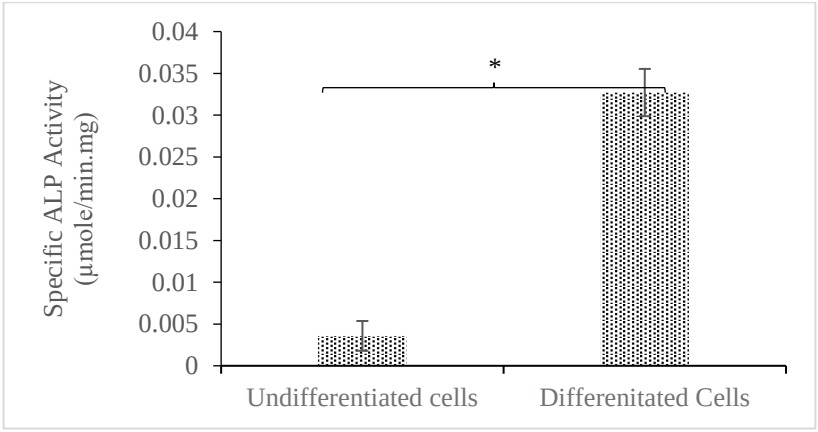

Figure 30. Specific ALP activity of the differentiated DP-MSCs after 21 days of osteogenic induction and the undifferentiated (control) DP-MSCs culture with the growth medium. (* p value < 0.05)

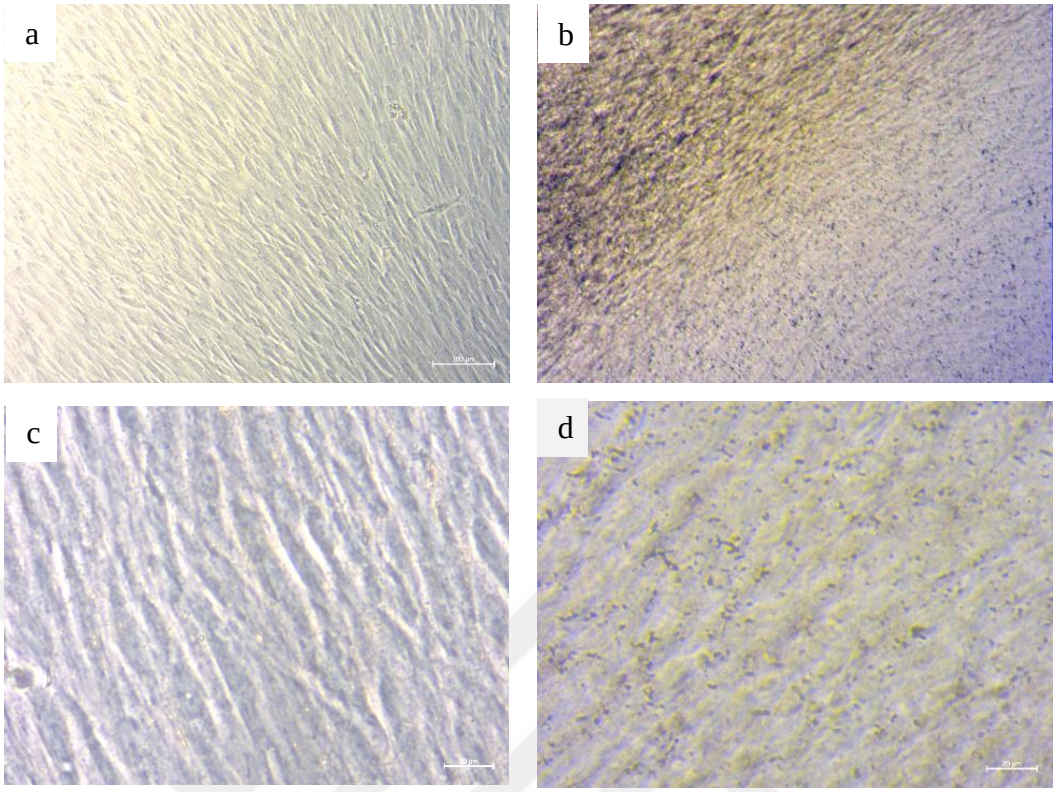

Figure 31. Light microscope images taken after von Kossa stainining of (a, c) DP-MSCs that were cultured for 21 days with the growth medium in undifferentiated state and (b, d) DP-MSCs with osteogenic induction medium. Magnifications: (a, b) X10, (c, d) X40; scale bars: (a, b) 100 μm, (c, d) 20 μm.

4.3.1.5 Chondrogenic differentiation of human DP-MSC

Alcian Blue which stained glucosaminoglycans and proteoglycans of the cartilage tissue as in blue color was used to evaluate chondrogenic differentiation. The differentiated DP-MSCs after 21 days of chondrogenic induction and the control, undifferentiated DP-MSCs, were stained with Alcian Blue and examined under light microscope (Figure 32). Compared to the undifferentiated DP-MSCs, the differentiated cells by chondrogenic induction displayed intense blue colored regions indicating the presence of cartilage tissue specific ECM components.

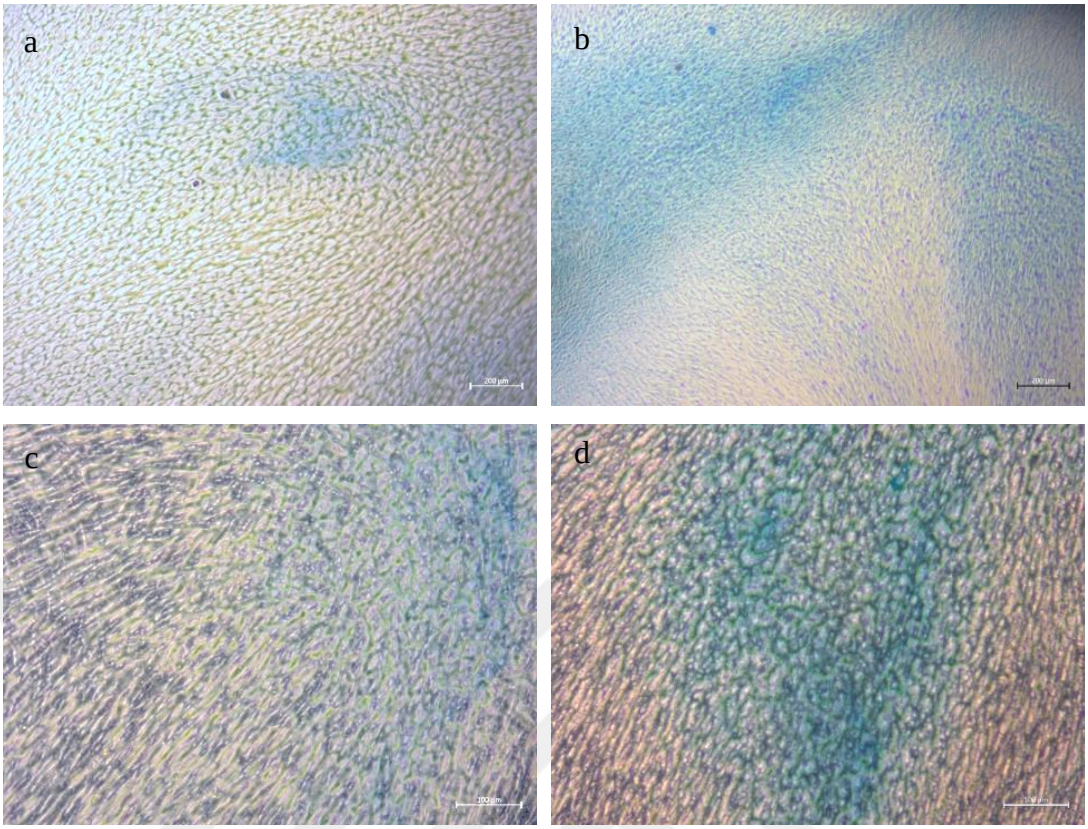

Figure 32. Light microscope images obtained after Alcian Blue stainining of (a, c) DP-MSCs that were cultured for 21 days with the growth medium in undifferentiated state and (b, d) DP-MSCs with chondrogenic induction medium. Magnifications: (a, b) X4, (c, d) X10; scale bars: 100 µm.

4.3.2 Spherical culture for chondrogenic differentiation

4.3.2.1 Culture of DP-MSCs as spheroids

Culturing of chondrogenic cells is difficult with standard cell culture procedures, since they have a tendency to de-differentiate into fibroblast-like cells and lose their cartilage-specific phenotypes in monolayers (117). In monolayer cultures, chondrogenic cells downregulate the synthesis of type II collagen during cell division and start to synthesize type I collagen, thus changing the proteoglycan synthesis pattern (118). There are culture conditions which would allow to keep chondrocyte phenotype of chondrogenic cells *in vitro*; (i) high initial plating density, (ii) using growth hormone supplements and (iii) doing suspension/pellet culture (119).

In this study, spheroids were formed using DP-MSCs and chondrogenic induction was done as mentioned in Section 3.2.3.3.1. It was observed that spheroids were successfully formed within a day (Figure 33). In addition, it was seen that their size was around 670 µm in diameter on 21st day of culture.

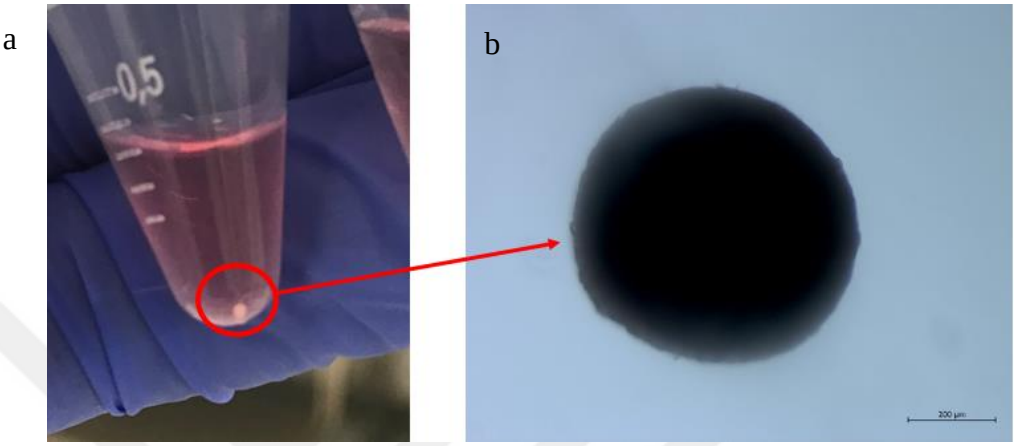

Figure 33. (a) Image of newly formed spheroid (day 1) that was indicated within red circle and (b) light microscope image of the spheroid (21 days). Magnification: (b) X10; scale bar: 200 µm.

4.3.2.1.1 Evaluation of chondrogenic differentiation with Alcian Blue

The most appropriate chondrogenic induction medium was determined by staining spheroids with Alcian Blue after their culture in three different induction media for 21 days (Figure 34). Compared to control group, undifferentiated cells, spheroids treated with each induction media stained intensely blue colored, which means that all induction media lead to chondrogenic differentiation at a certain level. However, the most prominent blue colored staining was seen in spheroids cultured with chondrogenic induction medium 1 among the others. As a conclusion, chondrogenic induction medium 1 was selected to be used for the chondrogenic differentiation of the spheroid culture in the further studies.

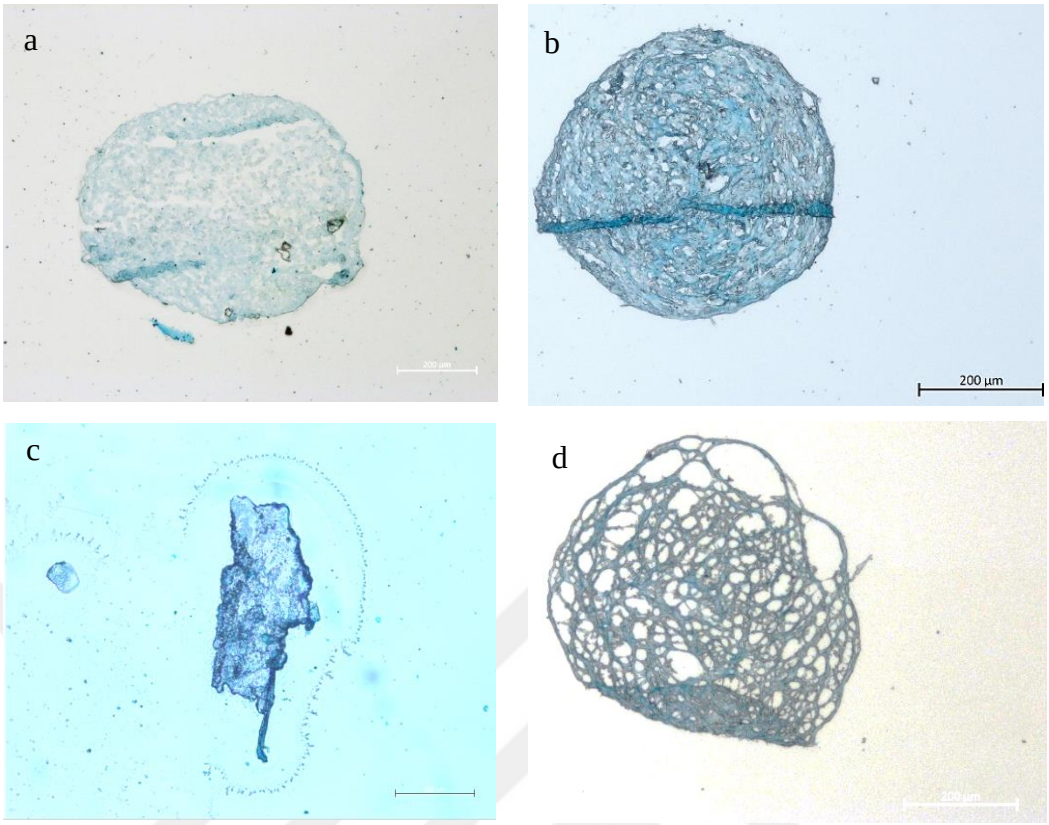

Figure 34. Light microscope images obtained after Alcian Blue staining of the spheroid cryosections. The spheroids cultured with (a) the growth medium (control), and with different chondrogenic induction mediums as (b) medium 1, (c) medium 2 and (d) medium 3. Magnifications: X10; scale bars: 200 µm

4.3.2.1.2 Evaluation of chondrogenic differentiation by immunostaining

After chondrogenic differentiation of spheroid's cells using the determined chondrogenic induction medium mentioned in Section 4.3.1.2., the expression of cartilage specific markers such a s collagen type II and aggrecan was investigated by immunostaining. It was seen that there was a significant expression of collagen type II and aggrecan in chondrogenic differentiated cells compared to DP-MSCs cultured with the growth medium (Figure 35). The immunostaining results also showed that the determined chondrogenic induction medium 1 provided chondrogenic differentiation of DP-MSCs with the spheroid culture.

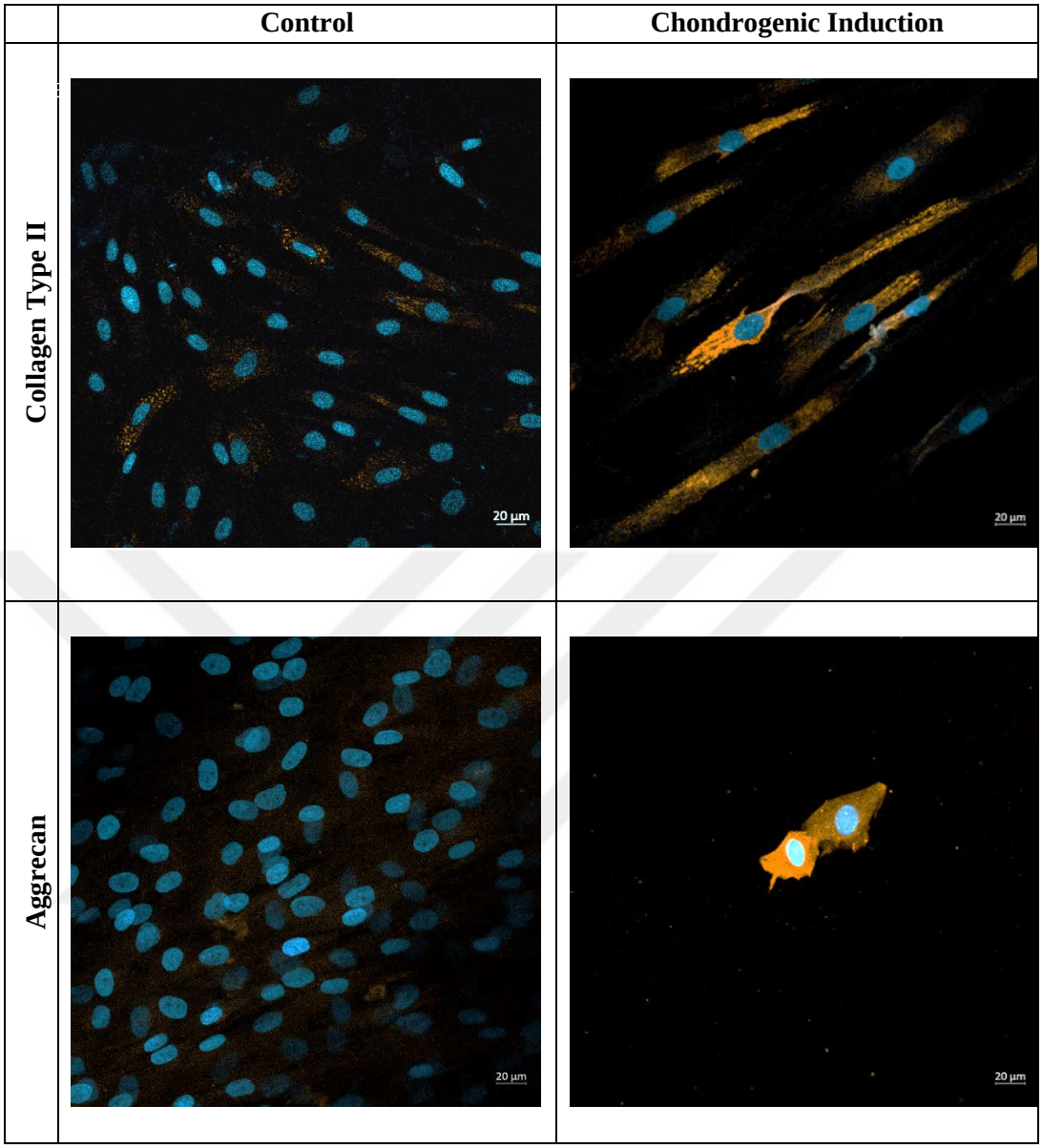

Figure 35. Immunostaining analysis of collagen type II and aggrecan expressions of DP-MSCs cultured with growth medium (control, undifferentiated cells) and with the chondrogenic induction medium for 21 days. Magnifications: 20X; scale bars; 20 µm

4.3.3 Cell behavior on the multilayered osteochondral scaffolds

4.3.3.1 Viability, proliferation and organization of DP-MSCs on the bone part of the scaffold

Live/Dead assay, MTS Assay and Phalloidin/DAPI staining were performed to investigate the viability, proliferation and organization of DP-MSCs within the β-TCP coated bone part of the multilayered scaffold, respectively.

At 5 days of DP-MSCs culture on the β-TCP coated bone part of the multilayered scaffold Live/Dead assay and Phalloidin/DAPI staining were performed. Live/Dead assay results indicated that allmost all cells were alive and the ratio of dead cells to live cells was very low (Figure 36). Both analyses showed that the cells adhered homogeneously to all filaments of the scaffolds and the cells were aligned along the filaments by sensing the topography (Figure 36 and 37). In addition, it was seen that the cells made contact with each other, which is a very important to enhance cell proliferation. In addition, it was observed that there was a high cell population also in the deep layers of the scaffold.

The proliferation and organization of DP-MSCs on the β-TCP coated bone part of the scaffold were studied at 1, 7, 14 and 21 days by MTS and Phalloidin/DAPI staining, respectively. MTS results showed that the number of cells on these scaffolds increased by time (Figure 38). The cells could survive and proliferated on these scaffolds, eventhough there was an insignificant increase in cell number on day 14 and 21. This may be a result of lack of space on the scaffold for cells to grow and start to detach from surface (Figure 38d). The significant increase in cell number by time on these scaffolds was also indicated in Phalloidin/DAPI staining (Figure 39). CLSM micrographs also revealed that the cells were spread all over the scaffold and made contact with each other. Moreover, it was seen that the cells preserved their alignment along the filaments even over time.

.

For the evaluation of the barrier-like function of the calcified cartilage part of the multilayered scaffolds, DP-MSCs were seeded onto the bone part and examined with the Phalloidin/DAPI staining after 5 days of culture as mentioned at 3.2.3.5.1. The multilayered scaffold was cut horizontally along the calcified cartilage part and the bone and cartilage parts were examined separately with CLSM. It was observed that the cells adhered to the filaments even at the deeper levels of the bone part (Figure 40a). However, almost no cells were seen on the cartilage part of the scaffolds (Figure 40b). This proved that the cells were not able to penetrate through the calcified cartilage part, as was intended. This result confirmed the ability of the calcified cartilage part in preventing the cell migration from the bone side to the cartilage part, as it was intended.

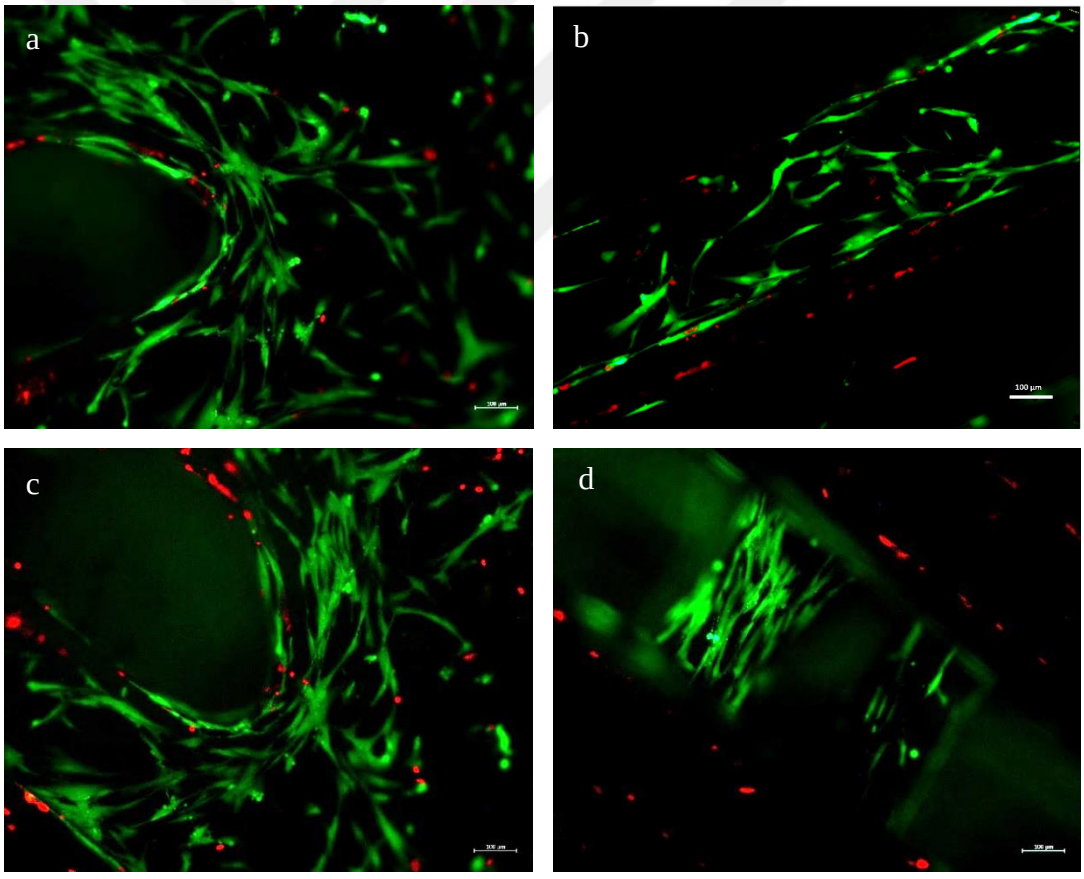

Figure 36. Fluorescene micrographs of DP-MSCs after application of Live (green)-Dead (red) assay. DP-MSCs cultured on the β-TCP coated bone part of the multilayered scaffold for 5 days. Magnifications: X10; scale bars: 100 µm

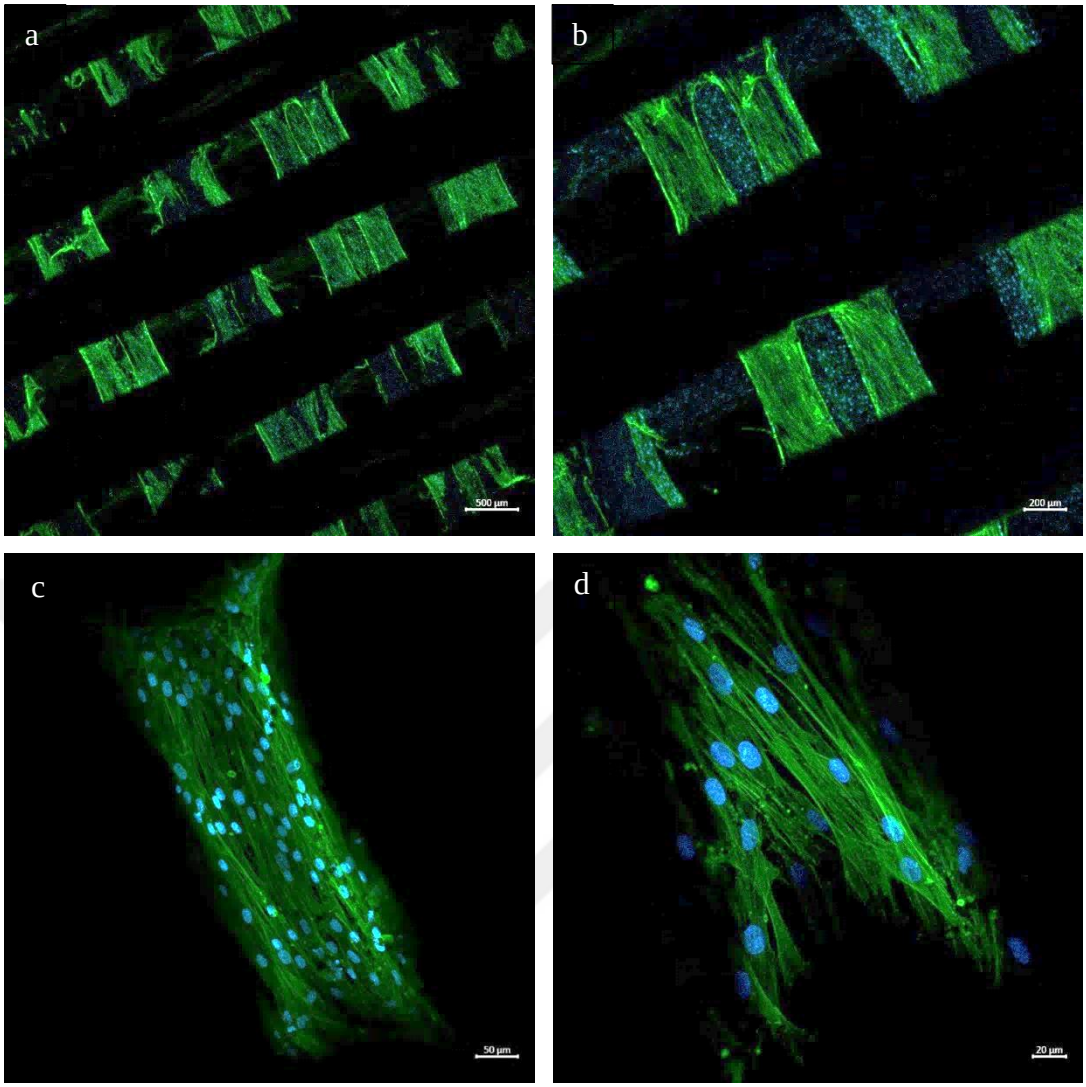

Figure 37. CLSM images of DP-MSCs stained with Phalloidin (green)-DAPI (blue) . DP-MSCs on the β-TCP coated bone part of the multilayered scaffold at day 5 of the culture. Magnifications: (a) X2.5, (b) X5, (c) X10, (d) X20; scale bars: (a) 500µm, (b)200µm, (c) 50 µm, (d) 20µm

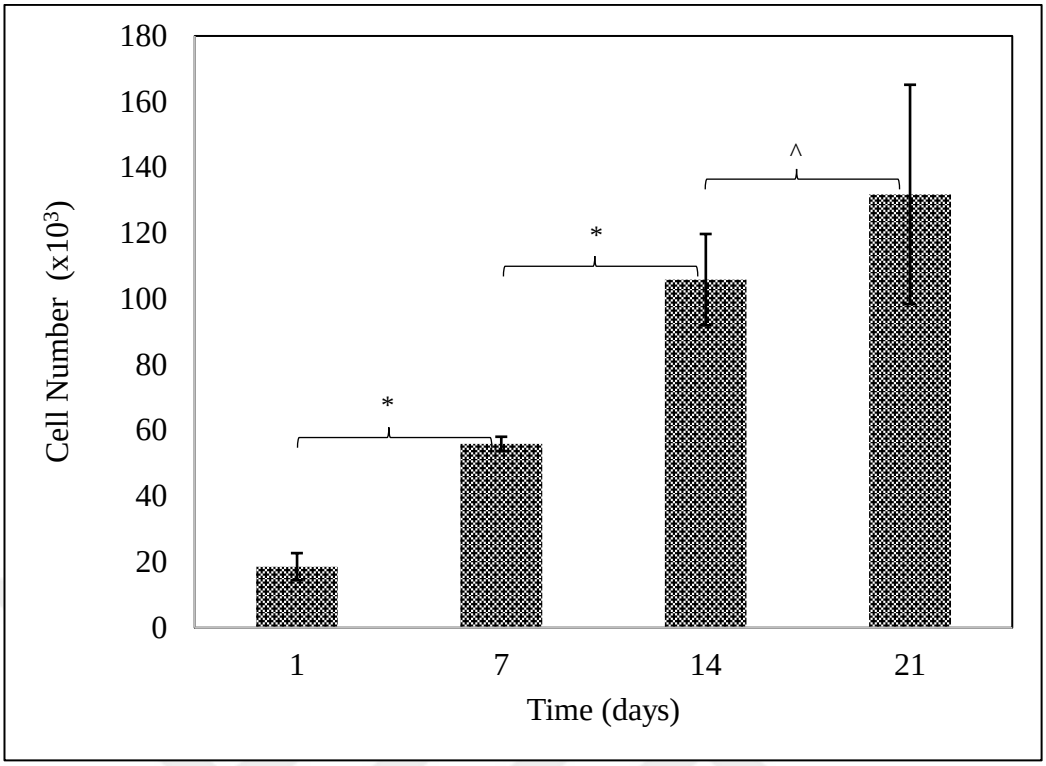

Figure 38. Proliferation of DP-MSCs cultured on β-TCP coated bone part of multilayered scaffold. (* p value < 0.05, ^ p value > 0.05)

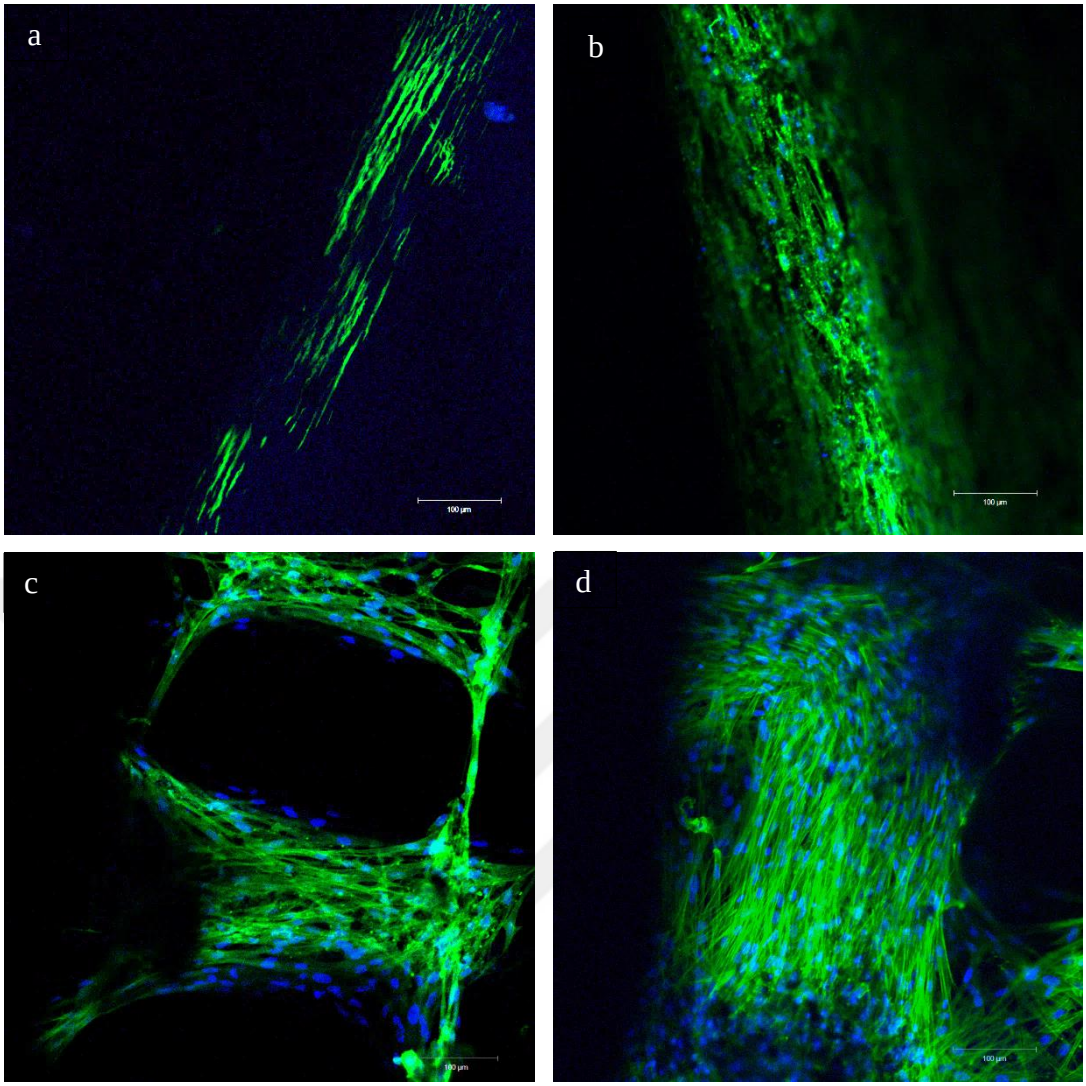

Figure 39. CLSM images of DP-MSCs stained with Phalloidin (green)-DAPI (blue). DP-MSCs on the β-TCP coated bone part of the multilayered scaffold at (a) day 1, (b) day 7, (c) day 14, (d) day 21 of the culture. Magnifications: 10X; scale bars: 100 µm.

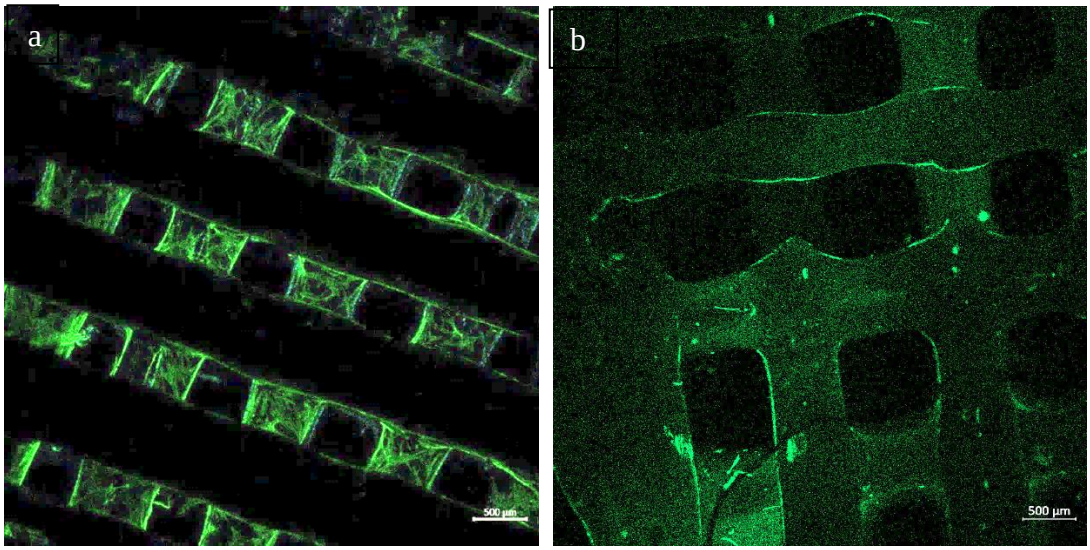

Figure 40. CLSM images of DP-MSCs stained with Phalloidin (green)/DAPI (blue). Images from (a) the β-TCP coated bone and (b) the cartilage parts of the multilayered scaffolds after seeding DP-MSC cells onto the bone part. Magnifications: X2.5, scale bars: 500µm

4.3.3.2 Evaluation of cell differentiation on the bone part of the multilayered scaffold

DP-MSCs were seeded on the β-TCP coated bone part of the scaffolds and cultured in the osteogenic induction medium for 21 days as mentioned in Section 3.2.3.5.2. Osteogenic differentiation of the cells on these scaffolds was evaluated via ALP assay, Alizarin Red staining and mineralization assay using tetracycline.

As mentioned before, ALP is an extracellular enzyme secreted from the osteogenic cells during the early stages of biomineralization and the produced amount of this enzyme is used as an osteogenic indicator in *in vitro* studies. Specific ALP activity results were presented in Figure 41. It was revealed that DP-MSCs on the scaffolds showed higher expression of specific ALP activity when cultured in osteogenic induction medium compared to the specific ALP activity of undifferentiated cells cultured in growth medium on the scaffolds and TCPS. Slightly high error bars of the specific ALP activity results might be due to trapping of the ALP product in the pores of the scaffold and inability to read the real amount of the product.

Alizarin red staining was performed to determine osteogenic differentiation via the demonstration of calcium phosphate deposition on scaffolds. It was observed that the bone part of the multilayered scaffold that housed DP-MSCs cultured in the osteogenic induction medium was intensely colored red after Alizarin Red staining (Figure 42a). However, the scaffold containing DP-MSCs that were cultured in the growth medium and cell-free scaffold used as a control was not stained significantly with Alizarin Red (Figure 42b and c). The results indicated that DP-MSCs differentiated into osteogenic cells on these scaffolds in the presence of osteogenic induction medium, and they produced the calcium phosphate deposition seen in red region on the scaffolds. Mineralization was also shown by labeling the formed calcium phosphate with tetracycline which is a widely used method for mineralization studies. CLSM micrographs showed that DP-MSCs cultured in the osteogenic induction medium with tetracycline gave fluorescence signals on the surface of the scaffolds (Figure 43b and d). The scaffolds housing undifferentiated cells without tetracycline application was used as a control, and it was indicated that there was no indication of autofluorescence signal from the scaffold or cells (Figure 43 a and c). In conclusion, all evaluation methods confirmed the osteogenic differentiation of DP-MSCs on the bone part of the scaffolds by osteogenic induction.

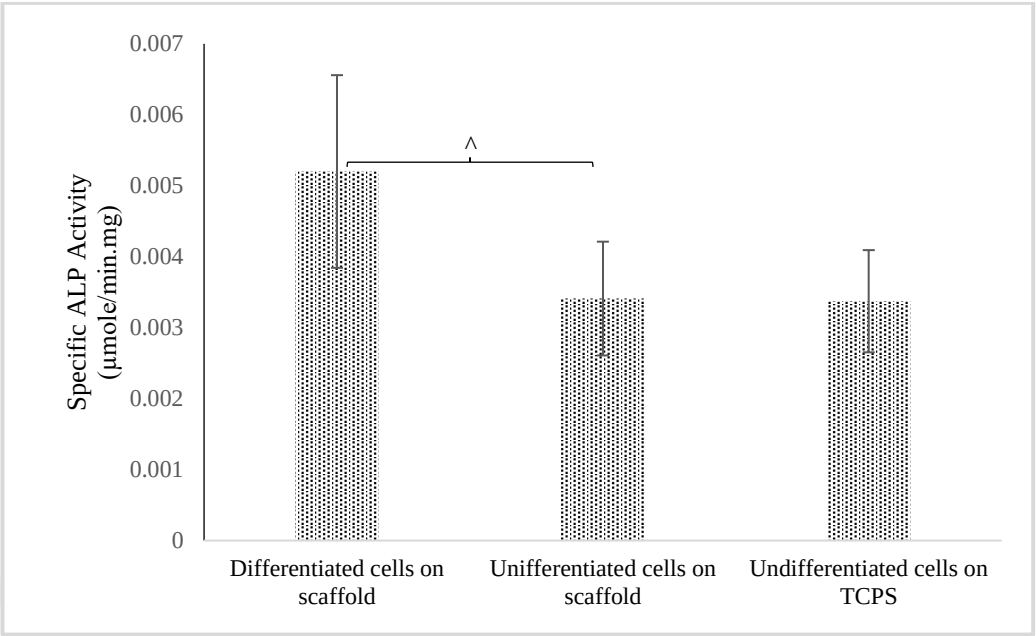

Figure 41. Specific ALP Activity of the cells. Differentiated DP-MSCs cultured with osteogenic medium and undifferentiated cells cultured with the growth medium on β-TCP coated bone part of the multilayered scaffold. DP-MSCs cultured with the growth medium on TCPS. (^ p value > 0.05)

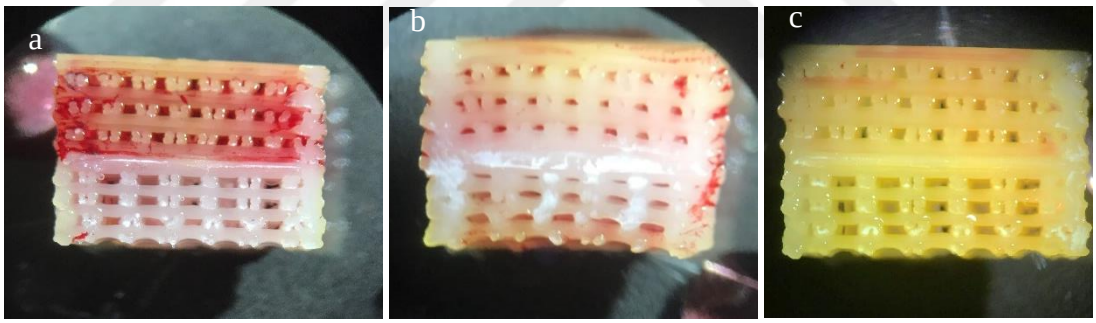

Figure 42. Stereomicrographs of the multilayered scaffolds after Alizarin Red staining. β-TCP coated bone part of the scaffolds were seeded with DP-MSCs and the cells were cultured (a) with osteogenic induction medium and (b) with the growth medium. (c) Cell-free scaffolds as a control for staining.

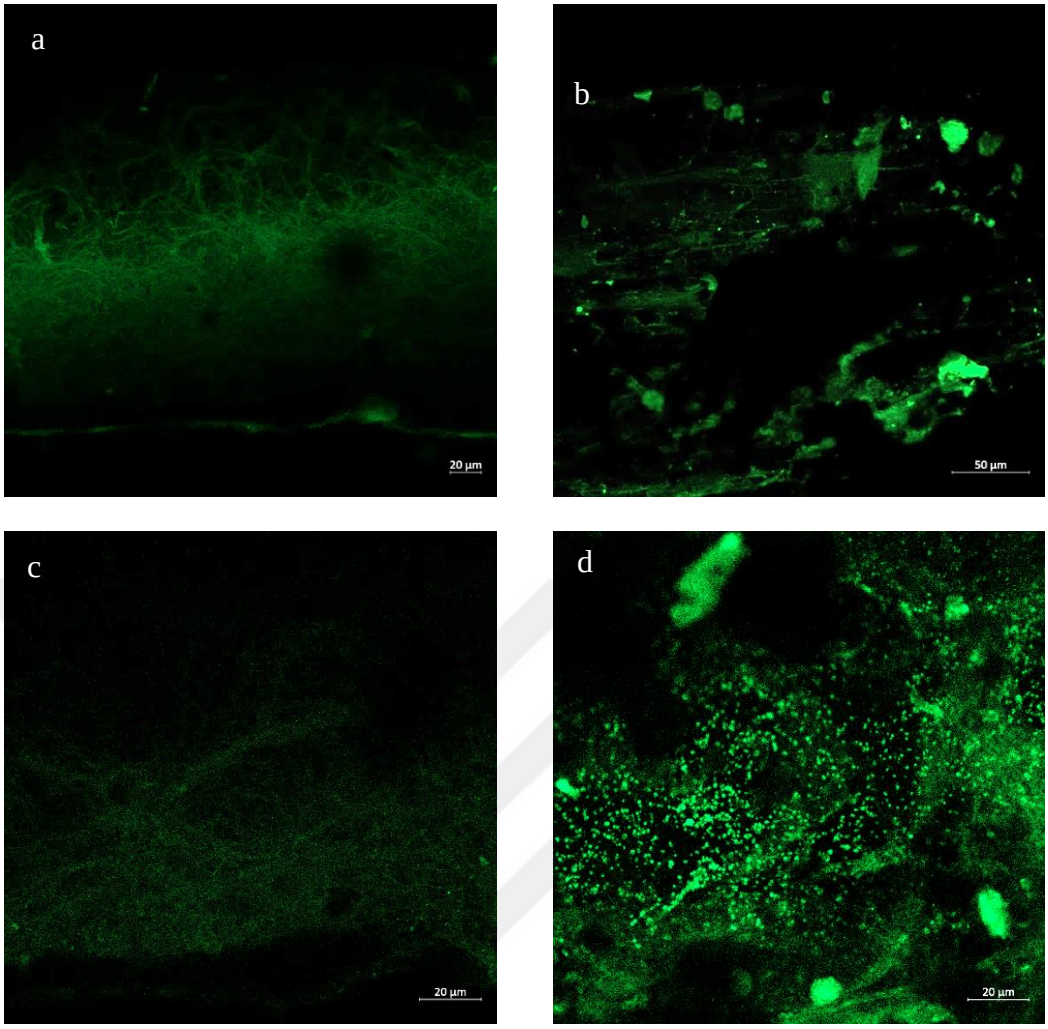

Figure 43. CLSM images of DP-MSCs on the bone part of the multilayered scaffold. (a, c) Undifferentiated cells without tetracycline application, (a) control for autofluorescence of cells and scaffolds. (b, d) Differentiated cells to which tetracycline was applied during osteogenic induction. Magnifications: (a, b) X20 (c, d) X40; scale bars: (b) 50 µm, (a, c, d) 20 µm.

4.3.3.3 Viability of cells after co-culture within the multilayered scaffold

DP-MSCs were cultured in the osteogenic induction medium for 21 days on the bone part of the osteochondral scaffolds, then hydrogel carrying chondrogenic cells of spheroid culture were placed into the cartilage part of the scaffold, and osteogenic and chondrogenic cells were co-cultured for a week (day 21-28 of culture) on the multilayered scaffolds to obtain osteochondral tissue equivalent. The cell viability and proliferation of both cells in the osteochondral tissue equivalents were studied by applying MTS assay. For the co-culture samples the scaffolds were cut in half horizontally along the calcium cartilage barrier and MTS assay was performed to the cartilage and the bone parts separately. In addition, inorder to check the chondrogenic cells viability on the scaffolds a separate set of samples prepared by loading chondrogenic cells with hydrogel to the cartilage part and MTS was done after one day. The proliferation results of the cells on the bone and the cartilage part of the osteochondral tissue equivalents were presented in Figure 44 and 445, respectively. It was observed that the number of DP-MSCs were significantly increased by time even in the presence of the chondrogenic induction medium (Figure 44). It was revealed that co-culture of the osteogenic cells with chondrogenic cells on the osteochondral scaffolds slightly decreased the rate of proliferation but still there was an increase in the number of the osteogenic cells at the end of co-culture on day 28. It was seen that despite the low chondrogenic cell number on the cartilage part of the scaffolds the cells were significantly increased in number when co-cultured with the osteogenic cells on the scaffolds (Figure 45).

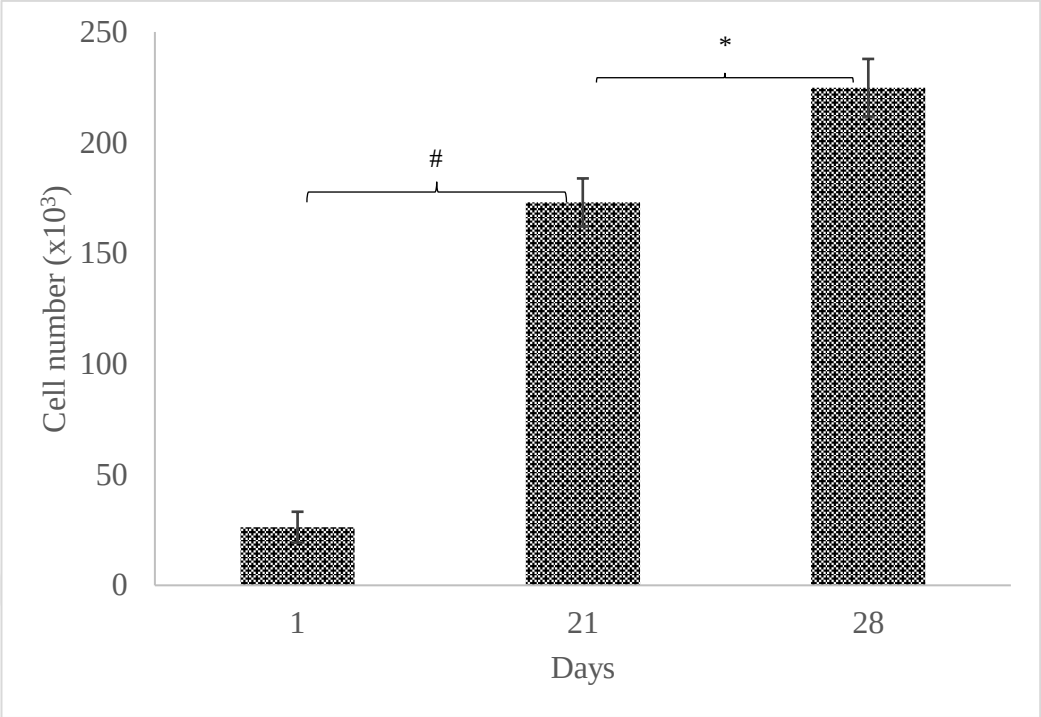

Figure 44. Proliferation of DP-MSCs on the bone part of the multilayered osteochondral scaffold. The cells were cultured with osteogenic induction medium for 21 days (Day 1- Day 21) followed by co-culture with chondrogenic cells for 1 week (Day 28). (* p value < 0.05, # p value < 0.0001)

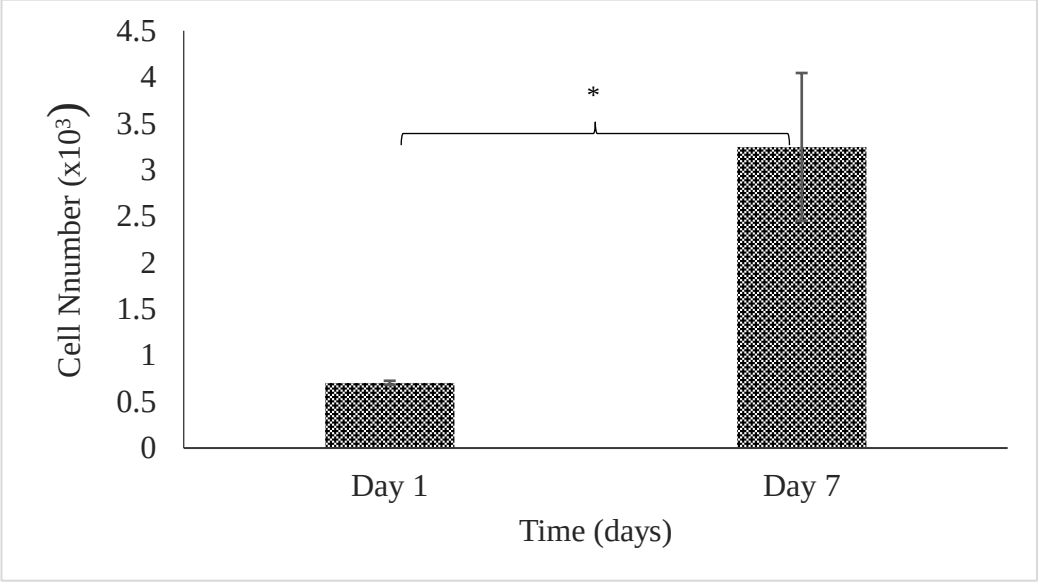

Figure 45. Proliferation of chondrogenic cells on the cartilage part of the multilayered osteochondral scaffold. The chondrogenic cells were co-cultured with osteogenic cells for 1 week (Day 28) (* p value < 0.05)

4.3.3.4 Immunostaining for the expression of osteogenic and chondrogenic markers of the cells after co-culture

The conservation of osteogenic and chondrogenic differentiation of DP-MSCs in the osteochondral tissue equivalent after co-culture was evaluated by immunostaining analysis of tissue specific osteogenic and chondrogenic markers. The undifferentiated DP-MSCs seeded on cover glass and cultured in the growth medium was used as control for immunostaining protocols.

For osteogenic differentiation osteonectin and osteopontin markers were selected. Osteonectin is a non-collagenous bone specific protein produced by osteoblasts (120) and osteopontin is a glycosated protein expressed at the early stages of osteogenesis by osteoblasts (121, 122). Immunostaining results showed that DP-MSCs, which were induced with osteoinductive stimulant for 21 days and then co-cultured with the chondrogenic cells in the chondrogenic induction medium for a week, intensely expressed the osteogenic specific markers, osteopontin and osteonectin, at protein level (Figure 46 and 47). In addition, CLSM images at lower magnifications demonstrated that the osteogenic cells preserved their alignment along the filaments of the bone part even at the end of co-culture (Figure 48). On the cartilage side, the chondrogenic cells derived from spheroid culture of DP-MSCs were immunostained against cartilage tissue specific markers, aggrecan and collagen type II, to determine whether they retained their phenotype under co-culture conditions. It was observed that the chondrogenic cells was significantly expressed both aggrecan and collagen type II markers despite of co-culture with the osteogenic cells on the osteochondral scaffolds (Figure 49 and 50). The immunostaining results showed that even after co-culture on the osteochondral scaffolds both osteogenic and chondrogenic cells preserved their differentiated state by the expression of each cells' tissue specific markers. Consequently, the results of site-specific tissue formation at cartilage and bone part indicated that multilayered, bifunctional osteochondral tissue substitute was obtained successfully.

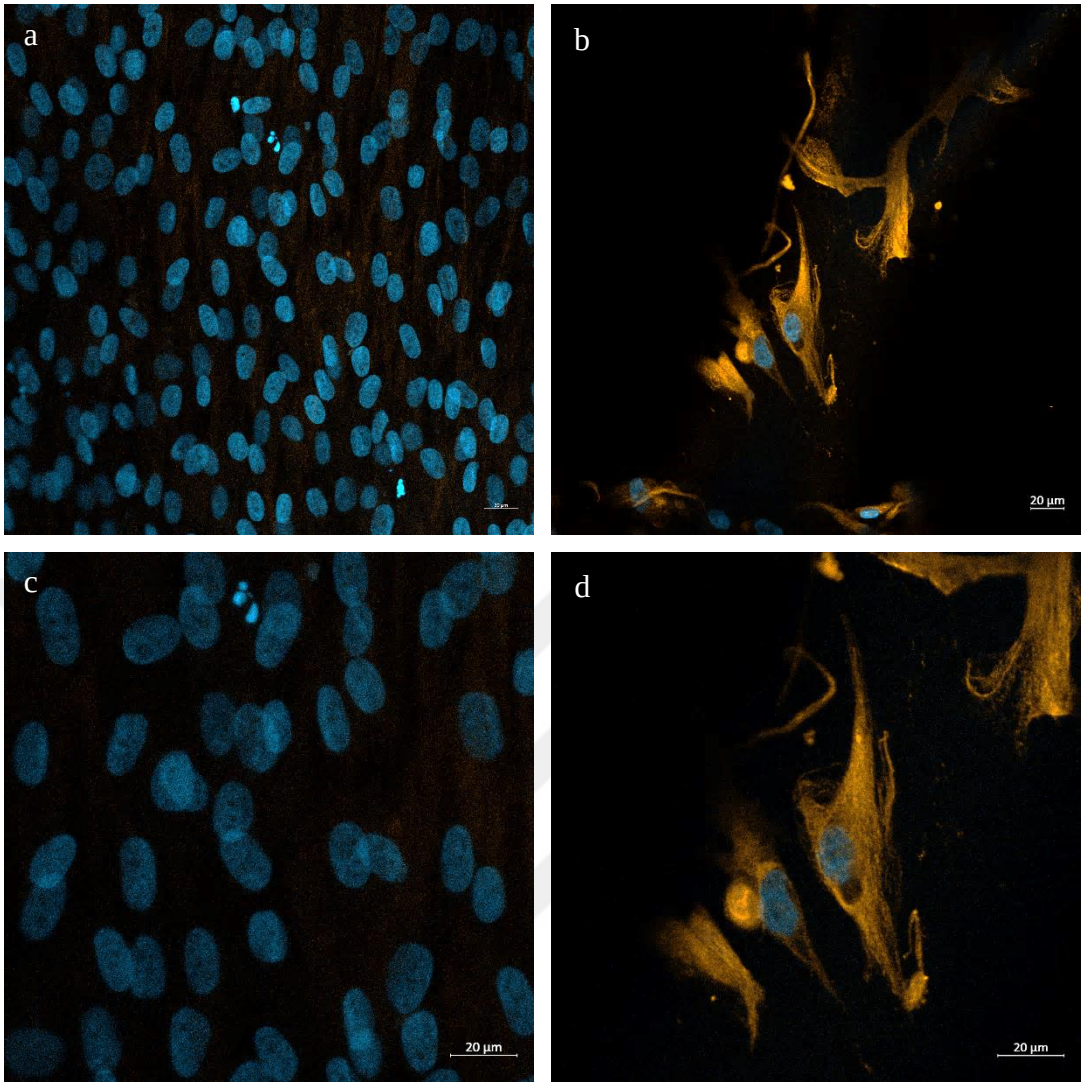

Figure 46. CLSM images of the cells immunostained against osteopontin (orange) and counterstained with DAPI for nucleus (blue). (a,c) Undifferentiated DP-MSCs on the cover glass (control) and (b,d) differentiated DP-MSCs on the bone part of the multilayered scaffold. Magnifications: (a,b) X20 (c,d) X40; scale bars: 20µm.

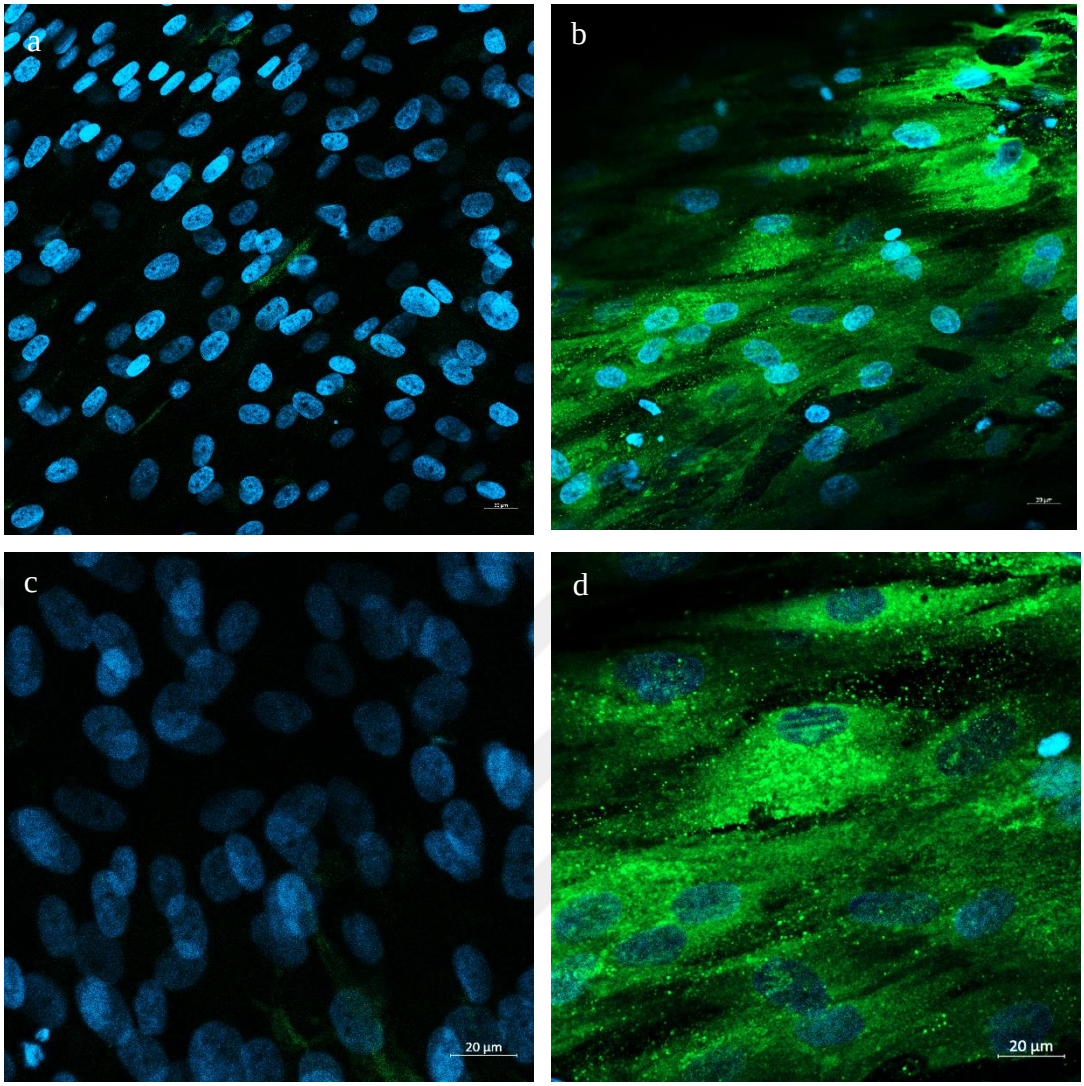

Figure 47. CLSM images of the cells immunostained against osteonectin (green) and counterstained with DAPI for nucleus (blue). (a,c) Undifferentiated DP-MSCs on the cover glass (control) and (b, d) differentiated DP-MSCs on the bone part of the multilayered scaffold. Magnifications: (a,b) X20 (c,d) X40; scale bars: 20µm.

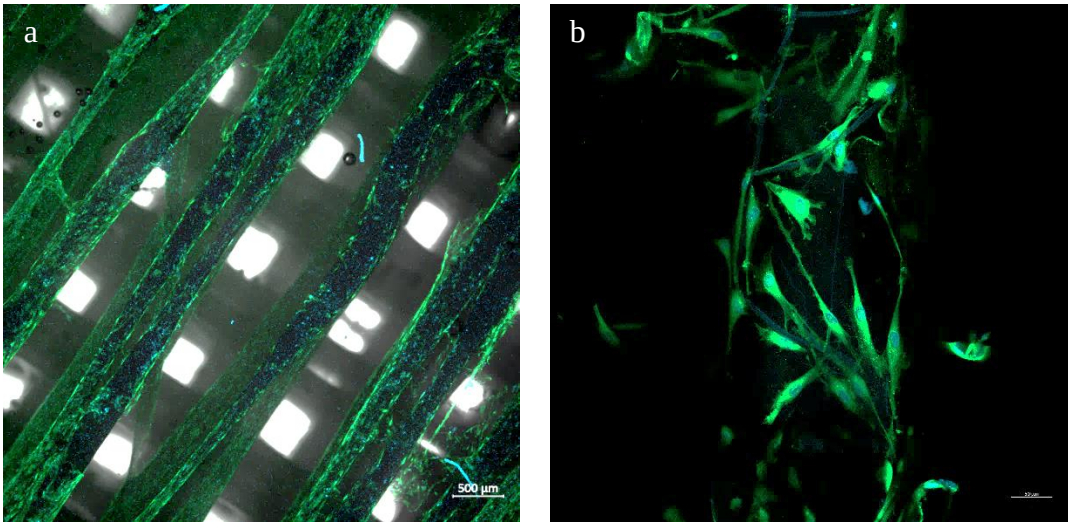

Figure 48. CLSM images of the differentiated DP-MSCs on the bone part of the multilayer scaffold after immunostaining against osteonectin (green) and counterstained with DAPI for nucleus (blue). Magnifications: (a) x2.5, (b) X10; scale bars: (a) 500 µm, (b) 50 µm.

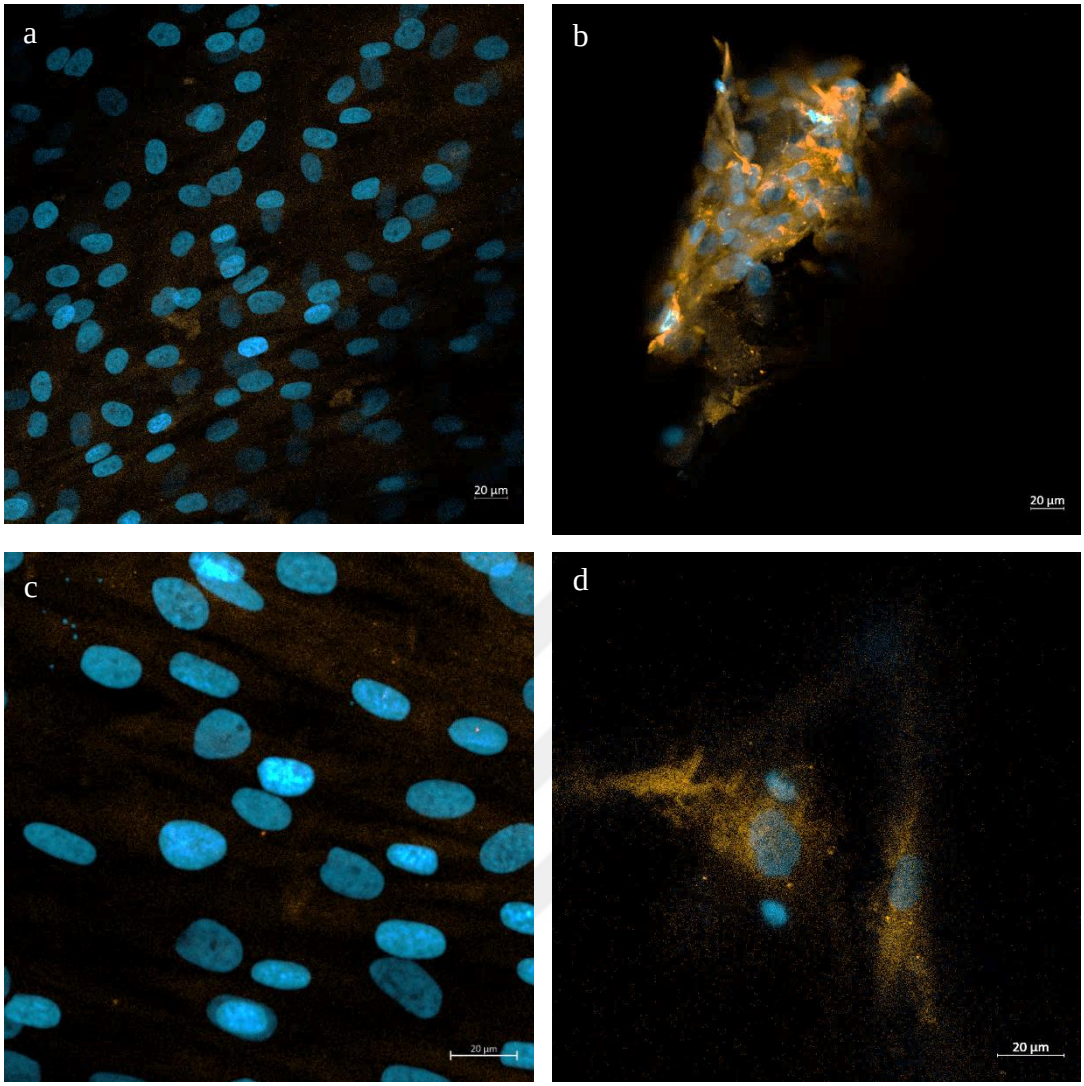

Figure 49. CLSM images of the cells immunostained against aggrecan (orange) and counterstained with DAPI for nucleus (blue). (a,c) Undifferentiated DP-MSCs on the cover glass (control) and differentiated DP-MSCs on the cartilage part of the multilayered scaffold. Magnifications: (a,b) X20 (c,d) X40; scale bars: 20µm.

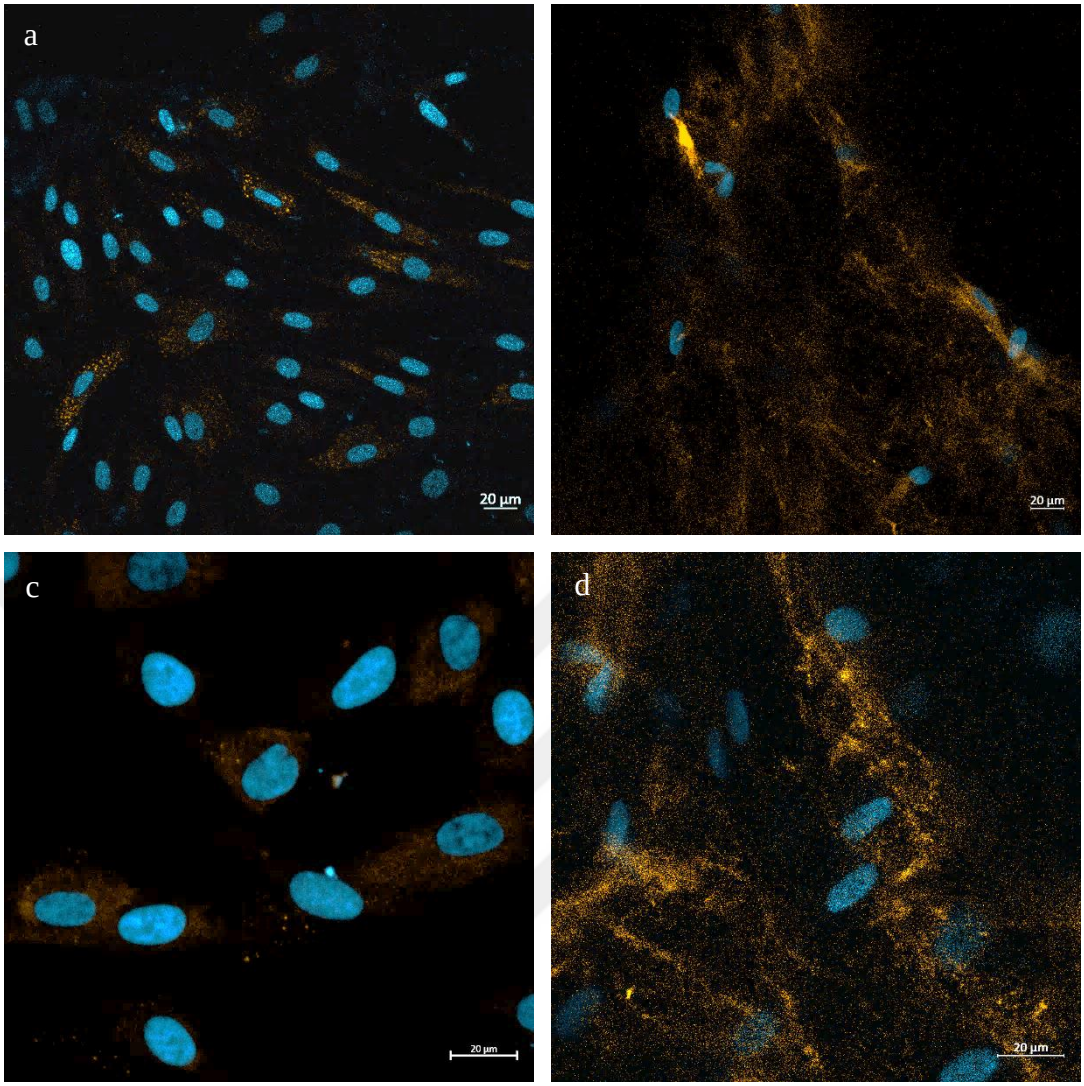

Figure 50. CLSM images of the cells immunostained against collagen type II (orange) and counterstained with DAPI for nucleus (blue). (a, c) Undifferentiated DP-MSCs on the cover glass (control) and differentiated DP-MSCs on the cartilage part of the multilayered scaffold. Magnifications: (a, b) X20 (c, d) X40; scale bars: 20µm.

5 DISCUSSION

Osteochondral defects may be caused by trauma or degenerative diseases such as osteoarthritis. Osteoarthritis is the most common musculoskeletal disease seen worldwide. OCDs are characterized by the unbalanced degeneration of articular cartilage and subchondral bone, causing swelling, pain, and joint immobilization (54). Even minor damage in the articular cartilage can lead to a full osteochondral defect reaching the subchondral bone, and if not treated or treated inappropriately it can result in an end-stage of OA and loss of joint function (4). There are several clinical approaches for the treatment of OCD. The current approach for the treatment of OCD involves harvesting an autologous OC graft from the non-load bearing part of the joint and implanting it on the defect site (e.g mosaicplasty). This approach has drawbacks such as donor site morbidity, lack of suitable healthy tissue at the joint, recurrency and failure in long-term outcomes. It has been reported that there is a 51% chance of failure in 8.4 years (123) that shows the need for repetitive surgeries for younger patients. Current clinical treatments are only palliative solutions, and for now, there is not seen any permanent solution for the regeneration of osteochondral tissue capable of withstanding joint loading in long term (124). Osteochondral tissue is a well-organized avascular and aneural tissue that ensures smooth joint movement and withstands high joint loading (125). It is a highly functionalized, heterogeneous tissue consisting of the articular cartilage, the calcified cartilage transitional zone, and the subchondral bone. Due to the avascular nature of the articular cartilage, it has a very low self-repairing capacity, while bone has an inherent regeneration potential as well as exhibits a continuous remodeling through adult time. Despite the structural and functional differences in its layers, the OC tissue coexists as a single functioning unit with extraordinary properties (83).

Osteochondral tissue engineering aims to create a tissue substitute that can guide the simultaneous regeneration and remodeling in the dissimilar layers of the osteochondral unit (57). In order to achieve a successful regeneration at the osteochondral defect, it is crucial for each layer to have mechanical and biological properties that match the surrounding tissue. Challenges in constructing a successful OC tissue substitute are related to the sophisticated properties of the native tissue such

as heterogeneous biological, biochemical, and biomechanical properties of the whole tissue, exposure to a cycle of high-pressure overtime, the limited endogenous healing capacity of cartilage, and the distinctive interaction between the bone and cartilage tissues. Despite the exciting improvements in the tissue engineering approaches, a perfect osteochondral tissue regeneration and remodeling could not have been achieved yet. The ideal osteochondral tissue substitute should be biocompatible, biodegradable, maintain the spherical chondrocyte morphology and phenotype, possess sufficient mechanical integrity, and promote cell differentiation and tissue regeneration at bone and cartilage parts simultaneously. In addition, a transitional layer between bone and cartilage layers to mimic calcified cartilage should be integrated to prevent site-specific cells' migration and not to allow vascularization of the cartilage part.

Primary ostechondral tissue engineering studies were focused on monophasic constructs for regeneration of cartilage neglecting the subchondral bone, due to having a single cell type in cartilage, and simplicity in processing (57). By harnessing the high healing capacity of the bone, a tissue formation at the implantation area was observed with monolayered approaches. However, unlike the native tissue, a homogeneous tissue formation was reported, also it was seen that a functional interface was not achieved due to the delamination and separation incidents of the cartilage phase (125). Even though these studies provide important information about the scaffold's interaction with the native tissue, the majority of these approaches lack the requirements for site-specific tissue regeneration. Moreover, it was seen that the integration of the tissue substitute was driven by the subchondral bone, and subchondral bone was vital for the successful repair of the overlying cartilage and OC defects (57). Thus, the subchondral bone was taken into consideration for further tissue engineering approaches, and bi-layered and multilayered constructs were designed. Bilayered scaffolds were capable of the regeneration of both bone and cartilage tissues simultaneously due to comprising two distinct layers with different mechanical, structural or biological properties (126). There are various biphasic scaffolds that have been studied under *in vitro* and *in vivo* conditions (127, 128). However, due to bi-layered scaffolds' lack of transitional phase between bone and cartilage layers, all osteochondral tissue requirements were not fulfilled. The calcified cartilage, a

transitional layer between bone and cartilage layers, provides structural integration while transferring and distributing the mechanical load from viscoelastic articular cartilage to stiff bone tissue. This interface of bone and cartilage is the key component in moderating the tensile, compressive, and shear forces from AC to bone (129).

Multilayered scaffolds were designed to mimic the bone, and cartilage layers and a transitional phase between them, resulting in a scaffold having a closer resemblance to the physiological structure of OC tissue. Multi-layered scaffolds can maintain cell viability and promote tissue regeneration by supplying appropriate site-specific biological and mechanical stimuli, and also provide a functional transitional zone between cartilage and subchondral bone (130). A trilayered scaffold composed of hyaluronan charged collagen fibers at the cartilaginous layer, biomineralized collagen at the osseous layer, and the same biomineralized collagen with a lower percentage of mineral at the transitional phase was developed over a ten years ago (131). Afterwards, different approaches were applied for stratification of the multilayer scaffold such as porosity, pore size, and content of minerals (81, 132-134). For instance, a single integrated multilayered construct was produced with the use of sodium alginate, chitosan, and HAp composite (132). The main challenge in construction of multilayered osteochondral tissue substitute is to provide a dissimilar tissue layer in one construct. Each layer with different biological and mechanical properties and different layers should provide different microenvironments for the site-specific cell proliferation and differentiation. In addition, each layer should have matching mechanical properties with the surrounding native tissue. In most of the studies, these different parts are generated and combined using different methods such as press-fitting, fibrin gluing, and suturing. Although these methods seem successful they create a weak point in the structure and this can lead to delamination or phase separation (67).

In this thesis study, a 3D multilayered osteochondral scaffold was designed providing different layers to promote site-specific regeneration and also having a structural integration between these layers using 3D printing. The 3D model was designed to have cartilage and bone parts with a transitional zone mimicking the calcified cartilage of native tissue.In addition, in the design of the cartilage part random

and columnar organization of the middle and deep zones were also considered. Formation of the different parts and structural integrity of the whole construct was ensured by 3D printing. The whole construct including multiple layers was 3D printed at once to prevent weak points in the scaffold structure to avoid delamination and phase separation. In addition, controlling inner architecture, porosity, and pore size of scaffolds is very difficult by conventional fabrication methods; however, all these features could be adjusted by computer-aided design programs and 3D printing. The results showed that the multilayered osteochondral scaffold having different inner structures and porosity in each layer was successfully fabricated by 3D printing. The scaffold should have appropriate pore size, porosity, and interconnection between pores to allow cell attachment, growth, proliferation, migration, and differentiation (135). The optimal pore size of the scaffold varies according to the targeted tissue. For instance, it was reported that pore sizes in the range of 300-450 μm were favorable for cell proliferation and osteogenic differentiation at the osseous part of the osteochondral scaffold (136). In this thesis study, the pore size in the bone part of the scaffold was determined as 453 ±44 μm which was close to the favorable pore size for the bone part of the osteochondral scaffold.

As mentioned above, integration of functional transitional zone between the cartilage and bone parts in the scaffolds is an important issue to better mimic native tissue, since calcified cartilage zone increases mechanical integrity, acts as a barrier to prevent cell migration and vascularization at cartilage side. The importance and the necessity of the calcified layer in tissue substitute were shown in an *in vivo* study, in which two different scaffolds with and without a transitional layer were implanted to the patellofemoral surface of rabbit (102). Microtomography imaging and histological results showed that there was a higher collagen and glycosaminoglycan content in regenerated tissue. In addition, it was reported that this compact transitional layer increased the interphase integration and enhanced the biomechanical properties of the scaffold and provided optimal microenvironment at each layer of the scaffold. In another study, the scaffolds with and without a transitional layer were implanted into an OCD model on the femoral condyles of a goat (137). Even though there was a tissue regeneration with both scaffolds, it has been reported that the organization of the

regenerated tissue was closer to the complex organization of the native tissue in the presence of transitional layer within the scaffold. In this thesis study, barrier-like, non-porous layer mimicking the calcified cartilage was integrated into the scaffold, and it was shown that it increased structural and mechanical integrity, and prevented cell migration from the bone part to the cartilage part.

The compression modulus of subchondral bone is in the range of 90-400 MPa, while the compression modulus of the cartilage is in the range of 2-10 MPa (3). In most of the studies, cartilage layer was composed of a softer construct such as natural or synthetic polymer-based hydrogels due to their hydrated nature and similarity to cartilage ECM, while osseous part contained strengthening materials such as ceramic and hard polymers. However, hydrogel constructs have weak mechanical properties thus they are not sufficient to withstand high levels of mechanical load upon implantation into damaged tissue. There are methods to enhance the mechanical properties of hydrogels such as increasing the cross-linking degree. Even though such methods can increase mechanical properties of hydrogels they might have negative effects on cellular activity within the scaffold and might inhibit ECM synthesis (138). Therefore, new fabrication strategies have been studied, and in one of that studies a PCL scaffold was combined with an alginate hydrogel to increase mechanical properties of the cartilage layer and provide a hydrated ECM mimicking the native cartilage tissue (139). In this thesis study, the chondrogenic cells were loaded with collagen-based hydrogel into the cartilage part of the multilayered scaffold to mimic the native ECM environment with its hydrated nature and components. It was observed that the bone part of our scaffold had a higher compression modulus compared to the cartilage part as intended. In addition, the compression modulus of the final scaffold with a calcified cartilage part was higher than the individual bone and cartilage parts. It was concluded that the calcified cartilage part of the scaffold increased the mechanical properties as it is in the native tissue.

PCL is an FDA-approved, biocompatible and biodegradable polymer that was selected for fabrication of the multilayered scaffold in this study due to its superior mechanical behaviors and easy-to-process properties with 3D printing because of having a low melting point (140). PCL is a widely used polymer for osteochondral

tissue engineering studies (141, 142). However, it is a hydrophilic polymer with a low bioactivity, therefore O_2 plasma treatment and β-TCP coating were done in this study to increase cell atatchment, bioactivity and osteoconductive property of the bone part of the scaffold.

In this thesis study, the electrospun fibrous mat was fixed on the cartilage part of the multilayer scaffold to mimic superficial zone of the articular cartilage. Collagen fibers at the superficial layer of the articular catilage are at high density and are organized parallel to the articulating surface. The organization and density of the collagen fibrils provides the tensile strenght against joint loading and contributes to the smooth joint movement. Also this layer acts as a barrier for large immunulogical molecules to pass from synovial fluid and creates a hypoxic environment which is essential for the metabolic activities of the chondrocytes. In one of the study, it was reported that electrospun fibrous mesh was added on the cartilage part of the multilayer scaffold to mimic superficial layer to increase the hypoxic conditions in the cartilage part and to act as a filter as in the native tissue it does (143). It was mentioned that the electrospun fiber mat improved the differentiation of MSCs into chondrocytes. This is the only study as we know which adds the electrospun mat onto the osteochondral scaffold to mimic the superficial layer

In clinical approaches and tissue engineering studies inorder to restore the OCDs, chondrocytes, which supply the function and structure of the cartilage tissue, are widely used as being the main residents of the articular cartilage (54). It has been reported that the use of chondrocytes embedded in 3D scaffolds could promote the hyaline caatilage formation (144-147). However, there are several important drawbacks with the mature chondrocytes such as low isolation efficiency, donor site mobidity and risk of infection during biopsy, low proliferation capacity and known de-differrentiation tendency of chondrocytes. For instance, the cell number required for implantation of autologous chondrocytes is around 5-30 million depending on the size of defect (148). However, only 450 000 chondrocytes can be isolated from a biopsy of 100 mg healthy cartilage. Besides, it was reported that most of the chondrocytes underwent de-differentiation in 2D expansion cultures while adapting a fibroblastic phenotype and morphology (149). Stem cells, especially MSCs, are potential cell

sources to overcome these limitiations. There are several studies that used a single cell source for bone and cartilage regeneration at different layers of the OC scaffolds. For instance, in one of the study the differentiaton of BMSCs into chondrogenic and osteogenic cells were carried out on the collagen-HAp based bi-phasic scaffold (150). In another study, adipose derived MSCs were used within the multilayered scaffold and site-specific differentiaton of ADMSCs was shown (67).

In this thesis study mesenchymal stem cells derived from dental pulp was used as a single cell source to promote site-specific cell differentiaiton at the cartilage and bone parts of the sscaffold. Dental pulp MSCs has a high potential for osteogenic differentiation and used for bone tisssue engineering studies (151, 152). Chondrogenic differentiation ability of DP-MSCs have also been shown in recent studies (109, 153). There is no report of a study which DP-MSC used for osteogenic and chondrogenic differentiation in a single scaffold for osteochondral tissue engineering. DP MSCs were preferred due to their availability, ease of harvesting without any invasion to the patients, and also their tendency to differentiate into both osteogenic and chondrogenic cells. MSCs can differentiate into ostegenic cells in monolayer cultures, while for chondrogenic differentiation it was revealed that spheroid culture methods were more suitable (107, 154). This culture system allows cell-to-cell interactions similar to the pre-cartilage condensation occurs during embryonic development (155). Therefore, in this study spheroid culture was conducted for the chondrogenic differentiation of DP-MSCs. As mentioned earlier hydrogels are widely used for the cartilage parts of the osteochondral tissue substitutes. Chondrocytes are known to be phenotypically unstable due to their susceptiblity and sensitivity to changes in their ECM microenvironment. During the development of the cartilage tissue, chondroblasts produce matrix around themselves and are entrapped within this matrix while differentiating into chondrocytes. This creates a three-dimensional ECM environment for the chondrocytes. If chondrocytes lose their 3D environment, they lose their typical protein synthesis and phenotype, which is called de-differentiation and they de-differentiate into fibroblast-like cells (156). To prevent de-differentiation of chondrocytes a scaffold should provide 3D environment as the natural ECM does (157). Hydrogels can maintain a highly hydrated 3D environment for the

chondrocytes, but they have weak mechanical properties and may fail upon implantation. In the light of these information, in this study MSC was loaded with collagen-based hydrogel to maintain their phenotypes, and then cell-loaded hydrogel was integrated into the cartilage part of 3D printed PCL construct to increase the mechanical properties of the cartilage tissue substitute. In addition, the obtained final bifunctional, multilayered osteochondral tissue substitute exhibited favorable mechanical properties, and site-specific cell differentiation was seen without de-differentiation of cells.

6 CONCLUSION

In this thesis, it was aimed to develop a bifunctional, multilayered osteochondral tissue substitute to promote simultaneous bone and cartilage tissue formation and site-specific cell differentiation at different layers to improve tissue regeneration at the defect site. The multilayered scaffold composed of cartilage, calcified cartilage, and bone parts was successfully fabricated by 3D printing, and the electrospun fibrous mesh was fixed onto the cartilage part to mimic the superficial layer of the articular cartilage. Bone and cartilage parts of the 3D printed construct were improved to promote cell proliferation, and site-specific tissue regeneration. The cartilage part was loaded with collagen-based hydrogel to enhance survival of cells loaded with hydrogel. The bone part was coated with β-TCP to enhance osteogenic differentiation. Mechanical test results showed that the bone part has a higher compression modulus compared to the cartilage part. In addition, the final osteochondral construct with a calcified cartilage part had the highest compression strength.

On the other hand, the isolated human dental pulp MSCs were characterized and their differentiation protocols were determined. DP MSCs were differentiated into osteogenic cells on the bone side for 21 days by applying osteogenic induction, and on day 21 DP MSC-derived chondrocytes loaded within the hydrogel to the cartilage side, and then the cells were co-cultured within the final construct for a week. The results showed that DP-MSCs were successfully proliferated on the scaffold and site-specific cell differentiation was accomplished mimicking the heterogenic nature of the osteochondral tissue, even after co-culture. The multilayered osteochondral tissue substitute developed in this study meets the desired properties with its heterogenic structure mimicking the native tissue layers with articular cartilage, calcified cartilage, and bone parts.

The developed bifunctional, multilayered osteochondral tissue substitute in this study has the potential to be tested in *in vivo* studies and could be a promising approach for the treatment of osteochondral defects in the clinic.

.

7 REFERENCES

1. Jimenez G, Cobo-Molinos J, Antich C, Lopez-Ruiz E. Osteoarthritis: Trauma vs Disease. Adv Exp Med Biol. 2018;1059:63-83.
2. Bodur H. Current review on osteoarthritis in Turkey and the world; epidemiology and socioeconomic aspect. Turkish Journal of Geriatrics. 2011;14.
3. Tamaddon M, Wang L, Liu Z, Liu C. Osteochondral tissue repair in osteoarthritic joints: clinical challenges and opportunities in tissue engineering. Biodes Manuf. 2018;1(2):101-14.
4. Datta P, Dhawan A, Yu Y, Hayes D, Gudapati H, Ozbolat IT. Bioprinting of osteochondral tissues: A perspective on current gaps and future trends. Int J Bioprint. 2017;3(2):007.
5. Pereira H, Cengiz IF, Vilela C, Ripoll PL, Espregueira-Mendes J, Oliveira JM, et al. Emerging Concepts in Treating Cartilage, Osteochondral Defects, and Osteoarthritis of the Knee and Ankle. Adv Exp Med Biol. 2018;1059:25-62.
6. Spencer V, Illescas E, Maltes L, Kim H, Sathe V, Nukavarapu S. Osteochondral Tissue Engineering: Translational Research and Turning Research into Products. Adv Exp Med Biol. 2018;1058:373-90.
7. Fu L, Yang Z, Gao C, Li H, Yuan Z, Wang F, et al. Advances and prospects in biomimetic multilayered scaffolds for articular cartilage regeneration. Regen Biomater. 2020;7(6):527-42.
8. Tamaddon M, Liu C. Enhancing Biological and Biomechanical Fixation of Osteochondral Scaffold: A Grand Challenge. Adv Exp Med Biol. 2018;1059:255-98.
9. Vyas C, Mishbak H, Cooper G, Peach C, Pereira RF, Bartolo P. Biological perspectives and current biofabrication strategies in osteochondral tissue engineering. Biomanufacturing Reviews. 2020;5(1):2.
10. McMahon LA, O'Brien FJ, Prendergast PJ. Biomechanics and mechanobiology in osteochondral tissues. Regen Med. 2008;3(5):743-59.
11. Mow VCG, Wei Yong Chen. Faye, Hui Chen. Structure and Function of Articular Cartilage and Meniscus. In: Mow VC, Huiskes R, editors. Basic orthopaedic biomechanics & mechano-biology. Third edition. ed. Philadelphia, Pennsylvania: Lippincott Williams & Wilkins; 2005. p. 181-214.
12. Athanasiou KA, Darling EM, Hu JC. Articular cartilage tissue engineering. Synthesis Lectures on Tissue Engineering. 2009;1(1):1-182.
13. Flik KR, Verma N, Cole BJ, Bach BR. Articular Cartilage. In: Williams RJ, editor. Cartilage Repair Strategies. Totowa, NJ: Humana Press; 2007. p. 1-12.
14. Akkiraju H, Nohe A. Role of Chondrocytes in Cartilage Formation, Progression of Osteoarthritis and Cartilage Regeneration. J Dev Biol. 2015;3(4):177-92.
15. Sophia Fox AJ, Bedi A, Rodeo SA. The basic science of articular cartilage: structure, composition, and function. Sports Health. 2009;1(6):461-8.
16. Eyre DR. The collagens of articular cartilage. Semin Arthritis Rheum. 1991;21(3 Suppl 2):2-11.

17. Knudson CB, Knudson W. Cartilage proteoglycans. Semin Cell Dev Biol. 2001;12(2):69-78.
18. Zhou L, Gjvm VO, Malda J, Stoddart MJ, Lai Y, Richards RG, et al. Innovative Tissue-Engineered Strategies for Osteochondral Defect Repair and Regeneration: Current Progress and Challenges. Adv Healthc Mater. 2020:e2001008.
19. Walsh WR, Walton M, Bruce W, Yu Y, Gillies RM, Svehla M. Cell Structure and Biology of Bone and Cartilage. In: An YH, Martin KL, editors. Handbook of Histology Methods for Bone and Cartilage. Totowa, NJ: Humana Press; 2003. p. 35-58.
20. Hu JCY, Athanasiou KA. Structure and Function of Articular Cartilage. In: An YH, Martin KL, editors. Handbook of Histology Methods for Bone and Cartilage. Totowa, NJ: Humana Press; 2003. p. 73-95.
21. Davis S, Roldo M, Blunn G, Tozzi G, Roncada T. Influence of the Mechanical Environment on the Regeneration of Osteochondral Defects. Front Bioeng Biotechnol. 2021;9:603408.
22. Bhosale AM, Richardson JB. Articular cartilage: structure, injuries and review of management. Br Med Bull. 2008;87:77-95.
23. Zhang Y, Wang F, Tan H, Chen G, Guo L, Yang L. Analysis of the mineral composition of the human calcified cartilage zone. Int J Med Sci. 2012;9(5):353-60.
24. Hoemann CD, Lafantaisie-Favreau CH, Lascau-Coman V, Chen G, Guzmán-Morales J. The cartilage-bone interface. J Knee Surg. 2012;25(2):85-97.
25. Luo Y, Sinkeviciute D, He Y, Karsdal M, Henrotin Y, Mobasheri A, et al. The minor collagens in articular cartilage. Protein & Cell. 2017;8(8):560-72.
26. Madry H, van Dijk CN, Mueller-Gerbl M. The basic science of the subchondral bone. Knee Surg Sports Traumatol Arthrosc. 2010;18(4):419-33.
27. Stewart HL, Kawcak CE. The Importance of Subchondral Bone in the Pathophysiology of Osteoarthritis. Front Vet Sci. 2018;5:178.
28. Johnston JD, Burnett WD, Kontulainen SA. Subchondral Bone Features and Mechanical Properties as Biomarkers of Osteoarthritis. In: Patel VB, Preedy VR, editors. Biomarkers in Bone Disease. Dordrecht: Springer Netherlands; 2017. p. 529-55.
29. Hart NH, Newton RU, Tan J, Rantalainen T, Chivers P, Siafarikas A, et al. Biological basis of bone strength: anatomy, physiology and measurement. J Musculoskelet Neuronal Interact. 2020;20(3):347-71.
30. Mohamed AM. An overview of bone cells and their regulating factors of differentiation. Malays J Med Sci. 2008;15(1):4-12.
31. Lin X, Patil S, Gao Y-G, Qian A. The Bone Extracellular Matrix in Bone Formation and Regeneration. Frontiers in Pharmacology. 2020;11.
32. Ramesh N, Moratti SC, Dias GJ. Hydroxyapatite-polymer biocomposites for bone regeneration: A review of current trends. J Biomed Mater Res B Appl Biomater. 2018;106(5):2046-57.
33. Outerbridge RE. The etiology of chondromalacia patellae. J Bone Joint Surg Br. 1961;43-B:752-7.

34. Howell M, Liao Q, Gee CW. Surgical Management of Osteochondral Defects of the Knee: An Educational Review. Curr Rev Musculoskelet Med. 2021;14(1):60-6.
35. Gikas PD, Aston WJ, Briggs TW. Autologous chondrocyte implantation: where do we stand now? J Orthop Sci. 2008;13(3):283-92.
36. Bentley G, Bhamra JS, Gikas PD, Skinner JA, Carrington R, Briggs TW. Repair of osteochondral defects in joints--how to achieve success. Injury. 2013;44 Suppl 1:S3-10.
37. Robert H. Chondral repair of the knee joint using mosaicplasty. Orthop Traumatol Surg Res. 2011;97(4):418-29.
38. Mithoefer K, Williams RJ, 3rd, Warren RF, Potter HG, Spock CR, Jones EC, et al. The microfracture technique for the treatment of articular cartilage lesions in the knee. A prospective cohort study. J Bone Joint Surg Am. 2005;87(9):1911-20.
39. Brittberg M, Lindahl A, Nilsson A, Ohlsson C, Isaksson O, Peterson L. Treatment of deep cartilage defects in the knee with autologous chondrocyte transplantation. N Engl J Med. 1994;331(14):889-95.
40. Abouna GM. Organ shortage crisis: problems and possible solutions. Transplant Proc. 2008;40(1):34-8.
41. Langer R, Vacanti JP. Tissue engineering. Science. 1993;260(5110):920-6.
42. Vacanti JP, Langer R. Tissue engineering: the design and fabrication of living replacement devices for surgical reconstruction and transplantation. Lancet. 1999;354 Suppl 1:SI32-4.
43. Khademhosseini A, Langer R. A decade of progress in tissue engineering. Nat Protoc. 2016;11(10):1775-81.
44. Polykandriotis E, Popescu LM, Horch RE. Regenerative medicine: then and now--an update of recent history into future possibilities. Journal of cellular and molecular medicine. 2010;14(10):2350-8.
45. Caddeo S, Boffito M, Sartori S. Tissue Engineering Approaches in the Design of Healthy and Pathological In Vitro Tissue Models. Front Bioeng Biotechnol. 2017;5:40.
46. de Isla N, Huseltein C, Jessel N, Pinzano A, Decot V, Magdalou J, et al. Introduction to tissue engineering and application for cartilage engineering. Biomed Mater Eng. 2010;20(3):127-33.
47. Hasirci V, Hasirci N. Tissue Engineering and Regenerative Medicine. In: Hasirci V, Hasirci N, editors. Fundamentals of Biomaterials. New York, NY: Springer New York; 2018. p. 281-302.
48. Ma PX. Biomimetic materials for tissue engineering. Adv Drug Deliv Rev. 2008;60(2):184-98.
49. Li JJ, Ebied M, Xu J, Zreiqat H. Current Approaches to Bone Tissue Engineering: The Interface between Biology and Engineering. Advanced Healthcare Materials. 2018;7(6):1701061.
50. Leal BBJ, Wakabayashi N, Oyama K, Kamiya H, Braghirolli DI, Pranke P. Vascular Tissue Engineering: Polymers and Methodologies for Small Caliber Vascular Grafts. Frontiers in Cardiovascular Medicine. 2021;7.
51. Gomes ME, Reis RL. Tissue engineering: key elements and some trends. Macromol Biosci. 2004;4(8):737-42.

52. Gaskell T, Englund MCO, Hyllner J. Human Embryonic Stem Cells. In: Steinhoff G, editor. Regenerative Medicine - from Protocol to Patient: 2 Stem Cell Science and Technology. Cham: Springer International Publishing; 2016. p. 27-49.
53. Nukavarapu SP, Dorcemus DL. Osteochondral tissue engineering: Current strategies and challenges. Biotechnology Advances. 2013;31(5):706-21.
54. Wei W, Dai H. Articular cartilage and osteochondral tissue engineering techniques: Recent advances and challenges. Bioact Mater. 2021;6(12):4830-55.
55. Jeong CG, Zhang H, Hollister SJ. Three-dimensional polycaprolactone scaffold-conjugated bone morphogenetic protein-2 promotes cartilage regeneration from primary chondrocytes in vitro and in vivo without accelerated endochondral ossification. J Biomed Mater Res A. 2012;100(8):2088-96.
56. Zhang B, Huang J, Narayan RJ. Gradient scaffolds for osteochondral tissue engineering and regeneration. J Mater Chem B. 2020;8(36):8149-70.
57. Pereira DR, Reis RL, Oliveira JM. Layered Scaffolds for Osteochondral Tissue Engineering. Adv Exp Med Biol. 2018;1058:193-218.
58. O'Shea TM, Miao X. Bilayered scaffolds for osteochondral tissue engineering. Tissue Eng Part B Rev. 2008;14(4):447-64.
59. Frenkel SR, Bradica G, Brekke JH, Goldman SM, Ieska K, Issack P, et al. Regeneration of articular cartilage--evaluation of osteochondral defect repair in the rabbit using multiphasic implants. Osteoarthritis Cartilage. 2005;13(9):798-807.
60. Cross LM, Thakur A, Jalili NA, Detamore M, Gaharwar AK. Nanoengineered biomaterials for repair and regeneration of orthopedic tissue interfaces. Acta Biomater. 2016;42:2-17.
61. Fu J-N, Wang X, Yang M, Chen Y-R, Zhang J-Y, Deng R-H, et al. Scaffold-Based Tissue Engineering Strategies for Osteochondral Repair. Frontiers in Bioengineering and Biotechnology. 2022;9.
62. Yousefi AM, Hoque ME, Prasad RG, Uth N. Current strategies in multiphasic scaffold design for osteochondral tissue engineering: A review. J Biomed Mater Res A. 2015;103(7):2460-81.
63. Levingstone TJ, Ramesh A, Brady RT, Brama PAJ, Kearney C, Gleeson JP, et al. Cell-free multi-layered collagen-based scaffolds demonstrate layer specific regeneration of functional osteochondral tissue in caprine joints. Biomaterials. 2016;87:69-81.
64. Zhou J, Xu C, Wu G, Cao X, Zhang L, Zhai Z, et al. In vitro generation of osteochondral differentiation of human marrow mesenchymal stem cells in novel collagen-hydroxyapatite layered scaffolds. Acta Biomater. 2011;7(11):3999-4006.
65. Deng T, Lv J, Pang J, Liu B, Ke J. Construction of tissue-engineered osteochondral composites and repair of large joint defects in rabbit. J Tissue Eng Regen Med. 2014;8(7):546-56.
66. Schaefer D, Martin I, Shastri P, Padera RF, Langer R, Freed LE, et al. In vitro generation of osteochondral composites. Biomaterials. 2000;21(24):2599-606.
67. Mellor LF, Nordberg RC, Huebner P, Mohiti-Asli M, Taylor MA, Efird W, et al. Investigation of multiphasic 3D-bioplotted scaffolds for site-specific chondrogenic and osteogenic

differentiation of human adipose-derived stem cells for osteochondral tissue engineering applications. J Biomed Mater Res B Appl Biomater. 2020;108(5):2017-30.

68. Levingstone TJ, Thompson E, Matsiko A, Schepens A, Gleeson JP, O'Brien FJ. Multi-layered collagen-based scaffolds for osteochondral defect repair in rabbits. Acta Biomater. 2016;32:149-60.
69. Liu X, Liu S, Liu S, Cui W. Evaluation of oriented electrospun fibers for periosteal flap regeneration in biomimetic triphasic osteochondral implant. J Biomed Mater Res B Appl Biomater. 2014;102(7):1407-14.
70. Hasirci V, Hasirci N. Introduction. In: Hasirci V, Hasirci N, editors. Fundamentals of Biomaterials. New York, NY: Springer New York; 2018. p. 1-14.
71. Ondrésik M, Oliveira JM, Reis RL. Advances for Treatment of Knee OC Defects. In: Oliveira JM, Pina S, Reis RL, San Roman J, editors. Osteochondral Tissue Engineering: Challenges, Current Strategies, and Technological Advances. Cham: Springer International Publishing; 2018. p. 3-24.
72. Bonani W, Singhatanadgige W, Pornanong A, Motta A. Natural Origin Materials for Osteochondral Tissue Engineering. In: Oliveira JM, Pina S, Reis RL, San Roman J, editors. Osteochondral Tissue Engineering: Nanotechnology, Scaffolding-Related Developments and Translation. Cham: Springer International Publishing; 2018. p. 3-30.
73. Lin HY, Tsai WC, Chang SH. Collagen-PVA aligned nanofiber on collagen sponge as bi-layered scaffold for surface cartilage repair. J Biomater Sci Polym Ed. 2017;28(7):664-78.
74. Chung C, Burdick JA. Influence of three-dimensional hyaluronic acid microenvironments on mesenchymal stem cell chondrogenesis. Tissue Eng Part A. 2009;15(2):243-54.
75. Shafiee A, Soleimani M, Chamheidari GA, Seyedjafari E, Dodel M, Atashi A, et al. Electrospun nanofiber-based regeneration of cartilage enhanced by mesenchymal stem cells. J Biomed Mater Res A. 2011;99(3):467-78.
76. Ondresik M, Oliveira JM, Reis RL. Advances for Treatment of Knee OC Defects. Adv Exp Med Biol. 2018;1059:3-24.
77. Eltom A, Zhong G, Muhammad A. Scaffold Techniques and Designs in Tissue Engineering Functions and Purposes: A Review. Advances in Materials Science and Engineering. 2019;2019:3429527.
78. Lee K-XA, Ng HY, Wei L-J, Shen Y-F. 16 - 3D functional scaffolds for cartilage tissue engineering. In: Deng Y, Kuiper J, editors. Functional 3D Tissue Engineering Scaffolds: Woodhead Publishing; 2018. p. 391-421.
79. Collins MN, Ren G, Young K, Pina S, Reis RL, Oliveira JM. Scaffold Fabrication Technologies and Structure/Function Properties in Bone Tissue Engineering. Advanced Functional Materials. 2021;31(21):2010609.
80. Yucel D, Kose GT, Hasirci V. Polyester based nerve guidance conduit design. Biomaterials. 2010;31(7):1596-603.

81. Bittner SM, Smith BT, Diaz-Gomez L, Hudgins CD, Melchiorri AJ, Scott DW, et al. Fabrication and mechanical characterization of 3D printed vertical uniform and gradient scaffolds for bone and osteochondral tissue engineering. Acta Biomaterialia. 2019;90:37-48.
82. Esposito Corcione C, Gervaso F, Scalera F, Padmanabhan SK, Madaghiele M, Montagna F, et al. Highly loaded hydroxyapatite microsphere/ PLA porous scaffolds obtained by fused deposition modelling. Ceramics International. 2019;45(2, Part B):2803-10.
83. Goncalves AM, Moreira A, Weber A, Williams GR, Costa PF. Osteochondral Tissue Engineering: The Potential of Electrospinning and Additive Manufacturing. Pharmaceutics. 2021;13(7).
84. Kilian D, Sembdner P, Bretschneider H, Ahlfeld T, Mika L, Lützner J, et al. 3D printing of patient-specific implants for osteochondral defects: workflow for an MRI-guided zonal design. Bio-Design and Manufacturing. 2021;4(4):818-32.
85. Turner B, Strong R, Gold S. A review of melt extrusion additive manufacturing processes: I. Process design and modeling. Rapid Prototyping Journal. 2014;20.
86. Martin I, Miot S, Barbero A, Jakob M, Wendt D. Osteochondral tissue engineering. J Biomech. 2007;40(4):750-65.
87. Mano JF, Reis RL. Osteochondral defects: present situation and tissue engineering approaches. J Tissue Eng Regen Med. 2007;1(4):261-73.
88. Ng J, Bernhard J, Vunjak-Novakovic G. Mesenchymal Stem Cells for Osteochondral Tissue Engineering. Methods Mol Biol. 2016;1416:35-54.
89. Pountos I, Giannoudis PV. Biology of mesenchymal stem cells. Injury. 2005;36(3, Supplement):S8-S12.
90. Friedenstein AJ, Chailakhyan RK, Gerasimov UV. Bone marrow osteogenic stem cells: in vitro cultivation and transplantation in diffusion chambers. Cell Tissue Kinet. 1987;20(3):263-72.
91. Riekstina U, Cakstina I, Parfejevs V, Hoogduijn M, Jankovskis G, Muiznieks I, et al. Embryonic Stem Cell Marker Expression Pattern in Human Mesenchymal Stem Cells Derived from Bone Marrow, Adipose Tissue, Heart and Dermis. Stem Cell Reviews and Reports. 2009;5(4):378-86.
92. Pierdomenico L, Bonsi L, Calvitti M, Rondelli D, Arpinati M, Chirumbolo G, et al. Multipotent Mesenchymal Stem Cells with Immunosuppressive Activity Can Be Easily Isolated from Dental Pulp. Transplantation. 2005;80(6).
93. In 't Anker PS, Scherjon SA, Kleijburg-van der Keur C, de Groot-Swings GM, Claas FH, Fibbe WE, et al. Isolation of mesenchymal stem cells of fetal or maternal origin from human placenta. Stem Cells. 2004;22(7):1338-45.
94. Erices A, Conget P, Minguell JJ. Mesenchymal progenitor cells in human umbilical cord blood. Br J Haematol. 2000;109(1):235-42.
95. Fan X-L, Zhang Y, Li X, Fu Q-L. Mechanisms underlying the protective effects of mesenchymal stem cell-based therapy. Cell Mol Life Sci. 2020;77(14):2771-94.
96. Wang N, Zhang R, Wang S-J, Zhang C-L, Mao L-B, Zhuang C-Y, et al. Vascular endothelial growth factor stimulates endothelial differentiation from mesenchymal stem cells via

Rho/myocardin-related transcription factor-A signaling pathway. The International Journal of Biochemistry & Cell Biology. 2013;45(7):1447-56.

97. Cho KJ, Trzaska KA, Greco SJ, McArdle J, Wang FS, Ye JH, et al. Neurons Derived From Human Mesenchymal Stem Cells Show Synaptic Transmission and Can Be Induced to Produce the Neurotransmitter Substance P by Interleukin-1α. Stem Cells. 2005;23(3):383-91.
98. Ercal P, Pekozer GG, Kose GT. Dental Stem Cells in Bone Tissue Engineering: Current Overview and Challenges. Adv Exp Med Biol. 2018;1107:113-27.
99. Seong JM, Kim BC, Park JH, Kwon IK, Mantalaris A, Hwang YS. Stem cells in bone tissue engineering. Biomed Mater. 2010;5(6):062001.
100. Nooeaid P, Salih V, Beier JP, Boccaccini AR. Osteochondral tissue engineering: scaffolds, stem cells and applications. J Cell Mol Med. 2012;16(10):2247-70.
101. Poole AR, Kojima T, Yasuda T, Mwale F, Kobayashi M, Laverty S. Composition and Structure of Articular Cartilage: A Template for Tissue Repair. Clinical Orthopaedics and Related Research®. 2001;391:S26-S33.
102. Da H, Jia SJ, Meng GL, Cheng JH, Zhou W, Xiong Z, et al. The impact of compact layer in biphasic scaffold on osteochondral tissue engineering. PLoS One. 2013;8(1):e54838.
103. biosystems D. Allevi Protocols 2022 [Available from: https://www.allevi3d.com/pcl-polycaprolactone-protocol/.]
104. Dominici M, Le Blanc K, Mueller I, Slaper-Cortenbach I, Marini F, Krause D, et al. Minimal criteria for defining multipotent mesenchymal stromal cells. The International Society for Cellular Therapy position statement. Cytotherapy. 2006;8(4):315-7.
105. Lian JB, Stein GS. CHAPTER 6 - Osteoblast Biology. In: Marcus R, Feldman D, Nelson DA, Rosen CJ, editors. Osteoporosis (Third Edition). San Diego: Academic Press; 2008. p. 93-150.
106. Layton C, Bancroft JD. 13 - Carbohydrates. In: Suvarna SK, Layton C, Bancroft JD, editors. Bancroft's Theory and Practice of Histological Techniques (Eighth Edition): Elsevier; 2019. p. 176-97.
107. Zhang L, Su P, Xu C, Yang J, Yu W, Huang D. Chondrogenic differentiation of human mesenchymal stem cells: a comparison between micromass and pellet culture systems. Biotechnology Letters. 2010;32(9):1339-46.
108. Johnstone B, Hering TM, Caplan AI, Goldberg VM, Yoo JU. In vitro chondrogenesis of bone marrow-derived mesenchymal progenitor cells. Exp Cell Res. 1998;238(1):265-72.
109. Longoni A, Utomo L, van Hooijdonk IE, Bittermann GK, Vetter VC, Kruijt Spanjer EC, et al. The chondrogenic differentiation potential of dental pulp stem cells. Eur Cell Mater. 2020;39:121-35.
110. Kenar H, Kose GT, Hasirci V. Tissue engineering of bone on micropatterned biodegradable polyester films. Biomaterials. 2006;27(6):885-95.
111. Watson TF, Atmeh AR, Sajini S, Cook RJ, Festy F. Present and future of glass-ionomers and calcium-silicate cements as bioactive materials in dentistry: biophotonics-based interfacial analyses in health and disease. Dent Mater. 2014;30(1):50-61.

112. Lee WD, Hurtig MB, Pilliar RM, Stanford WL, Kandel RA. Engineering of hyaline cartilage with a calcified zone using bone marrow stromal cells. Osteoarthritis and Cartilage. 2015;23(8):1307-15.
113. Wu J, editor Study on optimization of 3D printing parameters. IOP conference series: materials science and engineering; 2018: IOP Publishing.
114. Fazeli N, Arefian E, Irani S, Ardeshirylajimi A, Seyedjafari E. 3D-Printed PCL Scaffolds Coated with Nanobioceramics Enhance Osteogenic Differentiation of Stem Cells. ACS Omega. 2021;6(51):35284-96.
115. Abdulghani S, Morouço PG. Biofabrication for osteochondral tissue regeneration: bioink printability requirements. Journal of Materials Science: Materials in Medicine. 2019;30(2):20.
116. Wuchter P, Wagner W, Ho AD. Mesenchymal Stromal Cells (MSC). In: Steinhoff G, editor. Regenerative Medicine - from Protocol to Patient: 2 Stem Cell Science and Technology. Cham: Springer International Publishing; 2016. p. 295-313.
117. Otero M, Favero M, Dragomir C, Hachem KE, Hashimoto K, Plumb DA, et al. Human chondrocyte cultures as models of cartilage-specific gene regulation. Methods Mol Biol. 2012;806:301-36.
118. Costa E, González-García C, Gómez Ribelles JL, Salmerón-Sánchez M. Maintenance of chondrocyte phenotype during expansion on PLLA microtopographies. J Tissue Eng. 2018;9:2041731418789829.
119. Glowacki J, Trepman E, Folkman J. Cell shape and phenotypic expression in chondrocytes. Proc Soc Exp Biol Med. 1983;172(1):93-8.
120. Jundt G, Berghauser KH, Termine JD, Schulz A. Osteonectin--a differentiation marker of bone cells. Cell Tissue Res. 1987;248(2):409-15.
121. Zohar R, Cheifetz S, McCulloch CA, Sodek J. Analysis of intracellular osteopontin as a marker of osteoblastic cell differentiation and mesenchymal cell migration. Eur J Oral Sci. 1998;106 Suppl 1:401-7.
122. Nys Y, Le Roy N. Chapter 22 - Calcium Homeostasis and Eggshell Biomineralization in Female Chicken. In: Feldman D, editor. Vitamin D (Fourth Edition): Academic Press; 2018. p. 361-82.
123. Solheim E, Hegna J, Inderhaug E. Long-Term Survival after Microfracture and Mosaicplasty for Knee Articular Cartilage Repair: A Comparative Study Between Two Treatments Cohorts. Cartilage. 2020;11(1):71-6.
124. Zylinska B, Silmanowicz P, Sobczynska-Rak A, Jarosz L, Szponder T. Treatment of Articular Cartilage Defects: Focus on Tissue Engineering. In Vivo. 2018;32(6):1289-300.
125. Huey DJ, Hu JC, Athanasiou KA. Unlike bone, cartilage regeneration remains elusive. Science (New York, NY). 2012;338(6109):917-21.
126. Li X, Ding J, Wang J, Zhuang X, Chen X. Biomimetic biphasic scaffolds for osteochondral defect repair. Regenerative biomaterials. 2015;2(3):221-8.

127. Sherwood JK, Riley SL, Palazzolo R, Brown SC, Monkhouse DC, Coates M, et al. A three-dimensional osteochondral composite scaffold for articular cartilage repair. Biomaterials. 2002;23(24):4739-51.
128. Yan LP, Silva-Correia J, Oliveira MB, Vilela C, Pereira H, Sousa RA, et al. Bilayered silk/silk-nanoCaP scaffolds for osteochondral tissue engineering: In vitro and in vivo assessment of biological performance. Acta Biomater. 2015;12:227-41.
129. Mountcastle SE, Allen P, Mellors BOL, Lawless BM, Cooke ME, Lavecchia CE, et al. Dynamic viscoelastic characterisation of human osteochondral tissue: understanding the effect of the cartilage-bone interface. BMC Musculoskeletal Disorders. 2019;20(1):575.
130. Longley R, Ferreira AM, Gentile P. Recent Approaches to the Manufacturing of Biomimetic Multi-Phasic Scaffolds for Osteochondral Regeneration. Int J Mol Sci. 2018;19(6).
131. Tampieri A, Sandri M, Landi E, Pressato D, Francioli S, Quarto R, et al. Design of graded biomimetic osteochondral composite scaffolds. Biomaterials. 2008;29(26):3539-46.
132. Chen T, Bai J, Tian J, Huang P, Zheng H, Wang J. A single integrated osteochondral in situ composite scaffold with a multi-layered functional structure. Colloids and Surfaces B: Biointerfaces. 2018;167:354-63.
133. Kang H, Zeng Y, Varghese S. Functionally graded multilayer scaffolds for in vivo osteochondral tissue engineering. Acta Biomaterialia. 2018;78:365-77.
134. Korpayev S, Kaygusuz G, Şen M, Orhan K, Oto Ç, Karakeçili A. Chitosan/collagen based biomimetic osteochondral tissue constructs: A growth factor-free approach. International Journal of Biological Macromolecules. 2020;156:681-90.
135. Murphy CM, Haugh MG, O'Brien FJ. The effect of mean pore size on cell attachment, proliferation and migration in collagen–glycosaminoglycan scaffolds for bone tissue engineering. Biomaterials. 2010;31(3):461-6.
136. Duan P, Pan Z, Cao L, He Y, Wang H, Qu Z, et al. The effects of pore size in bilayered poly(lactide-co-glycolide) scaffolds on restoring osteochondral defects in rabbits. Journal of Biomedical Materials Research Part A. 2014;102(1):180-92.
137. Jia S, Wang J, Zhang T, Pan W, Li Z, He X, et al. Multilayered Scaffold with a Compact Interfacial Layer Enhances Osteochondral Defect Repair. ACS Applied Materials & Interfaces. 2018;10(24):20296-305.
138. Erickson IE, Huang AH, Sengupta S, Kestle S, Burdick JA, Mauck RL. Macromer density influences mesenchymal stem cell chondrogenesis and maturation in photocrosslinked hyaluronic acid hydrogels. Osteoarthritis and Cartilage. 2009;17(12):1639-48.
139. Critchley S, Sheehy EJ, Cunniffe G, Diaz-Payno P, Carroll SF, Jeon O, et al. 3D printing of fibre-reinforced cartilaginous templates for the regeneration of osteochondral defects. Acta Biomaterialia. 2020;113:130-43.
140. Dwivedi R, Kumar S, Pandey R, Mahajan A, Nandana D, Katti DS, et al. Polycaprolactone as biomaterial for bone scaffolds: Review of literature. J Oral Biol Craniofac Res. 2020;10(1):381-8.

141. Du Y, Liu H, Yang Q, Wang S, Wang J, Ma J, et al. Selective laser sintering scaffold with hierarchical architecture and gradient composition for osteochondral repair in rabbits. Biomaterials. 2017;137:37-48.
142. Huang Q, Goh JCH, Hutmacher DW, Lee EH. In Vivo Mesenchymal Cell Recruitment by a Scaffold Loaded with Transforming Growth Factor β1 and the Potential for in Situ Chondrogenesis. Tissue Engineering. 2002;8(3):469-82.
143. Wise JK, Yarin AL, Megaridis CM, Cho M. Chondrogenic differentiation of human mesenchymal stem cells on oriented nanofibrous scaffolds: engineering the superficial zone of articular cartilage. Tissue Eng Part A. 2009;15(4):913-21.
144. Heo DN, Kim H-J, Lee D, Kim H, Lee SJ, Lee H-R, et al. Comparison of polysaccharides in articular cartilage regeneration associated with chondrogenic and autophagy-related gene expression. International Journal of Biological Macromolecules. 2020;146:922-30.
145. Hong H, Seo YB, Kim DY, Lee JS, Lee YJ, Lee H, et al. Digital light processing 3D printed silk fibroin hydrogel for cartilage tissue engineering. Biomaterials. 2020;232:119679.
146. Li Y, Liu Y, Xun X, Zhang W, Xu Y, Gu D. Three-Dimensional Porous Scaffolds with Biomimetic Microarchitecture and Bioactivity for Cartilage Tissue Engineering. ACS Applied Materials & Interfaces. 2019;11(40):36359-70.
147. Camarero-Espinosa S, Calore A, Wilbers A, Harings J, Moroni L. Additive manufacturing of an elastic poly(ester)urethane for cartilage tissue engineering. Acta Biomaterialia. 2020;102:192-204.
148. Bentley G, Biant LC, Carrington RW, Akmal M, Goldberg A, Williams AM, et al. A prospective, randomised comparison of autologous chondrocyte implantation versus mosaicplasty for osteochondral defects in the knee. J Bone Joint Surg Br. 2003;85(2):223-30.
149. Khan IM, Gilbert SJ, Singhrao SK, Duance VC, Archer CW. Cartilage integration: evaluation of the reasons for failure of integration during cartilage repair. A review. Eur Cell Mater. 2008;16:26-39.
150. Zhou J, Xu C, Wu G, Cao X, Zhang L, Zhai Z, et al. In vitro generation of osteochondral differentiation of human marrow mesenchymal stem cells in novel collagen–hydroxyapatite layered scaffolds. Acta Biomaterialia. 2011;7(11):3999-4006.
151. Cristaldi M, Mauceri R, Tomasello L, Pizzo G, Pizzolanti G, Giordano C, et al. Dental pulp stem cells for bone tissue engineering: a review of the current literature and a look to the future. Regen Med. 2018.
152. Ercal P, Pekozer GG, Kose GT. Dental Stem Cells in Bone Tissue Engineering: Current Overview and Challenges. In: Turksen K, editor. Cell Biology and Translational Medicine, Volume 3: Stem Cells, Bio-materials and Tissue Engineering. Cham: Springer International Publishing; 2018. p. 113-27.
153. Nemeth CL, Janebodin K, Yuan AE, Dennis JE, Reyes M, Kim D-H. Enhanced Chondrogenic Differentiation of Dental Pulp Stem Cells Using Nanopatterned PEG-GelMA-HA Hydrogels. Tissue Engineering Part A. 2014;20(21-22):2817-29.

154. Johnstone B, Hering TM, Caplan AI, Goldberg VM, Yoo JU. In VitroChondrogenesis of Bone Marrow-Derived Mesenchymal Progenitor Cells. Experimental Cell Research. 1998;238(1):265-72.
155. Ryu NE, Lee SH, Park H. Spheroid Culture System Methods and Applications for Mesenchymal Stem Cells. Cells. 2019;8(12).
156. Yamaoka H, Asato H, Ogasawara T, Nishizawa S, Takahashi T, Nakatsuka T, et al. Cartilage tissue engineering using human auricular chondrocytes embedded in different hydrogel materials. J Biomed Mater Res A. 2006;78(1):1-11.
157. Armiento AR, Stoddart MJ, Alini M, Eglin D. Biomaterials for articular cartilage tissue engineering: Learning from biology. Acta Biomater. 2018;65:1-20.

8 APPENDIX

8.1 Appendix 1. Ethical Approval

Appendix 8.1 Ethical Approval (continued)

8.2 Appendix 2. Calibration Curves for Determination of Cell Number

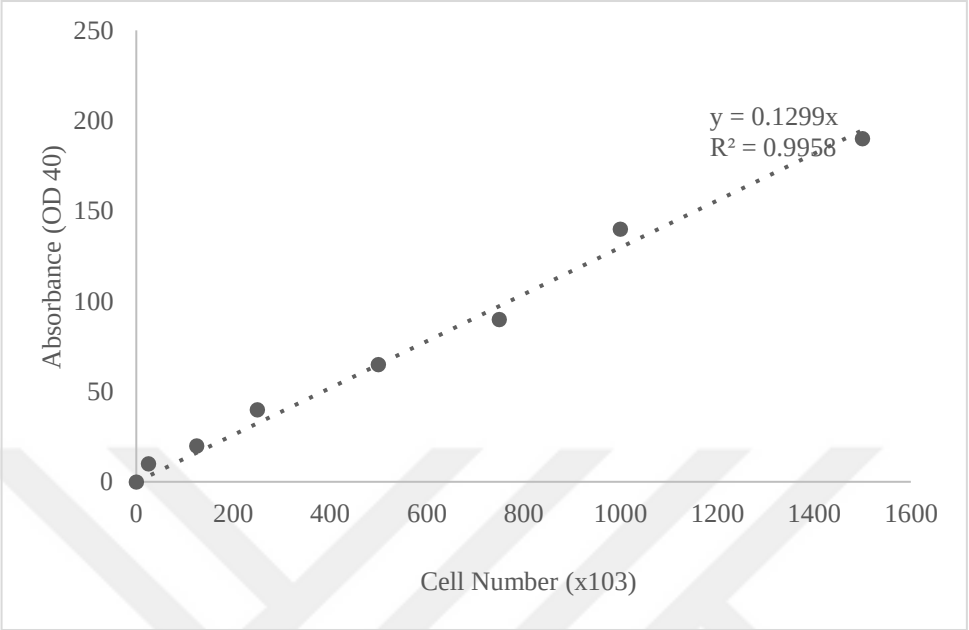

Figure A.1 The calibration curve obtained by WST-1 assay for cell number determination

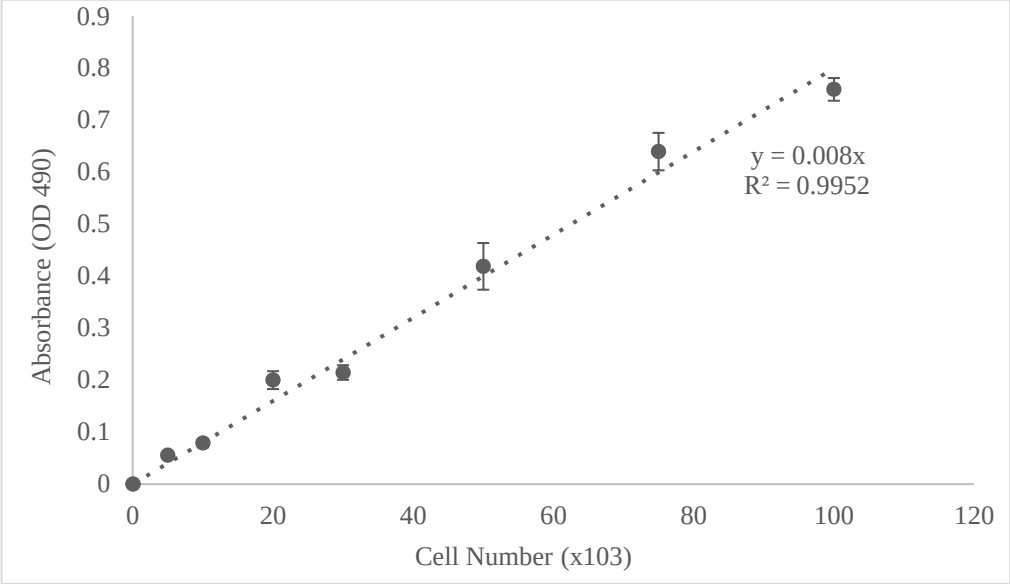

Figure A.2 The calibration curve obtained by MTS assay for cell number determination on scaffolds

8.3 Appendix 3 Calibration Curves for ALP Activity

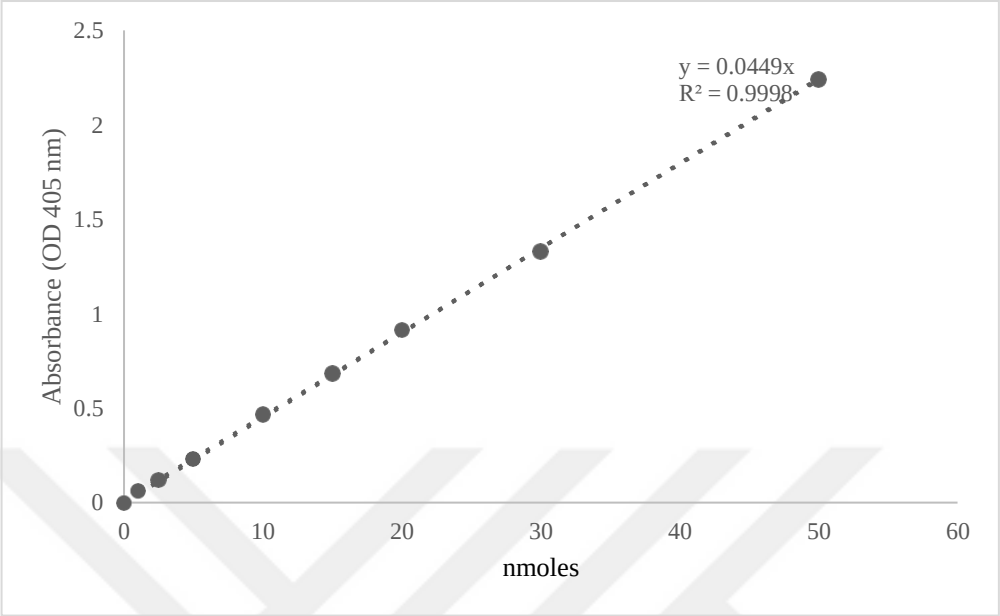

Figure A.3 The calibration curve for ALP activity prepared by p-nitrophenol at different concentrations

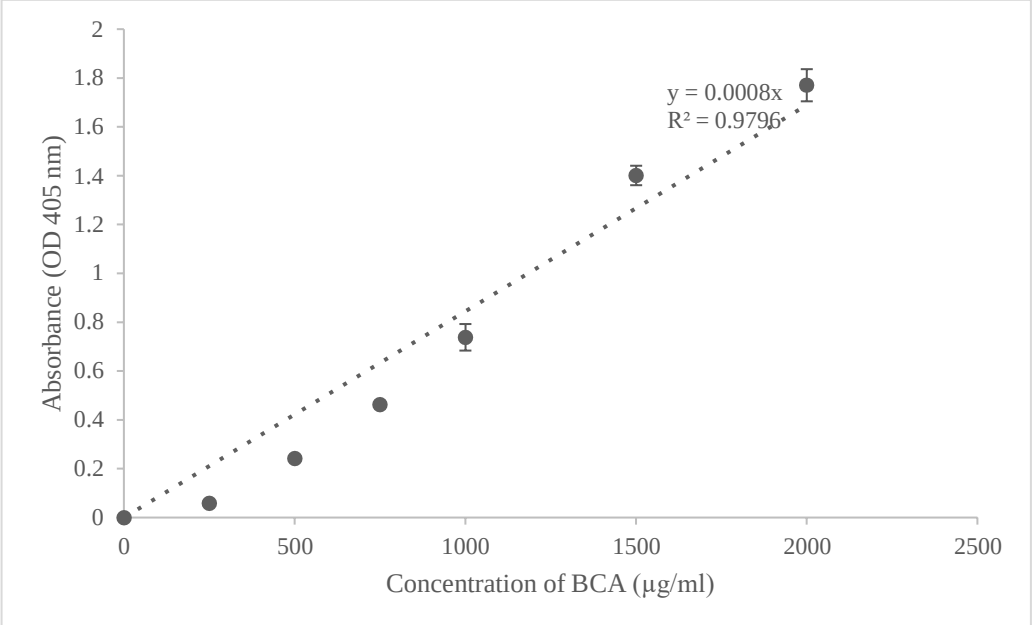

Figure A.4 The calibration curve for the determination of total protein concentration using BCA

9 CURRICULUM VITAE